SHORTWAVE SOLAR RADIATION FIELD INSIDE WILLOW CANOPY

MATTI MÕTTUS

This study was carried out at Tartu Observatory.

The dissertation was admitted on 22 June 2004 in partial fulfillment of the requirements for the degree of Doctor of Philosophy (in environmental physics) and allowed for defence by the Council of the Department of Physics, University of Tartu.

Supervisors:

Prof. Juhan Ross , Tartu Observatory, member of the Estonian Academy of Sciences

Prof. Tiit Nilson, Tartu Observatory

Prof. Hannes Tammet, Institute of Environmental Physics, University of Tartu

Opponents:

Dr. Pauline Stenberg, University of Helsinki

Dr. Piia Post, University of Tartu

Defence: 15 October 2004 at the University of Tartu.

CONTENTS

LIST OF ORIGINAL PUBLICATIONS

I **Ross, J., Mõttus, M., 2000.** Statistical treatment of umbra length inside willow coppice. Agricultural and Forest Meteorology 100, 89–102.

II **Ross, J., Mõttus, M., 2000.** Statistical treatment of sunfleck length inside willow coppice. Agricultural and Forest Meteorology 104, 215–231.

III **Mõttus, M., Ross, J., Sulev, M., 2001.** Experimental study of ratio of PAR to direct integral solar radiation under cloudless conditions. Agricultural and Forest Meteorology 109, 161–170.

IV **Mõttus, M., Ross, J., Ross, V., 2002.** Shape and area of simple narrow leaves. Proceedings of the Estonian Academy of Sciences. Biology. Ecology 51, 147–62.

V **Mõttus, M., 2004.** Measurement and modelling of the vertical distribution of sunflecks, penumbra and umbra in willow coppice. Agricultural and Forest Meteorology 121, 79–91.

VI **Mõttus, M., Sulev, M., 2004.** Comparison of modeled canopy transmittance and radiation fluxes with measurements inside a willow canopy. Submitted to Agricultural and Forest Meteorology.

MAIN RESULTS

- A geometrical model describing the willow coppice as consisting of vertical stems, applied to predicting the distribution of the intensity of direct solar radiation in penumbra and to modeling radiation fluxes inside the willow stand is shown to produce results agreeing well with the measured characteristics of the radiation field.

- A leaf shape function is proposed for the description of simple narrow leaves.

- The effect of clumping on the penetration of direct solar radiation is shown to be similar to that of variation in leaf inclination angle.

- The clumping index introduced into the equation of radiative transfer is shown to improve the estimates of downward fluxes at the cost of adding a parameter determined from radiation measurements; the improvement in predicting upward fluxes is not so evident.

1   INTRODUCTION

The biological and biochemical processes inside a plant are determined by the environment of the plant and whether or not the plant has adapted to such conditions during its evolution. The set of conditions experienced by individual organisms is called their microenvironment, the physical factors of this environment constitute the microclimate the organism has to endure or prosper in.

To understand the functioning of an ecosystem, quantitative measurements of its microclimate have to be carried out. Depending on the required detailedness of the description of the environment, different constituents of microclimate might be measured at different scales. However, one of the most fundamental characteristics of any system is its energy budget. Generally, the energy budget of a plant consists of the exchange of heat by conductance or advection, latent heat flux, accumulation of incident shortwave radiation, energy loss due to thermal infrared radiation and the small fraction of energy accumulated in the chemical bonds of organic compounds. But when looking at the subject with a broader perspective, it is evident that all energy exchanged by an organism has its roots in a single source.

Biosphere receives its energy either directly or indirectly from the thermonuclear reactions inside the fiery core of our closest star—the Sun. This energy traverses the empty space between the Sun and the Earth as a flux of photons. On the spectral scale, most of the solar radiative energy is transported by photons with wavelengths below 4 μm, or equivalently, ignoring the relatively small contribution of gamma- and X-rays, most of the energy arrives in the ultraviolet, visible and short infrared wavebands.

After interacting with the atmosphere, this radiation affects directly the functioning of a plant canopy. A direct consequence of the solar radiation absorbed by plants is an increase in temperature. For normal growth and development of plants, the temperature has to be above a (somewhat species-specific) threshold (Campbell and Norman, 1998). On the other hand, high temperatures decrease the rate of photosynthesis and can cause large evaporation rates leading to excess water loss.

The air surrounding the plant may be heated indirectly, by advection of warm air, creating a favorable environment for growth. However, this thermal energy can not be directly used for supporting biological processes, and for plants, the primary source of chemical energy is the process known as photosynthesis. One of the irreplaceable requirements for photosynthesis is the presence of shortwave radiation; thus it may be said that after learning to photosynthesize at the very beginning of their evolution, plants are directly dependent on solar radiation.

Besides energy, photosynthesis also provides the basic construction material for plant cells, carbon contained in various organic compounds. This organic material is used by other organisms inhabiting our planet, initiating a number of food chains, some of which allow for the existence of human beings. The ability of green plants to produce organic compounds from atmospheric carbon serving as a foundation to all life on our planet is well appreciated by modern man and much scientific attention has been paid to this phenomenon.

By determining the well-being of a plant, microclimate is an indicator of plant health. The physical parameters constituting the plant microclimate may be measured directly for a characterization of a small area chosen as a test site or to represent a specific ecosystem. For larger areas or even on the global scale, remote sensing techniques have to be used.

Only a few variables describing the microclimate of a plant canopy can be directly measured using remote sensing methods. The temperature of plants can be measured using the thermal radiation emitted by the vegetation as the atmosphere is almost transparent to radiation in the spectral interval of 8 to 13 μm where bodies at room temperature emit quite efficiently. Most of the remaining parameters have to be determined indirectly.

Although with the advent of lidars, active methods of remote sensing in the visible and infrared spectral regions are being actively developed for military, scientific and commercial purposes, passive sensors are still cheaper and more widely used. Thus, using the Sun as the source, radiation reflected by the canopy in one or several directions is measured. Being emitted by a body with a much higher temperature, this radiation is not at an equilibrium with the canopy and thus does not characterize the microclimate directly.

This does not mean that the shortwave radiation field inside the plant canopy is not a micrometeorological element. Shortwave radiation is one of the key ingredients of the microclimate, determining plant growth. Remote sensing methods do not permit the measurement of the shortwave radiation field inside the canopy. However, many of the parameters determining the distribution of solar radiation inside the canopy also determine the distribution of reflected radiation. Thus, the two topics—characterizing vegetation microclimate and passive shortwave remote sensing—are tightly connected.

Besides monitoring the state of an ecosystem with a known dependence of reflectance on the condition of the system, a different and more complex problem is often encountered in remote sensing. If a large amount of reflectance data is obtained from a remote sensing satellite or some other system capable of covering large vegetated areas, a physical interpretation is needed. With a limited prior knowledge of the species composition, canopy structure or health status, the characteristics of the observed ecosystem have to be determined.

Any attempt to solve this problem has to be preceded by a detailed study of the interactions between plants and radiation. Enough data has to be gathered to falsify or corroborate various theories, so that models describing the many sides of the microclimate can produce realistic values of the measured parameters.

The basic characteristics of the microclimate are determined by macroclimate; plants have only a few mechanisms to alter their environment. Plants can not choose the area they inhabit and mostly have to adjust to their surroundings. At the same time, accommodation to the macroclimatic conditions of a habitat can also include a modification of the microclimate inside and around the plant canopy.

Different adaptations allow plants to regulate the interception of light both in the short term (seconds to minutes) and in the longer term (hours to days). Some effects, like leaf movement, are more evident—some plants change the orientation of leaves according to the direction of the Sun, either actively, using a pulvinus attaching the leaf blade to the petiole or the stem, or passively, as a consequence of water stress in tissues without secondary cell walls. Many species, mostly from arid climates, are capable of changing leaf reflectance by varying the degree of pubescence for regulating light interception in the longer term; another mechanism of coping with varying radiation level is changing leaf transmittance by rearranging the chloroplasts within each cell (Björkman and Demmig-Adams, 1995).

Besides these modulative adaptations, long-term irreversible changes occur during plant development and growth. For example, low values of radiation intensity may limit the carbon available for support, decreasing the total area of leaves attached to a shoot and their horizontal coverage, limiting in turn photosynthetic efficiency (Niinemets et al., 2004); the width of a conifer needle increases with light availability (Stenberg et al., 1999). Even slower, almost unnoticeable modifications within plant species are also constantly taking place forming the process known as evolution.

While these examples demonstrate the ability of plants to adapt to new environments, these changes also modify the radiation field inside the canopy, modifying the penetration of shortwave radiation. Naturally, plants can also modify other components of the microclimate: besides radiation, temperature is also determined by heat advection which depends on the shape and the aerodynamic properties of leaves and on canopy architecture; and also by latent heat fluxes that can be controlled by evaporation; many of these factors also influence local transport of atmospheric gases, like carbon dioxide. However, these variables are not discussed in this work—natural processes are almost infinitely complex, they have to be divided into more tractable problems that can be solved separately before a general picture of their functioning can be assembled.

The radiation field inside a plant canopy is determined by the field above the canopy, the geometrical and optical properties of plant elements (leaves, branches, etc.) and the reflectance of the ground. For an understanding of the functioning of a plant, all these factors have to be known, as the distribution of shortwave radiation has a direct effect on canopy photosynthesis.

Most plants orient their leaves so that as few leaves as possible are continuously exposed to direct radiation and so that most leaves are in semi-shade. Erect leaves, leaves positioned in profile and those with curved surfaces intercept incoming radiation at an acute angle, thus avoiding injuries from strong irradiation and overheating (Larcher, 1995). Minimizing the risk of overheating and photooxidative destruction of the photosynthetic apparatus with steeply oriented foliage and moderate self-shading comes with an increased cost in terms of potential carbon gain (Valladares and Pugnaire, 1999; Falster and Westoby, 2003).

Structural avoidance of excessive radiation efficiently prevents the risk of damage by intense irradiance, has no special maintenance costs, and is biomechanically cheaper than enhanced light harvesting by a horizontal canopy, which points to structural photoprotection as a very effective strategy to cope with high irradiance stress in poor and adverse habitats (Valladares and Pugnaire, 1999). For example, at smaller radiation intensities, Niinemets et al. (2004) found that the shoots of the *Nothofagus* species became more horizontal and flatter to increase radiation capture.

Besides creating small-scale fluctuations in the light microclimate, leaf size has an indirect effect on canopy transmittance. Species with smaller leaves tend to have greater within-shoot self-shading as small leaves can be more crowded together and are attached closer to the stem. This self-shading, rather than the distribution of leaf angles, can explain most variance in light capture for some species (Falster and Westoby, 2003). In conifers, the grouping of needles into shoots considerable changes the distribution of radiation (Stenberg, 1995); according to Niinemets et al. (2004), shoot architecture significantly affects light interception and photosynthesis also in broad-leaved trees.

The spatial distribution of leaves and their size determine how large are the gaps between them where direct solar radiation can penetrate into the lower canopy layers. Sunflecks, or areas where direct solar radiation is considerable, are of considerable importance to the carbon gain of many species (Pearcy and Pfitsch, 1995). However, the contribution of sunflecks depends not only on the canopy structure, but also on the definition of a sunfleck. Underneath a tall dense canopy where diffuse radiation is scarce, the occasional sunrays penetrating the upper stories can be vital for understory growth. In such a "sunfleck", radiation intensity only occasionally reaches that of direct solar radiation above the canopy

(e.g., Vierling and Wessman, 2000), and the radiation field is largely penumbral even in sunflecks.

In the largely varying radiation field, the effects of penumbra and canopy structure on canopy photosynthesis cannot be ignored. The importance of penumbra depends on the size of phytoelements and also on the depth within the canopy (Stenberg, 1995): the variance of the visible fraction of the Sun is a function of the distance, size and shape of leaf projections on a plane perpendicular to the sunrays. In conifer canopies that consist of long and narrow needles and have a large depth, penumbral effects in between-shoot shading dominate, the shading from a Scots pine shoot already at about 30 cm is highly penumbral (Palva et al., 1998).

Even for canopies consisting of leaves, penumbra cannot be ignored. For example, in a 70-year-old alder canopy, many small gaps exist that have sizes that are less than the apparent size of the Sun (Kucharik et al., 1998); Vierling and Wessman (2000) report that penumbra has a strong influence on the sunfleck regime beneath a rain forest.

The finite size of the solar disc and a deep canopy with depth many orders of magnitude larger than the size of a phytoelement help to distribute light more evenly. Stenberg (1998) suggested that the even distribution of irradiance can help conifers to effectively utilize absorbed photosynthetically active radiation (PAR) because, at a fixed rate of absorbed PAR by the canopy, the rate of photosynthesis would be highest if all leaves operated in the linear part of the photosynthetic response curve. Thus, although the fraction of absorbed radiation is saturated if the leaf area index (LAI) of the canopy reaches about 5, higher leaf area indices may be maintained by plants for more efficient photosynthesis. According to her modeling results, for moderate values of LAI, penumbra increased the rate of photosynthesis by as much as 40%.

According to Oker-Blom (1985), the photosynthetic response of a Scots pine shoot is highly dependent on the proportions of direct and diffuse irradiance, being higher the greater the proportion of diffuse radiation. In conifers, light interception per unit needle area of a shade shoot receiving 10% of the light received by a "sun shoot" can be about 30% of the interception of the sun shoot due an increase in the ratio of projected to total shoot area (measured as the sum of the total areas of all needles comprising the shoot) and an increase in the specific leaf area of a needle in the shade shoot (Stenberg et al., 1999). Although grouping decreases the relative amount of intercepted shortwave radiation, the loss in intercepted radiation becomes minor in dense and extensive canopies (Stenberg, 1998).

Thus, considering that the intensity of shortwave solar radiation illuminating the leaf is non-uniform, that the leaves do not have equal photosynthetical po-

tential due to their varying locations and orientations, and the non-linearity of photosynthesis with absorbed shortwave radiation, it is not surprising that the photosynthetic rate of single leaves is often not representative of photosynthetic behavior for the entire canopy (Beyschlag et al., 1995). To assess the photosynthetic capability of a plant stand, it must be modeled as a coherent system with numerous interacting components and feedback systems.

Shortwave radiation was detailed above as consisting of the ultraviolet, visible and short infrared wavebands. Ultraviolet radiation is mostly absorbed by the atmosphere, its contribution to the energy budget (but not necessarily its effect on plants) of a plant canopy is small and is ignored in this work.

Visible radiation, or radiation in the spectral interval of 400 to 700 nm is referred to as photosynthetically active radiation (PAR). This component of shortwave radiation is the driving force behind photosynthesis. The rest of solar radiation with wavelength longer than 700 nm is called near-infrared radiation (NIR). There is no universally accepted upper bound for the NIR interval, but it is convenient to use this term for the spectral region where the intensity of solar radiation is still significant while the thermal emittance of cooler objects (about 300 K) can be neglected. In the current work, the upper bound of the NIR region is chosen as 2500 nm.

The division of shortwave radiation into PAR and NIR is justified by the spectral properties of green plants. A very large fraction of incident PAR is absorbed by vegetation while in the NIR region, the reflectance of green leaves is high. Thus, vegetation viewed in the PAR (or visible) interval is much darker than when photographed with a near-infrared filter.

The experimental part of this study was carried out in a short-rotation energy forest. Two willow species were studied, *Salix viminalis* and *Salix dasyclados*. The maximum height of the forest was 8 m; thus the physical dimensions of the canopy allowed to measure regularly and thoroughly both the radiation field and the stand architecture. Compared with natural forests, the willow stand was more homogeneous and regular, but as the planting density was high, this regularity does not have a large effect on the radiation regime. Thus, effects like canopy clumping should be evident in the radiation measurements.

The main objectives of this work are to

- demonstrate an application of allometric formulae to a plant canopy for determining various canopy characteristics;

- describe the detailed structure of the fast growing willow stand;

- give an overview of the radiation measurements carried out in the willow coppice;

- compare the sunfleck, umbra and penumbra characteristics calculated for the two willow species;

- describe and model the penetration of direct solar radiation inside the willow coppice;

- compare measured radiation fluxes and canopy transmittance with various modeling results;

- describe the effect of canopy clumping on both direct and diffuse fluxes inside the willow canopy.

This thesis is structured as follows:

First, an overview of the general approaches to modeling canopy structure is given followed by a description of the willow coppice during different growing years. Allometric formulae are developed to allow the calculation of various canopy characteristics.

The radiation measurement system is described followed by a short overview of the various components of the radiation field and the basic theory of radiative transfer as applied to plant canopies. Various formulae of canopy transmittance are presented followed by a discussion of the clumping index.

Finally, various measurement and modeling results are reported. Most of the obtained results have been published in articles I, II, V and VI; in this thesis, an attempt is made to connect the modeling results with the theoretical information presented in the first sections and thus give a more complete and better-integrated picture of the radiation field.

2 BIOMETRICAL DESCRIPTION OF A PLANT CANOPY

2.1 Leaf area index and canopy models

To give a meaningful description of the radiation field inside a plant canopy, the canopy itself must also be described mathematically. Contrary to the atmosphere or the ocean that can be described as continuous media with continuous scattering and absorbing properties, plant canopy consists of elements with finite sizes—leaves, flowers, branches, etc.

Elements of the plant canopy, or phytoelements, can be described by their location in 3D space, orientation, spectral properties, etc. As giving the exact location of each leaf, branch, or twig and calculating their interaction properties with radiation requires extensive and laborious data collection and also much computing power, a statistical approach is most often used.

Leaves are usually treated as infinitesimally thin objects, characterized only by their area and orientation. Let us denote the one-sided leaf area in a small volume ΔV around the point $\mathbf{r} = (x, y, z)$ by $\Delta S_{L,\Delta V}$; then the one-sided leaf area density at that point equals

$$u_L(\mathbf{r}) = \lim_{\Delta V \to 0} \frac{\Delta S_{L,\Delta V}}{\Delta V}. \tag{2.1}$$

Due to the fact that leaves are treated as two-dimensional objects having a finite area in three-dimensional space, the limit converges to a delta function, or an "indicator function". To avoid this, the volume ΔV has to remain large enough for a meaningful physical interpretation. In actual canopies, however, this causes no problems due to uncertainties related to measuring the coordinates of individual leaves and leaf flutter caused by wind.

Integrating Eq. 2.1 downwards from the top of the canopy we obtain the downward cumulative leaf area index

$$L(x, y, z) = \int_z^{z_{max}} u_L(x, y, \zeta) d\zeta, \tag{2.2}$$

where z_{max} is the height of the plant stand. The value of the downward cumulative leaf area index at the bottom of the plant canopy, $L(x, y, 0)$, the one-sided area of leaves per unit ground area, is the leaf area index (LAI). Generally, LAI is a function of the horizontal coordinates x and y, but it is commonly averaged over some area or the whole plant stand as its value at a single point below the canopy is not a good characteristic of the (always somewhat random) stand. In the current work, the downward cumulative leaf area index (Eq. 2.2) is considered only as a function of the vertical coordinate z, $L(x, y, z) = L(z)$, ie. the value of

$L(x, y, z)$ is averaged over the x and y coordinates. Thus, LAI characterizes the whole plant stand or at least the part of the stand where radiation measurements where carried out.

The same approach can be used to describe the area of stems, branches, flowers, or needles in case of conifers. In this case, the corresponding indices are sometimes called the stem, branch, flower, or needle area index, respectively; the sum of these indices, including LAI, is the plant or foliage area index.

As these foliage elements cannot be adequately described as two-dimensional objects, further methodological difficulties arise.

For ideal cylindrical needles, several surface areas are defined (Nilson and Ross, 1997): total two-sided area, equal to the surface area of the cylinder; one-sided area, equal to half the two-sided area; and silhouette area, approximately equal to $\frac{2}{\pi}$ times the one-sided area. Real needles are never cylindrical and approximation formulae have to be used to relate the total one- or two-sided area to silhouette area (e.g., Palmroth et al, 1999). In their review paper, Gower et al. (1999) recommend to use half the total needle surface area, or hemisurface area. A theoretical survey of general relationships between surface areas of solids and their projections targeted at calculation of surface areas of leaves, needles, and branches was carried out by Lang (1991) concluding that the total area of needles, twigs, and branches can be obtained from π times the average projected area where the entity is essentially cylindrical or rotated about its long axis. Measurements carried out on the needles of *Picea abies* suggested that the ratio of total to projected leaf area is between 2.5 and 4.0 (Stenberg et al., 1999).

For modeling radiative transfer within canopies of coniferous trees, the shoot may be used as the basic unit (Nilson and Ross, 1997); according to Stenberg et al. (1994), measuring canopy transmittance gives an estimate of shoot silhouette area index rather than leaf area index.

Even for broadleaves, LAI value depends on the definition of the area of a single leaf. Although the thickness of the leaf is almost never an important issue, leaves are usually non-flat or convex. Chen and Black (1992) suggested that the leaf area index of non-flat leaves be defined as half the total intercepting area per unit ground surface area and that the definition of LAI based on the projected leaf area be abandoned. For randomly-oriented flat leaves, this definition coincides with the simple notion of one-sided leaf area. However, this proposition was not too well greeted by the scientific community.

In the present study, leaf area is defined as measured with a planimeter: the area of the leaf when stretched out on a flat surface (i.e. the area contained in the leaf's contour) is measured. This method is best suited for the non-complex willow leaves that have a simple shape (Ross, 1981). This method can not guarantee absolute accuracy, as in natural conditions willow leaves are not flat, even a slight

wind causes them to flutter, and damaged leaves can also have ragged edges or holes in them. Still, as the intercepting area of a leaf depends on view angle, is ambiguously related to leaf biomass, and its measurement is difficult (if not impossible) to carry out in field, the planimetric method can still be considered the preferred approach for determining leaf area.

When describing the radiation field inside a plant canopy, the variable L (Eq. 2.2) is often used as the vertical coordinate: from Eq. 2.2, it follows that

$$dL = -u_L(z)dz. \tag{2.3}$$

Integrating the last equation gives

$$L(z) = -\int_{z_{max}}^{z} u_L(\zeta)d\zeta = \int_{z}^{z_{max}} u_L(\zeta)d\zeta. \tag{2.4}$$

As $u_L(z) \geq 0$, L is a unique function of z.

From the radiation point of view, the description of a plant canopy using the $u_L(z)$ function assumes that it consists of numerous (infinitesimally) small scattering and absorption centers, i.e. that it is a horizontally homogeneous 'turbid medium'. Although this is a fruitful approach, natural canopies have an inherent structure. That structure can be described by some kind of parameterization, or a wholly different approach, detailed 3D modeling, can be used.

A more detailed description of the canopy, including the non-homogeneous case, can be given using an indicator function:

$$\chi(\mathbf{r}) = \begin{cases} 1, & \text{if } \mathbf{r} \in \text{vegetation} \\ 0, & \text{otherwise} \end{cases}$$

and a fine spatial mesh is introduced. Inside each cell, $u_L(\mathbf{r})$ is considered constant (Shabanov et al, 2000). The next step towards more detail is the complete 3D description of a (model) canopy, where the exact locations and orientations of phytoelements are given (Chen et al., 1994; Andrieu et al., 1995; Ivanov et al., 1995; España et al., 1998, 1999a,b; Castro and Fetcher, 1999; Fournier et al, 1996; Génard et al., 2000; Lewis, 1999; Myneni et al., 1986; Pommel et al., 2001; Sinoquet et al., 1991, 1998). This requires an accurate knowledge of the plant canopy, taken from detailed measurements or using more general considerations (like plant growth models) for creating model structures.

A compromise between the detailed 3D canopy models and the turbid medium approach are the geometric-optical models. In these models, tree crowns are approximated by geometrical figures: cones, cylinders, ellipsoids, etc.; the distribution of leaf area within each crown is homogeneous. These models allow for fast computation and model inversion while retaining some information about canopy

structure (e.g., Li and Strahler, 1986; Nilson and Peterson, 1991; Li and Strahler, 1992; Kuusk and Nilson, 2000; Zhang and Xu, 2002).

In the current work, radiation field is studied only inside a willow coppice, where the leaves are the major factors determining the scattering and attenuation of solar radiation. According to modeling results, stems absorb or scatter less than 1% of direct solar radiation penetrating the canopy. The stems inside a willow canopy are surrounded by leaves shielding them from both direct and diffuse radiation. Thus, only the optical properties of leaves and their areas are considered in this work, i.e. plant area index is taken equal to leaf area index. For other canopy types, the role of tree stems and branches can be considerably larger and they cannot be ignored. For woody plants, stem material plays a significant role in determining canopy reflectance, especially for canopies with LAI < 5; however, this is also dependent on the location of woody material within the canopy (Asner, 1998).

According to Jonckheere et al. (2004), LAI values range between 0.40 for a low-density willow stand and 16.9 for an old-growth stand; for deciduous forest, LAI values can normally be as high as 8; the LAI values measured in Estonian deciduous forests are generally close to 3. The *Salix viminalis* stand under observation in the current work reached its maximum LAI value of 8 during the fourth growing year when canopy height was more than 6 m; maximum height of the *Salix dasyclados* stand was about 5 m, maximum LAI 5.

2.2   Leaf orientation

The scattering centers inside a plant canopy are generally not rotationally invariant nor do have random orientation. Thus, a method has to be devised to describe the orientation of leaves using the turbid medium approach.

Let $g_L(x, y, z, \mathbf{\Omega}_L)$ be the probability density of the leaf normal distribution at the point (x, y, z) with the normalization

$$\frac{1}{4\pi} \int_{4\pi} g_L(x, y, z, \mathbf{\Omega}_L) d\mathbf{\Omega}_L = 1, \tag{2.5}$$

i.e. the probability that a leaf normal is pointing to the solid angle $d\mathbf{\Omega}_L$ around the direction $\mathbf{\Omega}_L$ is $\frac{1}{4\pi} g_L(x, y, z, \mathbf{\Omega}_L) d\mathbf{\Omega}_L$ (Ross, 1981). Then the mean projection of unit foliage area on the plane normal to direction of photon travel (denoted as $\mathbf{\Omega}$) can be calculated as

$$G(x, y, z, \mathbf{\Omega}) = \frac{1}{4\pi} \int_{4\pi} g_L(x, y, z, \mathbf{\Omega}_L) \left| \mathbf{\Omega} \cdot \mathbf{\Omega}_L \right| d\mathbf{\Omega}_L. \tag{2.6}$$

The integrals in Eqs. 2.5 and 2.6 are taken over the solid angle of 4π, or the whole sphere. Sometimes, leaf normals are restricted to the upper hemisphere

and the integral is taken only over the upper 2π, denoted as $\int_{2\pi+}$. Restricting leaf normals to one hemisphere is justified only if the optical properties of the abaxial and adaxial sides of the leaf are identical, otherwise the direction of the normal should always point from the adaxial surface of the leaf and integration must be carried out over 4π.

Generally, both g and G are functions of the three spatial coordinates x,y,z and the two variables defining a direction $\mathbf{\Omega}$ in 3D space, azimuth and zenith angles: $g \equiv g(x, y, z, \mathbf{\Omega}_L)$, $G \equiv G(x, y, z, \mathbf{\Omega})$. The assumption of horizontal homogeneity removes the dependence on x and y; the dependence of Eqs. 2.5 and 2.6 on the height z can rarely be verified by measurement. Thus it is customary to assume that the functions describing leaf orientation can be written as $g(x, y, z, \mathbf{\Omega}_L) \equiv g(\mathbf{\Omega}_L)$ and $G(x, y, z, \mathbf{\Omega}) \equiv G(\mathbf{\Omega})$. Also, when not studying row crops or plants with distinct directional preferences, these functions are averaged over the azimuth angle and are treated as functions of the zenith angle ϑ only.

3   MEASUREMENTS OF CANOPY STRUCTURE

Leaf area index and its vertical distribution in the willow coppice was determined using allometric relations. To estimate various canopy parameters, destructive sampling was carried out at a reasonable distance from the radiation measurement location periodically during the growing period. This method is well suited for collecting biometric data for phytoactinometric purposes; in their review, Gower et al. (1999) concluded that this type of approach using site-specific allometric relations is the preferred method for an accurate determination of LAI.

3.1   General description of the willow coppice

A small (area 0.4 ha) short-rotation willow plantation was established at Tartu Observatory, Estonia (latitude 58°16'N, longitude 26°28'E, altitude 70 m above sea level) in May 1993. The cuttings were planted in double rows on the flat top of a small hill on light pseudopodzolic soil (Planosol). Distance between the plants in a row was 0.5 m, distance between the rows was 0.75 and 1.25 m, planting density was 20,000 cuttings per ha. The azimuth angle of the rows was 75° E. A photo of the coppice on 18 August 1995 is shown in Figure 3.1.

The area of the plantation was divided between two species: *Salix viminalis*, clone 78021, and *Salix dasyclados*, clone 81090. Biometrical measurements were carried out in parallel in the two stands, but as radiation measuring equipment

Figure 3.1: Willow coppice at Tartu Observatory on 18 August 1995.

required more effort to relocate, radiation measurements were carried out in one stand for a month or two before the equipment was moved to the other stand.

At the end of 1993, all shoots were cut at the height of 0.1 m and the first growing year began in the middle of May 1994. At the end of 1997, the shoots were cut again, and 1998 was the first growing year of a new coppice.

As *S. dasyclados* was severely damaged by pests in 1998, more radiation data are available for *S. viminalis*. The two species have significantly different stand structures—the leaves of *S. viminalis* are longer and narrower compared with the leaves of *S. dasyclados*, also, the stems of *S. dasyclados* are more convex and less vertical than the stems of *S. viminalis*. Thus, it might be possible to trace the differences in the radiation field measured inside the two stands back to the differences in stand parameters; however, as the number of measurements in the *S. dasyclados* coppice is insufficient, the current study is mainly concentrated on the radiation field within the *S. viminalis* stand.

During the first growing year (1994 and 1998), the stand structure was the simplest: the coppice consisted of nearly vertical stems with no branches and the number of parameters required to describe the coppice was at a minimum. At the beginning of the second growing year, branches sprouted from the apex of the first-year stem, making the architecture considerably more complex.

During the first year, the foliage could be described as a single 'cylindrical foliage layer', a layer of almost vertically oriented stem foliage cylinders, the number of stems per stool ranged from 2 to 16. The second-year stems sprouting from the apex of the first-year stem elongated and formed lateral branches, whose number varied between 1 and 8 (Ross and Ross, 1998). The uppermost parts of the most vigorous stems and branches formed the new upper cylindrical foliage layer.

The layer below the cylindrical layer that formed at the beginning of the second foliated season consisted of leaves and small branches located on the stems. This layer can more accurately be described as a turbid medium as the canopy was completely closed. The bottom canopy layer was almost leafless and consisted of nearly vertical first-year stems. Below the dense willow canopy, undergrowth was sparse.

For a more detailed description of the first growth cycle of the *S. viminalis* coppice, see (Ross and Ross, 1998).

3.2   Leaf shape and area

The length, maximum width, and area of *S. viminalis* and *S. dasyclados* leaves were measured with a CI-203 Area Meter, CID, Inc. in July and August 1996. In total, about 3000 *S. viminalis* and 1500 *S. dasyclados* leaves were measured.
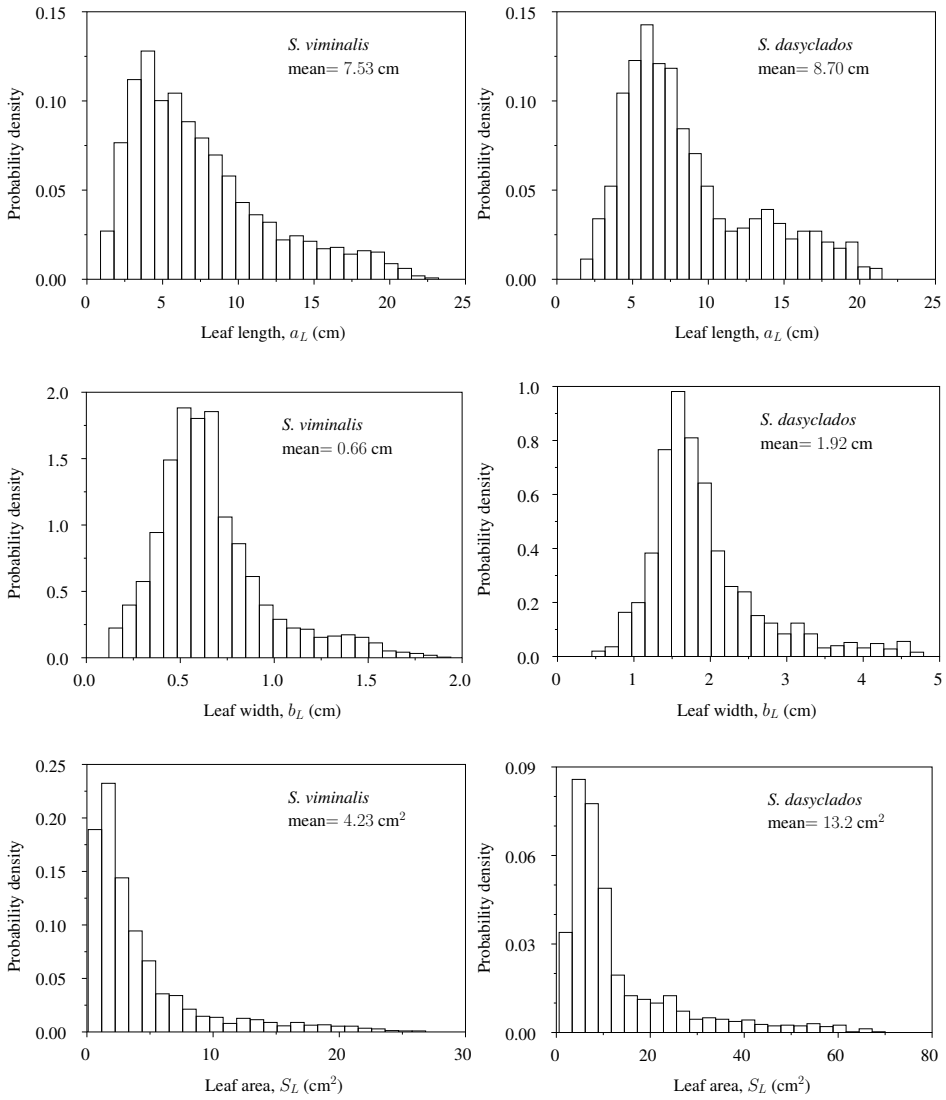
Figure 3.2: Distribution of leaf width, length and area for *S. viminalis* and *S. dasyclados.*

Table 3.1: Statistical parameters of the leaves of *S. viminalis* and *S. dasyclados*.

	Mean value	Standard deviation	min	max
S. viminalis				
Leaf length, a_L (mm)	75.2	45.6	9	232
Leaf max. width, b_L (mm)	6.6	2.9	1.2	19
Leaf area, S_L (mm^2)	423	465	10	2684
S. dasyclados				
Leaf length, a_L (mm)	87.0	43.9	16	215
Leaf max. width, b_L (mm)	19.1	7.3	4.5	48
Leaf area, S_L (mm^2)	1317	1290	60	7000

Additionally, the areas of some leaves were measured using an ordinary document scanner: leaves were scanned as black and white images and their areas were determined by counting black pixels in the image. The difference between the leaf areas obtained using the two techniques were very small.

The histograms of the distributions of leaf length, (maximum) width, and area are shown in Figure 3.2, some basic distribution parameters are given in Table 3.1.

Leaf length a_L and width b_L, and leaf length a_L and area S_L were strongly correlated,

$$b_L = 0.0564a_L + 0.238, R^2 = 0.76; \quad S_L = 0.0482a_L^2 + 0.499, R^2 = 0.94 \tag{3.1}$$

for *S. viminalis*, and

$$b_L = 0.153a_L + 0.583, R^2 = 0.85; \quad S_L = 0.131a_L^2 + 0.780, R^2 = 0.96 \tag{3.2}$$

for *S. dasyclados*. Regression formulae without an offset can also be constructed:

$$b_L = 0.0796a_L; \quad S_L = 0.0508a_L^2 \tag{3.3}$$

for *S. viminalis*, and

$$b_L = 0.207a_L; \quad S_L = 0.135a_L^2 \tag{3.4}$$

for *S. dasyclados*.

The leaves of *S. viminalis* were smaller and narrower than the leaves of *S. dasyclados*, for obtaining the same LAI, the number of *S. viminalis* leaves had to be about three times larger.
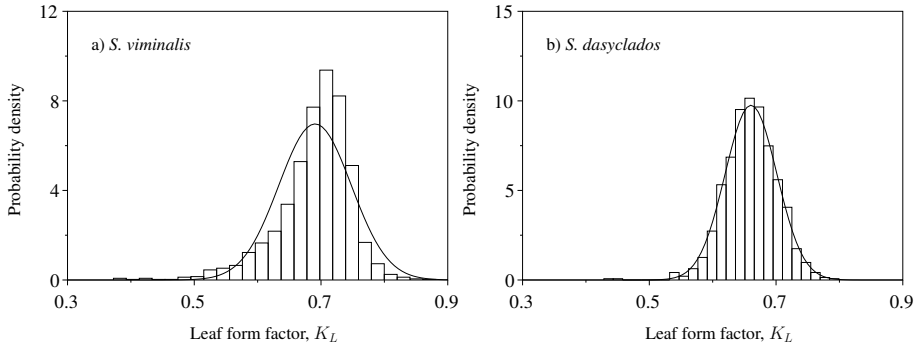
Figure 3.3: Measured leaf form factors for a) *S. viminalis* and b) *S. dasyclados* fitted with the normal distribution.

	Mean	Std. deviation
S. viminalis	0.691	0.057
S. dasyclados	0.661	0.041

The measurable dimensions of leaves exhibited large variations. Usually, the standard deviation equaled about one half of the measured quantity, the standard deviation of the area of a *S. viminalis* leaf even exceeded the mean value (Table 3.1). A more stable characteristic of the leaf is its form factor K_L defined by the formula for calculating leaf area

$$S_L = K_L a_L b_L, \tag{3.5}$$

(Kvet and Marshall, 1971; Ross, 1981). According to Sinoquet and Andrieu (1993), for many species, the form factor varies between 0.61 and 0.81. The measured form factors are shown in Figure 3.3, the average value of the form factor was 0.69 for *S. viminalis* and 0.66 for *S. dasyclados*.

From Figure 3.3 it may be concluded that K_L is a species-specific parameter that has a most probable value with a certain amount of natural dispersion as its measurements can be well fitted by the normal distribution; the mean values for the two *Salix* species distribution were significantly different ($p < 0.01$).

The geometric properties of the leaves of *S. viminalis* were also studied by Verwijst and Wen (1996). Their results were similar to those reported in this work: form factor $K_L = 0.74$, and R^2 value for the correlation between a_L and S_L was somewhat higher, $R^2 = 0.998$. Although Verwijst and Wen (1996) also reported that the relation between the product $a_L b_L$ and S_L was intrinsically nonlinear, the linear model performed superbly and could be applied without hesitation; mea-

surements at Tartu Observatory also showed no correlation between leaf area and form factor.

The difference between the leaf form factor of *S. viminalis* calculated as the slope of the regression line of S_L on $a_L b_L$ from Tõravere measurement data and that calculated by Verwijst and Wen (1996) is statistically significant ($p < 0.01$), indicating genetic differences or differences in growing conditions.

The basic geometrical properties of willow leaves described above were used for modeling the plant canopy. Mõttus et al. (2002) proposed the following function for modeling the shape of a simple narrow leaf:

$$f_L(x, \beta, a_L, b_L) = \pm \frac{b_L}{2}\left(1 - \beta\frac{x}{a_L}\right)\left[\frac{x}{a_L} - \left(\frac{x}{a_L}\right)^2\right]^{\beta} v(\beta), \qquad (3.6)$$

where the parameter β ($0 \le \beta \le 1$) describes leaf shape and $v(\beta)$ is a characteristic function. To apply the function, the x-axis has to be directed along the leaf midrib from the leaf insertion point and the positive and negative values of the function f_L draw the blade of the leaf: $|f_L(x, \beta, a_L, b_L)|$ is the half-width of the leaf at the distance x along its midrib.

Despite the apparent complexity of Eq. 3.6, it contains only three independent variables. Two of these variables, a_L and b_L, can be measured directly, and the shape parameter β is a unique function of the form factor K_L. The characteristic function $v(\beta)$ is required for normalization, it is defined using the equality

$$
\begin{aligned}
\frac{b_L}{2} &= f_L(x_{max}, \beta, a_L, b_L) \\
&= \frac{b_L}{2}\left(1 - \beta\frac{x_{max}}{a_L}\right)\left[\frac{x_{max}}{a_L} - \left(\frac{x_{max}}{a_L}\right)^2\right]^{\beta} v(\beta), \qquad (3.7)
\end{aligned}
$$

where x_{max} is the position of maximum leaf width. From Eq. 3.7 it follows that

$$v(\beta) = \left(1 - \beta\frac{x_{max}}{a_L}\right)^{-1}\left[\frac{x_{max}}{a_L} - \left(\frac{x_{max}}{a_L}\right)^2\right]^{-\beta}. \qquad (3.8)$$

The value of the first derivative of Eq. 3.6 with respect to x at the point $x = x_{max}$ has to equal zero; from this condition it can be found that

$$x_{max} = a_L\frac{2 + \beta - \sqrt{5 - 2\beta + \beta^2}}{2(1 + 2\beta)}. \qquad (3.9)$$

Substituting the previous equation into Eq. 3.8 gives

$$v(\beta) = \frac{2^{1+\beta}(1 + 2\beta)^{1+2\beta}}{\left(2 + \beta - \beta^2 + \beta u(\beta)\right)\left(\beta^2 + 5\beta - 4 + (1 - \beta)u(\beta)\right)^{\beta}}, \qquad (3.10)$$
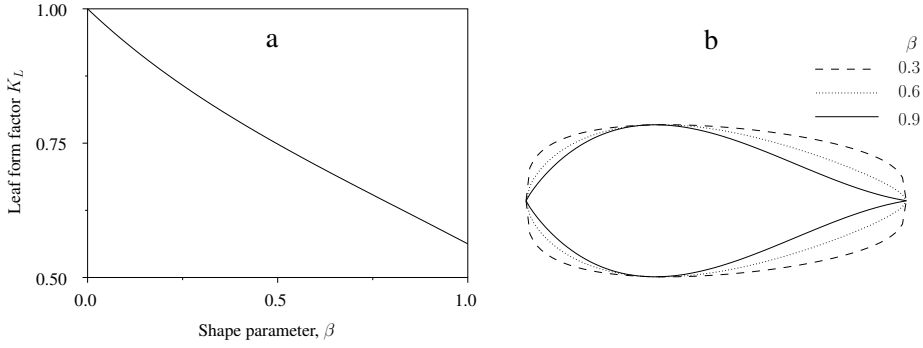
26

Figure 3.4: a) dependence of the form factor K_L on the shape parameter β, b) various leaf shapes obtained by modifying the shape parameter β.

where $u(\beta) = \sqrt{5 - 2\beta + \beta^2}$.

Integration of Eq. 3.6 yields for the leaf area

$$S_L = a_L b_L v(\beta) \left[B(1 + \beta, 1 + \beta) - \beta B(2 + \beta, 1 + \beta) \right], \qquad (3.11)$$

where $B(p, q) = \int_0^1 u^{p-1} (1 - u)^{q-1} du$ is the beta-function.

Thus, all parameters in Eq. 3.6 can be obtained from measurements. The leaf form factor K_L as a function of the parameter β is shown in Figure 3.4. The dependence of K_L on β is quasilinear, and to further simplify calculations, a linear approximation can be used without compromising accuracy. But as the parameter β can vary only between 0 and 1, the form factor K_L varies between $\frac{9}{16} = 0.56$ and 1. This means that the parameter β can not be determined for all measured *S. viminalis* leaves (Figure 3.3), but the range $[0.56, 1]$ suits most measured leaves as well as leaves of many other species.

A few leaf blades together with the shape calculated using Eq. 3.6 are depicted in Figure 3.5 and a quantitative description of these leaves is given in Table 3.2.

The increased mathematical complexity is the cost of keeping the number of parameters at the lowest possible value and of retaining physical interpretation of the parameters. Decreasing the number of parameters leads to a fixed leaf form factor (e.g. ellipses, squares, or triangles); further increasing independent variables introduces more undetermined parameters to the formula. For example, Bonhomme and Varlet-Grancher (1978), Prevot and Brunet (1993), Ivanov et al. (1995), Fournier and Andrieu (1998), and España et al. (1999b) used polynomials to describe the contour of the leaf, using a larger number of parameters.

Although Eq. 3.6 does not account for leaf curvature, non-flat leaves can be modeled if the shape function is plotted (in a local coordinate system) on a non-
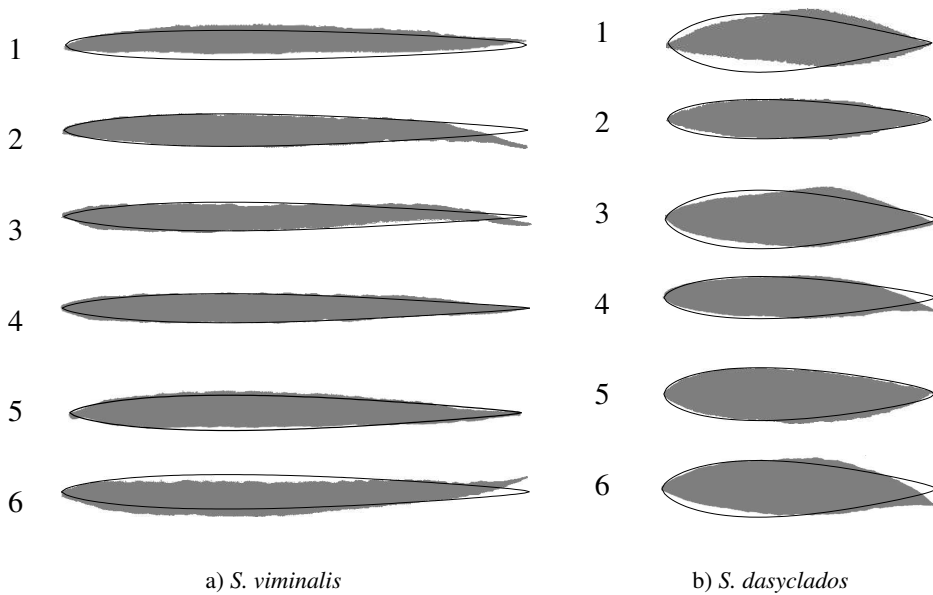
a) *S. viminalis*   b) *S. dasyclados*

Figure 3.5: Leaf blades and fitted shape functions for a) *S. viminalis* and b) *S. dasyclados* leaves; leaf lengths are normalized. Properties of the leaves are summarized in Table 3.2.

Table 3.2: Some measured characteristics of the leaves depicted in Figure 3.5.

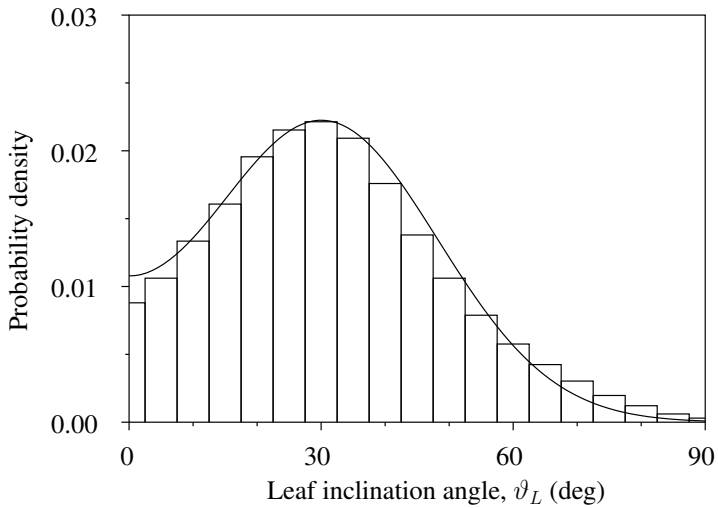| leaf number	1	2	3	4	5	6
a) *S. viminalis*						
length, mm	141	169	205	216	197	204
width, mm	9	12	13	14	16	16
area, mm^2	950	1420	1770	1960	2080	2290
form factor	0.748	0.698	0.666	0.647	0.681	0.590
b) *S. dasyclados*						
length, mm	72	107	97	122	143	145
width, mm	16	16	21	19	28	30
area, mm^2	760	1240	1390	1630	2900	3020
form factor	0.656	0.724	0.681	0.703	0.725	0.695

Figure 3.6: Measured and modeled leaf inclination angles. 0° denotes a horizontal leaf.

flat surface, although data for constructing such a surface realistically is difficult to obtain.

3.3   Leaf inclination

The distribution of leaf inclination angles of *S. viminalis* was measured on three days in 1994 and 1995 (Ross and Ross, 1998). As the measured distributions were similar, the results were added.

The measured distribution of the inclination angles of leaf laminae is shown in Figure 3.6. Leaves were divided into a number of inclination angle classes; larger non-flat leaves were cut into pieces and contributed to several classes. An inclination angle of 0° denotes a horizontal leaf and an inclination angle of 90° a vertical one.

As can be seen in Figure 3.6, willow leaves were mostly close to horizontal with the preferred inclination angle of about 30°. But the inclination angle measured in the way described above does not adequately describe leaf orientation, even if leaf azimuth angle is ignored: this method does not discriminate between upward- and downward tilting leaves and Figure 3.6 gives just the distribution of the absolute value of leaf inclination angle.

To solve this problem, the most probable inclination angle was estimated as 30° with leaves tilted upwards. This assumption was based on a visual observation of the natural *S. viminalis* canopy. The measured distribution was then
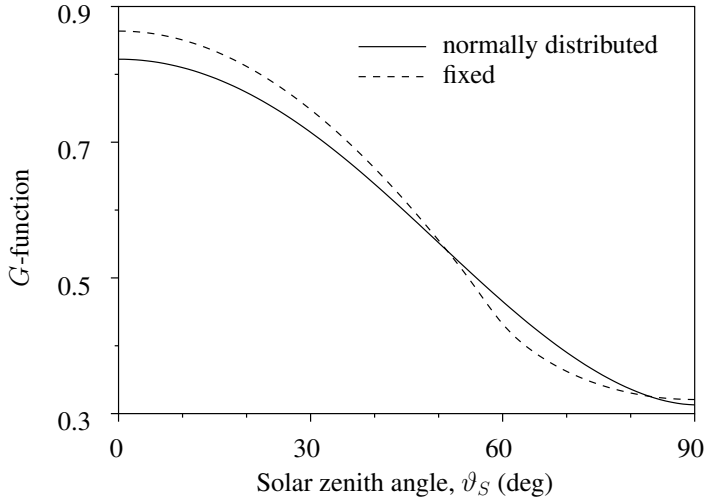
Figure 3.7: The effect of two models of leaf inclination on the mean projection of unit foliage area on the plane normal to the direction of direct solar radiation (G-function, Eq. 2.6). Normally distributed: leaf inclination angles are distributed normally with $\langle \vartheta_L \rangle = 30.3°$ and $\sigma_{\vartheta_L} = 18.0°$; fixed: leaves have a fixed inclination angle of $30.3°$.

fitted by the normal distribution, assigning a negative inclination angle to downward tilted leaves. The distribution of the absolute value of leaf inclination angle was then calculated by adding the contribution of negative inclination angles, the result is shown in Figure 3.6 superimposed on the measured histogram. The parameters of the fitted normal distribution are: mean $30.3°$ (0.528 rad) and standard deviation $18.0°$ (0.314 rad).

This leaf inclination model assumes that the adaxial surface of the leaf was always facing upward, and thus all leaf normals were in the upper hemisphere. Although some leaves were inverted in a natural canopy, i.e. their abaxial surfaces were facing upward, their fraction was small and this simplification did not cause considerable errors.

Two other models of leaf inclination are used in this work besides the one described above. As a simplification of the normal distribution, leaf inclination angles are taken fixed at the most probable value, $30.3°$; and a completely isotropic model is also used, where leaves have no directional preferences. For the isotropic model, the mean projection of unit foliage area on the plane normal to the direction of direct solar radiation, $G(\vartheta_S)$, equals 0.5 (Eq. 2.6); dependence of G on the solar zenith angle ϑ_S for the other two leaf inclination models is shown in Figure 3.7.

For leaves with the fixed zenith angle of leaf normal ϑ_L^0 and uniformly distributed azimuths (dashed line in Figure 3.7) an analytical formula for $G(\vartheta_S)$ can be given. Integration of Eq. 2.6 yields

$$
G(\vartheta_S) = \begin{cases} \cos \vartheta_L^0 \cos \vartheta_S, & \vartheta_S \leq \frac{\pi}{2} - \vartheta_L^0 \\ \frac{\pi - 2\phi_{L,cr}}{\pi} \cos \vartheta_L^0 \cos \vartheta_S + \\ \quad + \frac{2}{\pi} \sin \phi_{L,cr} \sin \vartheta_L^0 \sin \vartheta_S, & \vartheta_S > \frac{\pi}{2} - \vartheta_L^0 \end{cases} , \qquad (3.12)
$$

where

$$
\phi_{L,cr} = \arccos \left(\cot \vartheta_L^0 \cot \vartheta_S \right). \qquad (3.13)
$$

Due to the symmetry of the models, G is a function of the solar zenith angle ϑ_S only and is independent of the azimuth angle. Eq. 3.12 is equivalent to Eqs. 6e and 6f in (Nilson, 1971).

3.4 Distribution of foliage along the shoot stem

To describe the distribution of leaf area along the shoot stem, the shoot was divided into 20 or 30 cm sections and the fresh or dry mass of leaves of each section was measured. Using the measured values of leaf mass (fresh or dry) per unit leaf area, these weights were turned into the density of leaf area per unit stem length. The density was then normalized by dividing it by the total leaf area of the shoot.

As an illustration, some of measured normalized leaf area densities are plotted in Figure 3.8 as functions of relative distance from shoot tip. Measured data for two years are shown, both will be used later in modeling the radiation field inside the willow stand.

Figure 3.8a describes the willow coppice at the end of the first growing year. Eight shoots with lengths between 1.95 and 2.80 m were measured. The shape of the leaf area density curve is similar to that in Figure 8c in Ross and Ross (1998) where leaf area density is given at the end of the foliated season of 1994; both 1998 and 1994 were the first growing years of the willow coppice. The leaf area density curve shows a distinct maximum near the tip of the shoot where the youngest and largest leaves are located.

Figure 3.8b sums up the year 1995 that was the second growing year. Measurements of the distribution of leaf area along the shoot stem were made on 6 days and a total 74 shoots with lengths between 1.10 and 3.50 m were measured.

For modeling purposes, the measured leaf area density was fitted by a polynomial. For 7 September 1998 (Figure 3.8a), a fifth order polynomial was used:

$$
S_L^C = \begin{cases} 32.5x - 175x^2 + 400x^3 - 426x^4 \\ \quad + 170x^5, & 0 < x < 0.78 \\ 0, & x > 0.78 \end{cases} , \qquad (3.14)
$$
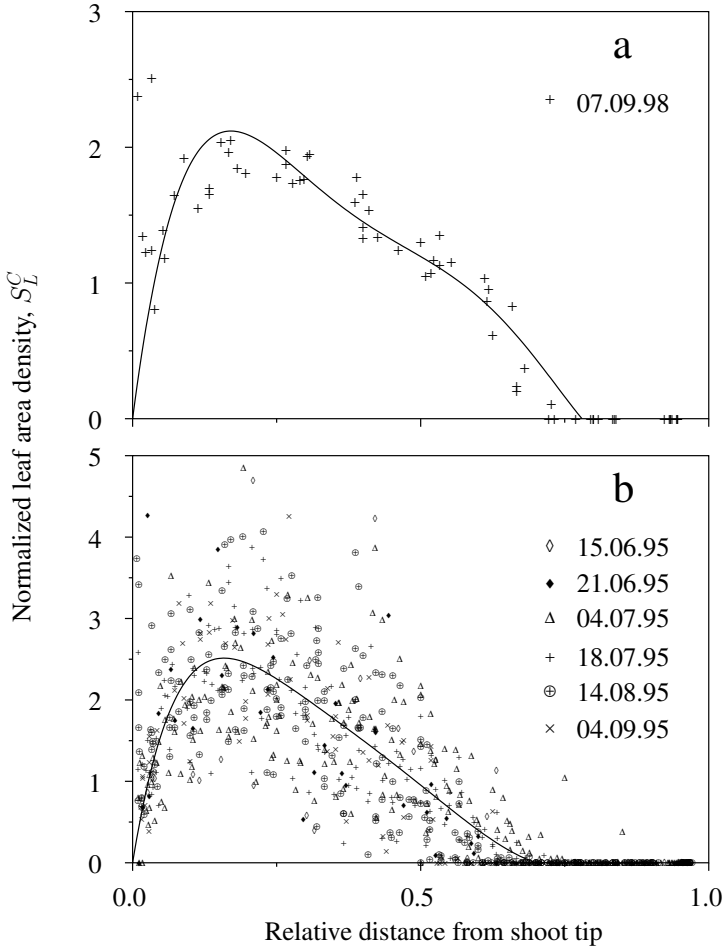
Figure 3.8: Distribution of leaf area along the shoot axis: a) September 1998, b) various days in 1995; *S. viminalis.*

where S_L^C is the normalized leaf area density and x is the relative distance from shoot tip. For the year 1995 (Figure 3.8b), the following 6th order polynomial was used:

$$S_L^C = \begin{cases} 43.5x - 273x^2 + 804x^3 - 1294x^4+ \\ \quad +1066x^5 - 347x^6, & 0 < x < 0.70 \\ 0, & x > 0.70 \end{cases} . \quad (3.15)$$

Eqs. 3.14 and 3.15 are normalized so that $\int_0^1 S_L^C dx = 1$.

The number of leaves on each measured section of the shoot stem was also recorded. Measurement results for 28 July 1994 and 7 September 1998 are shown
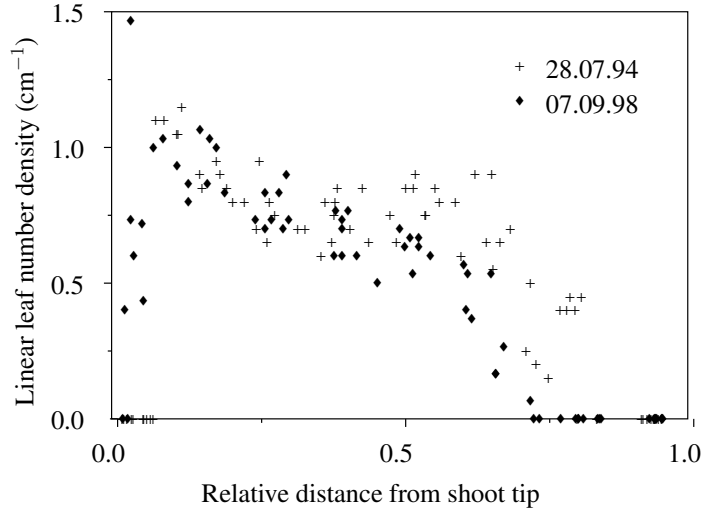
Figure 3.9: Number of leaves per unit stem length as measured on 28 July 1994 and 7 September 1998.

in Figure 3.9. The linear leaf number density was not constant but varied with the relative location of the leaf on the shoot. Consistently with Figure 3.8, no leaves were attached to the lower part of the shoot. For the rest of the shoot, linear leaf number density was almost constant. For modeling purposes, the fractional length of the lower, leafless part of the shoot was taken from the modeled leaf area distribution (Eqs. 3.14 and 3.15).

For 28 July 1994, the mean linear leaf number density in the upper part of the shoot was 55.1 leaves per meter, or 0.557 cm^{-1}. On 7 September 1998, the number of leaves was 61.7 m^{-1}.

3.5   Dependence of shoot leaf area on shoot length

The total leaf area of a shoot as a function of its length is one of the most basic characteristic of the willow stand. Knowing it and counting the number of shoots makes it possible to calculate LAI, as destructive LAI measurement near the radiation measurement site is unconceivable. The shoots of a one-year-old coppice start from the ground, for later growing years the shoot cylinders start from a previous-year stem. The results of shoot leaf area measurements are plotted against shoot length in Figure 3.10.
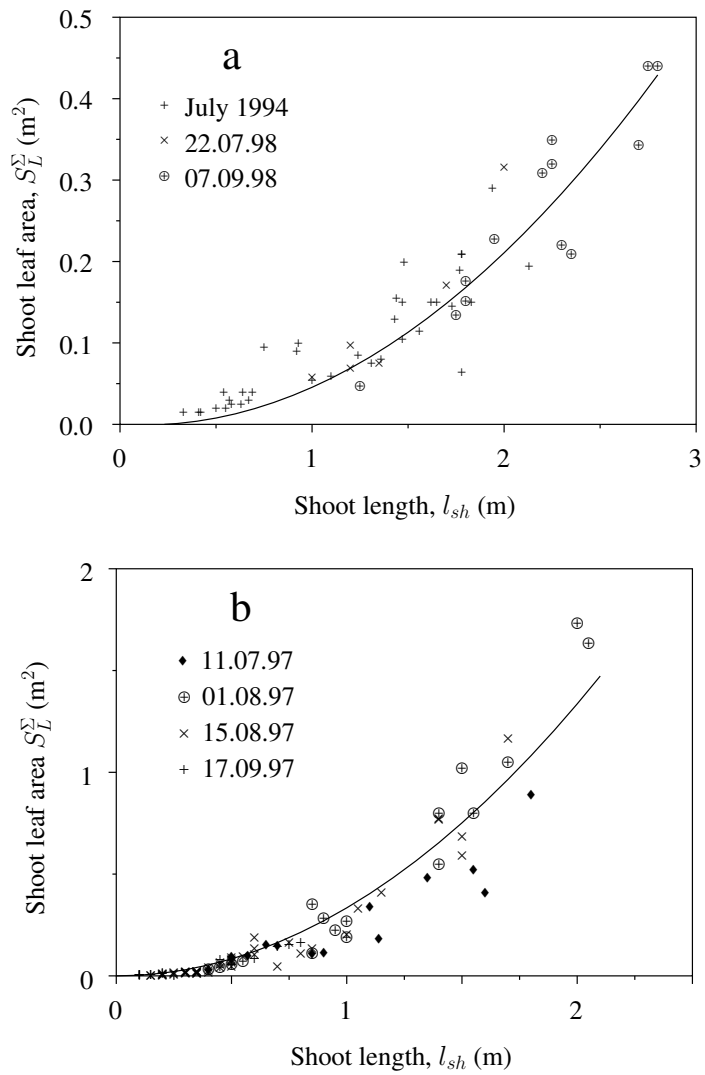
Figure 3.10: Dependence of shoot leaf area on shoot length. Measured during a) the first and b) the fourth growing year in the *S. viminalis* coppice.

The dependence of shoot leaf area on shoot length is clearly nonlinear: longer shoots have more leaf area per unit length than shorter shoots. The solid lines in Figure 3.10 are the regression curves

$$S_L^\Sigma = 0.334 l_{sh}^2 \qquad (3.16)$$

and

$$S_L^\Sigma = -0.0144 l_{sh} + 0.060 l_{sh}^2, \quad l_{sh} > 0.24, \qquad (3.17)$$

where the shoot length l_{sh} is measured in meters and the shoot leaf area S_L^Σ in square meters, calculated for 1997 and 1998, respectively.

Both 1994 and 1998 were the first growing year for the stand. It is noteworthy that although the coppice was more than twice higher at the end of the unusually warm and wet summer of 1998 compared with the end of the summer of 1994, the dependence of shoot area on shoot length was similar for the two years (Figure 3.10a).

3.6 Distribution of shoot length and shoot base height

If the dependence of shoot area on shoot length is known and the number of shoots is counted, only a measurement of the distribution of shoot length is needed to calculate LAI. The results of such measurements carried out in the *S. viminalis* coppice are summarized in Figure 3.11a,b for two days, 14 July 1997 and 9 September 1998. The distributions are noticeably different: the one-year-old coppice in Figure 3.11b is dominated by taller shoots with lengths approximately equally distributed in the interval from 1 to 3 meters. In a several-years-old coppice (Figure 3.11a), a large number of short shoots has sprouted from previous-year stems.

To find out not only the value of LAI, but also the downward cumulative leaf area index $L(z)$ (Eq. 2.2), or, equivalently, the leaf area density $u_L(z)$ (Eq. 2.1) for the year 1998, only the knowledge of the distribution of leaf area along the shoot stem and the distribution of stem inclination angle is required. Modeling the former by Eq. 3.15 and taking the latter equal to the delta function δ(shoot inclination $- 0$), i.e. assuming all shoots were vertical, gives realistic values for $L(z)$ and $u_L(z)$; results are shown in Figure 3.12. Assuming that all shoots were vertical does not cause a large error since the distribution is narrowly peaked around the vertical orientation (Ross and Ross, 1998).

For 1997, when not all shoots started from the ground, the distribution of shoot base height (Figure 3.11c) and the relation between shoot height and shoot base height (Figure 3.11c) has to be considered; the modeled $L(z)$ and $u_L(z)$ are shown in Figure 3.12. The distribution of leaf area on the shoot was not measured in 1997, so the approximation formula for 1995 (Eq. 3.15) was used.
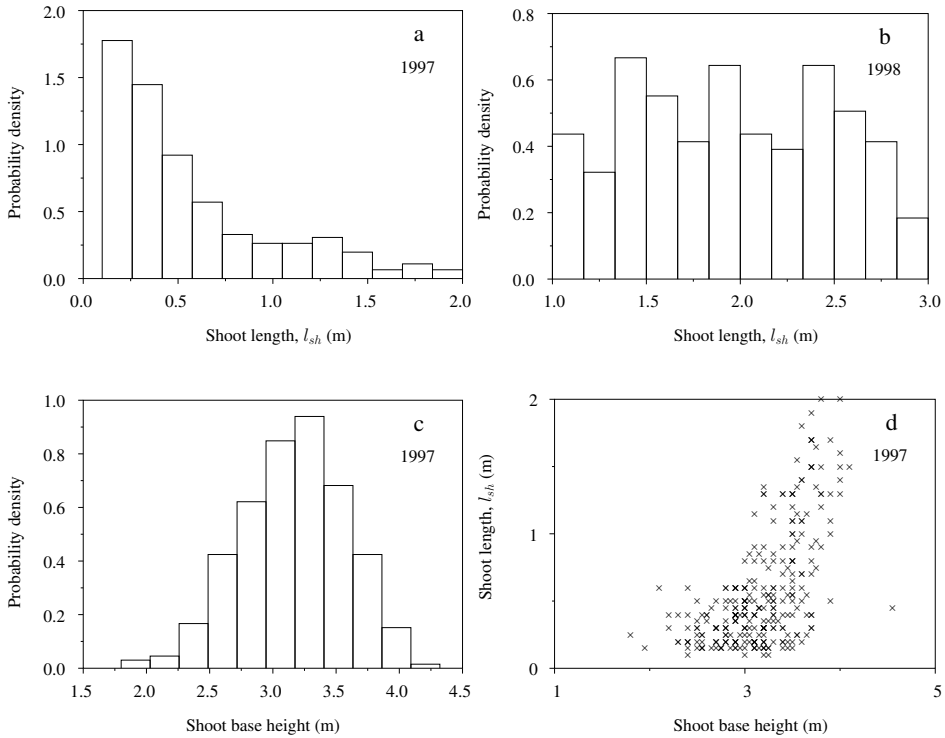
Figure 3.11: a) Distribution of shoot length on 14 July 1997; b) distribution of shoot length on 9 September 1998; c) distribution of shoot base height on 14 July 1997; d) dependence of shoot length on shoot base height on 14 July 1997. All measurements were made in the radiation measurement area in the *S. viminalis* stand and were used to estimate LAI for modeling radiative transfer.

The dependence of u_L on z in Figure 3.12 is not very smooth as it was calculated from unfitted distributions of shoot height and shoot base height. The values of $L(z)$ and $u_L(z)$ obtained in this manner are not valid for the whole coppice as only measurements made near the radiation measurement system were taken into account.

Figure 3.12: Downward cumulative leaf area index $L(z)$ (Eq. 2.2) and leaf area density $u_L(z)$ (Eq. 2.1) of the *S. viminalis* stand calculated by converting the shoot height distributions in Figure 3.11 into shoot areas using Eqs. 3.16 and 3.17 for 14 July 1997 and 9 September 1998, respectively.

4   RADIATION MEASUREMENTS

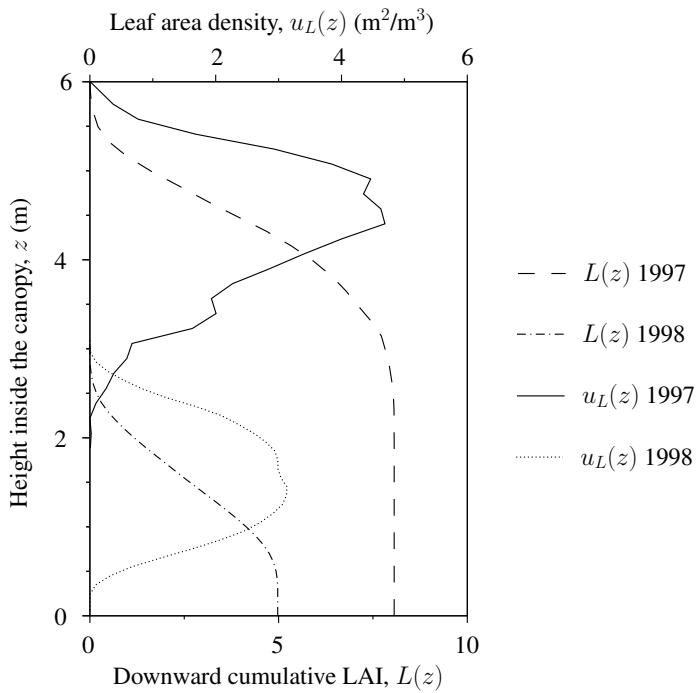A special measurement system was designed for the experimental study of the variability of radiation characteristics within the willow coppice (Ross et al., 1998). The measurement system consisted of a 6-meter long horizontal bar placed perpendicularly to the rows inside the willow plantation with a sensor carriage moving along it at 30 mm s^{-1}. Two Reemann pyranometers (TR-3) for measuring downward and upward fluxes of global radiation, two LI-COR quantum sensors (LI-190SA) for measuring downward and upward fluxes of photosynthetically active radiation (PAR), a miniature Reemann net radiometer (MB-1) for measuring net radiation, and a sunfleck indicator for detecting sunfleck and umbra were mounted on the carriage (Figure 4.1).

The height of the horizontal bar carrying the sensor carriage inside coppice could be changed from 0.4 to 6 m. One measurement scan consisted of a transit of the carriage perpendicular to willow rows from one end of the bar to the other and back with a total scan length of about 12 m. Because of leaf flutter caused by the wind, the data obtained from the two transits were not identical; to increase the statistical reliability of the sample, the data from the two transits were considered as one measurement. The scan took about 6 minutes to complete.

Depending on the time constant of the instrument, the number of measurements varied: the sampling interval for the slower thermoelectric instruments, the two pyranometers and the net radiometer, was longer, and only up to 400 measurements were made during each scan. The distance between two consecutive measurements with the more responsive instruments making about 2000
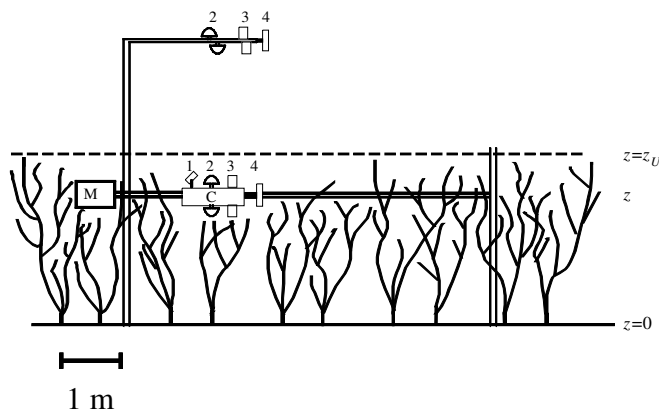

Figure 4.1: Radiation measurement system inside the willow coppice. M – drive, C – carriage, 1 – sunfleck indicator, 2 – pyranometer, 3 – quantum PAR sensor, 4 – net radiometer.

Figure 4.2: Photo of the sensor carriage inside the *S. viminalis* coppice.

measurements during a scan, the two quantum PAR sensors and the sunfleck indicator, was about 6 mm.

The sunfleck indicator used for measuring direct solar radiation was, in principle, a miniature actinometer, consisting of a collimating tube and a silicon detector. The collimator tube was manually directed towards the Sun at the beginning of each scan. The field of view of the instrument was 10° in the vertical direction and 15° in the horizontal direction, the receiving area of the photodiode was limited by a round diaphragm with a diameter of 1 mm. Such an angle of view guaranteed that the Sun remained completely in the field of view for 6 minutes, the accuracy of determination of the linear dimensions of sunflecks and umbrae was ±5 mm.

Although the sunfleck indicator was originally designed for detecting unobstructed sunlight and umbra, the response of the silicon photodiode used in the sunfleck indicator can be considered linear with the intensity of incident radiation. Thus, an approximate calibration was applied to the sunfleck indicator by comparing its output voltage with the actinometer reading when measuring above the canopy or in sufficiently long sunflecks. The largest errors in the calibration were due to the different spectral sensitivities of the instruments, the non-standard field of view and the bending of the aluminium bar under the weight of the carriage, i.e so the sensor was no longer pointed directly towards the Sun.

Concurrently with measurements inside the coppice, background measurements of upward and downward fluxes of both global and photosynthetically ac-

tive radiation were carried out; a Yanishevsky type actinometer AT-50 for recording global direct solar radiation and a phytoactinometer for recording direct PAR outside the coppice were mounted on a mechanical sun-tracker at a distance of about 30 m from the measuring site. The phytoactinometer is a specially constructed device for measuring direct PAR consisting of a LI-COR LI-190SA Quantum Sensor supplied with a view-limiting tube analogous to that of the Yanishevsky actinometer. The actinometer was regularly calibrated by comparison with the reference pyrheliometer of Tõravere Meteorological Station. For more information on the instrumentation for measuring direct solar radiation outside the willow coppice, see (Mõttus et al., 2001).

Data acquisition system consisted of a multi-channel data logger (Delta-T Devices) and a PC, recording data from all the sensors both inside and outside the canopy.

The measurements were carried out on different cloudless days during the whole growth period from June until October for solar zenith angle of 35–70° in the years 1995, 1996, 1997, 1998 and 1999. Simultaneously with radiation measurements, air temperature and humidity inside and outside the coppice, surface temperature beneath the coppice, and wind speed above the canopy were recorded.

5 QUANTITATIVE DESCRIPTION OF RADIATION FIELD

5.1 Intensity and radiation flux density

The theory of radiative transfer used in this work is based on the concepts of geometric optics. Effects like interference, diffraction and ray bending due to variations in the refraction index are ignored. The basic concept of geometric optics, and also the theory of radiative transfer, is a narrow ray of light, or the radiation pencil, whose energy is concentrated in a well-defined (infinitesimal) volume and that has a specific propagation direction. Polarization of light is also ignored here, although it is often used in describing the radiation regime of a plant canopy and can be incorporated into the classical theory of radiative transfer.

The spectral intensity of radiation or radiance is defined as the energy d^4E that has passed through a small surface dA propagating in a solid angle $d\Omega$ around a direction Ω in a time interval dt over a small increment of frequency $d\nu$,

$$I_\nu = \frac{d^4E}{\cos\vartheta\, dA dt d\Omega d\nu}, \qquad (5.1)$$

where ϑ is the angle between the direction Ω and the normal of the surface dA (Thomas and Stamnes, 1999). Intensity is a scalar quantity describing the angular variation of radiation flow and how this angular variation depends upon position.

To calculate the flow of radiative energy across a surface A located at some specific position, the contributions of angular beams have to be added. It is convenient to divide the flow into two oppositely directed positive energy flows into the two regions separated by the surface A.

As the beams do not interact, they may be treated separately and the total hemispherical flux, or the rate of radiative energy flow through the surface A within the small spectral range ν to $d\nu$ is just the integral

$$\Phi_\nu^+ = \frac{d^2E}{dt d\nu} = \int_A \left(\int_{2\pi+} I_\nu(\mathbf{r}) \cos\vartheta \, d\Omega \right) dA, \qquad (5.2)$$

where ϑ is the angle between the direction Ω and the normal of the surface dA, $\mathbf{r} \in A$ and '+' denotes integration over the hemisphere where $\cos\vartheta < 0$. A similar formula can be written for Φ_ν^-, integrated over directions where $\cos\vartheta > 0$. The net flux Φ_ν is defined as the difference of the two fluxes, $\Phi_\nu = \Phi_\nu^+ - \Phi_\nu^-$.

The second integral in Eq. 5.2 taken over the hemisphere $2\pi+$ denotes the radiation flux density, or irradiance, at the point $\mathbf{r}$,

$$F_\nu^+ = \frac{d\Phi_\nu^+}{dA} = \int_{2\pi+} I_\nu(\mathbf{r}) \cos\vartheta \, d\Omega. \qquad (5.3)$$

If the radiation field is isotropic, i.e. I_ν is constant over the whole hemisphere, Eq. 5.3 yields

$$F_\nu^+ = \int_{2\pi+} I_\nu \cos \vartheta d\mathbf{\Omega} = I_\nu \int_{2\pi+} \cos \vartheta \, d\mathbf{\Omega} = \pi I_\nu. \qquad (5.4)$$

Measured flux densities are always integrated over some frequency interval $\Delta\nu$ using the response curve characteristic of the receiving instrument, even when measuring in a narrow spectral interval. When measuring broadband radiation, e.g. direct or diffuse solar irradiance, the spectral composition of incident radiation has to be considered as the sensitivity of a sensor is rarely uniform in a wide spectral interval.

5.2 BRDF

The bidirectional reflectance distribution function (BRDF) for monochromatic radiation with the frequency ν is defined as the ratio of reflected intensity to the intensity of an infinitesimally narrow incident beam:

$$r(\nu, \mathbf{\Omega}', \mathbf{\Omega}) = \frac{dI_{\nu r}^+(\mathbf{\Omega})}{I_\nu^-(\mathbf{\Omega}') \cos \vartheta' d\mathbf{\Omega}'}, \qquad (5.5)$$

where $\mathbf{\Omega}'$ is the direction of incident radiation, $\mathbf{\Omega}$ is the direction of reflected radiation, $dI_{\nu r}^+(\mathbf{\Omega})$ is the intensity of reflected light leaving the reflecting surface within a cone of solid angle $d\mathbf{\Omega}$, I_ν^- is the incoming beam of radiation within a cone of solid angle $d\mathbf{\Omega}'$, and ϑ' is the angle between the surface normal and $\mathbf{\Omega}'$. Adding the contributions from all directions and using Eq. 5.5, the total reflected intensity is

$$I_{\nu r}^+(\mathbf{\Omega}) = \int_{2\pi-} dI_{\nu r}^+(\mathbf{\Omega}) = \int_{2\pi-} \cos \vartheta' r(\nu, \mathbf{\Omega}', \mathbf{\Omega}) I_\nu^-(\mathbf{\Omega}) d\mathbf{\Omega}'. \qquad (5.6)$$

Analogously to BRDF (Eq. 5.5), the bidirectional transmittance function can be defined:

$$t(\nu, \mathbf{\Omega}', \mathbf{\Omega}) = \frac{dI_{\nu t}^-(\mathbf{\Omega})}{I_\nu^-(\mathbf{\Omega}') \cos \vartheta' d\mathbf{\Omega}'}, \qquad (5.7)$$

where $dI_{\nu t}^-(\mathbf{\Omega})$ is the intensity of transmitted light leaving the surface within a cone of solid angle $d\mathbf{\Omega}$.

Generally, BRDF described by Eq. 5.5 is a function of both incidence and observation angles. If the reflected intensity is completely uniform regardless of the direction of incidence, i.e.

$$r(\nu, \mathbf{\Omega}', \mathbf{\Omega}) = r_L(\nu), \qquad (5.8)$$

the surface is said to be a Lambert (or Lambertian) surface. The reflected intensity is then simply (using Eq. 5.6)

$$I_{\nu L}^+ = \int_{2\pi-} r_L(\nu) \cos \vartheta' I_\nu^-(\mathbf{\Omega}) d\mathbf{\Omega}' = r_L(\nu) F_\nu^-, \tag{5.9}$$

and the reflected flux (using Eq. 5.4)

$$F_{\nu L}^+ = r_L(\nu) \int_{2\pi+} I_{\nu L}^+ \cos \vartheta d\mathbf{\Omega} = \pi r_L(\nu) F_\nu^- = R(\nu) F_\nu^-, \tag{5.10}$$

where $R(\nu) = \pi r_L(\nu)$ is the (spectral) albedo of the Lambertian surface.

5.3 Equation of radiative transfer

The differential equation describing the first component of the Stokes vector, intensity I (Eq. 5.1, index ν is dropped for simplicity, all equations in this subsection apply to monochromatic radiation) in a horizontally homogeneous scattering and absorbing medium can be written as

$$-\mu \frac{\partial I(z, \mathbf{\Omega})}{\partial z} + \sigma(z, \mathbf{\Omega}) I(z, \mathbf{\Omega}) = \int_{4\pi} I(z, \mathbf{\Omega}') \sigma_s(z, \mathbf{\Omega}' \to \mathbf{\Omega}) d\mathbf{\Omega}' + Q(z, \mathbf{\Omega}),$$

$$\tag{5.11}$$

where $\mu = \cos \vartheta$ is the cosine of the polar angle of photon travel direction ($\mu < 0$ denotes a downward traveling photon), $\mathbf{\Omega}$ is the direction of photon travel, σ is the interaction cross-section, $\sigma_s(z, \mathbf{\Omega}' \to \mathbf{\Omega})$ is the differential scattering cross-section from $\mathbf{\Omega}'$ into a solid angle of $d\mathbf{\Omega}$ around the direction $\mathbf{\Omega}$, z is the vertical coordinate and $Q(z, \mathbf{\Omega})$ is the source function (Chandrasekhar, 1960; Knyazikhin and Marshak, 1991).

The total interaction cross-section σ is defined as the sum of absorbing and scattering cross-sections, $\sigma = \sigma_a' + \sigma_s'$. The absorbing cross-section σ_a is defined so that the probability of a photon being absorbed while traveling the distance ds is

$$p_a(z, \mathbf{\Omega}) = \sigma_a'(z, \mathbf{\Omega}) ds. \tag{5.12}$$

A similar relation holds between the scattering cross-section σ_s' and the probability p_s of a photon being scattered; additionally, directional dependence of the scattering direction is described by introducing the differential scattering cross-section σ_s with the normalization

$$\int_{4\pi} \sigma_s(z, \mathbf{\Omega}' \to \mathbf{\Omega}) d\mathbf{\Omega} = \sigma_s'(z, \mathbf{\Omega}) ds = p_s(z, \mathbf{\Omega}). \tag{5.13}$$

When dealing with shortwave (visible and near-infrared wavelengths) radiation in plant canopies, the source term $Q(z, \mathbf{\Omega}) = 0$ and the interaction cross-section σ depends on foliage area density and leaf orientation:

$$\sigma(z, \mathbf{\Omega}) = G(z, \mathbf{\Omega})u_L(z), \tag{5.14}$$

where $G(z, \mathbf{\Omega})$, the mean projection of unit foliage area on the plane normal to direction of photon travel, is defined by Eq. 2.6 and $u_L(z)$ is the one-sided leaf area density defined by Eq. 2.1.

In phytoactinometric investigations it is customary to use the area scattering phase function $\frac{1}{\pi}\Gamma(z, \mathbf{\Omega}' \to \mathbf{\Omega})$ which is defined by the relation

$$\frac{1}{\pi}\Gamma(z, \mathbf{\Omega}' \to \mathbf{\Omega}) = \frac{1}{4\pi}\int_{4\pi} g_L(z, \mathbf{\Omega}_L)\left|\mathbf{\Omega}' \cdot \mathbf{\Omega}_L\right|\gamma_L(z, \mathbf{\Omega}_L, \mathbf{\Omega}' \to \mathbf{\Omega})d\mathbf{\Omega}_L,$$
$$\tag{5.15}$$

where $\frac{1}{4\pi}g_L(z, \mathbf{\Omega}_L)$ is the probability density function of leaf normal distribution (Eq. 2.5), $\mathbf{\Omega}_L$ is the direction of the leaf outward normal and $\gamma_L(z, \mathbf{\Omega}_L, \mathbf{\Omega}' \to \mathbf{\Omega})$ is the leaf scattering phase function characterizing the fraction of intercepted energy from photons initially traveling in direction $\mathbf{\Omega}'$ that are scattered after an interaction with a leaf with the outward normal $\mathbf{\Omega}_L$ into a unit solid angle around the direction $\mathbf{\Omega}$. The differential scattering cross-section σ_s can be written for plant canopies as

$$\sigma_s(z, \mathbf{\Omega}' \to \mathbf{\Omega}) = \frac{1}{\pi}\Gamma(z, \mathbf{\Omega}' \to \mathbf{\Omega})u_L(z). \tag{5.16}$$

Also, instead of the vertical coordinate z, the downward cumulative leaf area index $L(z)$ (Eq. 2.2) is used.

Thus, the equation of radiative transfer in plant canopies is usually written as

$$-\mu\frac{\partial I(L, \mathbf{\Omega})}{\partial L} + G(\mathbf{\Omega})I(L, \mathbf{\Omega}) = \frac{1}{\pi}\int_{4\pi} I(L, \mathbf{\Omega}')\Gamma(\mathbf{\Omega}' \to \mathbf{\Omega})d\mathbf{\Omega}', \tag{5.17}$$

where, as in Section 2.2, the dependence of canopy characteristics on the height z is ignored.

To solve the equation of radiative transfer, boundary conditions have to be given. Under natural illumination, these include direct solar radiation, diffuse sky radiation, and the BRDF of the underlying surface. The distribution of direct and diffuse radiation above a plant canopy is discussed in Section 5.7; for studying radiative transfer in various media, several prototype models are also used (e.g. Thomas and Stamnes, 1999).

Another complication of the solution of Eq. 5.17 are features characteristic of the plant canopy: for non-uniform leaf normal distribution, extinction is a function of the direction of photon travel and the transfer function is not rotationally

invariant as it depends on the directions $\mathbf{\Omega}$ and $\mathbf{\Omega}'$ and not just the scattering angle, $\cos^{-1}(\mathbf{\Omega}\mathbf{\Omega}')$ (Myneni et al., 1988). A detailed treatment of problems related to the radiative transfer equation (Eq. 5.17) and its solutions for plant canopies is given by Myneni et al. (1991).

5.4 Direct solar radiation

The first step in solving the radiative transfer equation, Eq. 5.17, is the separation of uncollided direct solar radiation. Besides making it easier to solve the equation, direct solar radiation plays an important role in many canopy layers as its intensity is by several orders of magnitude larger than the intensity of diffuse sky radiation. Direct solar radiation is also frequently utilized for determining canopy transmittance and LAI.

As the only process affecting direct solar radiation is attenuation by scattering or absorption, the following equation holds:

$$-\mu_0\frac{\partial I(L,\mathbf{\Omega}_0)}{\partial L} + G(\mathbf{\Omega}_0)I(L,\mathbf{\Omega}_0) = 0, \tag{5.18}$$

where $\mathbf{\Omega}_0$ is the direction of propagation of direct solar radiation and $\mu_0 = -\cos\vartheta_S$, ϑ_S is the solar zenith angle. Assuming azimuthal symmetry and rewriting Eq. 5.18:

$$\frac{\partial I_0}{\partial L} = -\frac{G(\vartheta_S)I_0}{\cos\vartheta_S}, \tag{5.19}$$

allows for an easy solution by integration:

$$I_0 = \hat{I}_0\exp\left(-\frac{G(\vartheta_S)L}{\cos\vartheta_S}\right), \tag{5.20}$$

where $\hat{I}_0$ and $I_0 = I(L,\vartheta_S)$ are the intensities of direct solar radiation above and inside the canopy, respectively, and L is the downward cumulative leaf area index (Eq. 2.2).

The canopy beam transmittance a_S is defined as the ratio of direct solar irradiance inside the canopy to that above the canopy. From Eq. 5.20, the theoretical value of a_S is given by

$$a_S(\vartheta_S,z) = \frac{I_0}{\hat{I}_0} = \exp\left(-\frac{G(\vartheta_S)L(z)}{\cos\vartheta_S}\right). \tag{5.21}$$

Eq. 5.21 can also be used to calculate the direct solar radiation flux density S inside a plant canopy. According to Eq. 5.3,

$$
\begin{aligned}
S &= \int_{2\pi+} I_0(\boldsymbol{\Omega}) \cos \vartheta d\boldsymbol{\Omega} \\
&= \int_{2\pi+} I_0 \cos \vartheta \delta(\boldsymbol{\Omega} - \boldsymbol{\Omega}_0) d\boldsymbol{\Omega} \\
&= I_0 \cos \vartheta_S
\end{aligned}
\tag{5.22}
$$

and we obtain the obvious result

$$
\frac{S}{S_0} = \frac{I_0 \cos \vartheta_S}{\hat{I}_0 \cos \vartheta_S} = a_S,
\tag{5.23}
$$

where S_0 is the direct solar irradiance above the canopy.

Eq. 5.21, also known as the Poisson model in the context of penetration of direct solar radiation in vegetation, is only valid for a completely random canopy. The structure inherent in all real plant canopies has a noticeable effect on canopy beam transmittance: clumping tends to increase canopy transmittance while special regular arrangements of leaves can have the opposite effect. Several other formulae for predicting the frequency of gaps in plant stands were proposed by Nilson (1971): the binomial models, where the canopy is divided into a finite number of layers with equal thicknesses ΔL,

$$
a_S = \exp \left[\frac{L}{\Delta L} \ln \left(1 - \frac{G}{\cos \vartheta_S} \Delta L \right) \right]
\tag{5.24}
$$

and

$$
a_S = \exp \left[-\frac{L}{\Delta L} \ln \left(1 + \frac{G}{\cos \vartheta_S} \Delta L \right) \right];
\tag{5.25}
$$

and the Markov model, based on the theory of Markov chains,

$$
a_S = \begin{cases} 1 - GL/\cos \vartheta_S, & \text{if } L \leq \Delta L \\ \left(1 - \frac{G\Delta L}{\cos \vartheta_S} \right) \exp \left[\left(\frac{L}{\Delta L} - 1 \right) \ln \left(1 - \lambda_0 \frac{G\Delta L}{\cos \vartheta_S} \right) \right], & \text{if } L \geq \Delta L \end{cases},
\tag{5.26}
$$

where

$$
\lambda_0 \leq \frac{1}{1 - G\Delta L/\cos \vartheta_S}
\tag{5.27}
$$

is a constant related to the conditional probability of observing a contact between sunrays and foliage elements in a layer with the thickness ΔL. Eq. 5.24 is known as the positive binomial model and describes regular dispersion of foliage with a transmittance smaller than that of a random canopy; Eq. 5.25 is the negative

binomial model describing a clumped foliage with less absorption than a random canopy.

In the case $\Delta L \to 0$, the transmittance of the Markov model (Eq. 5.26) becomes

$$a_S = \exp\left(-\frac{\lambda_0 GL}{\cos\vartheta_S}\right). \tag{5.28}$$

From Eq. 5.27, it follows that if $\Delta L \to 0$, the Markov model describes only a random or a clumped canopy as $\lambda_0 \leq 1$.

To apply the Poisson model (Eq. 5.21) to non-random canopies, Lang and Xiang (1986) used different averaging lengths for a_S, assuming the canopy to be random for each averaging path.

Mann et al. (1977) derived a more general formula for the expected fraction of the transect which is sunlit. In this context the Sun is considered to be a point source, no penumbrae exist and thus sunfleck fractional area equals the canopy beam transmittance a_S. When the number M of leaves that are projected onto the transect by the Sun's rays and the widths D of these projections are known, the fractional area of sunflecks is derived from the theory of probability. The locations of leaf projections along the transect are assumed to be identically and independently distributed random variables with an absolutely continuous distribution function; the widths of leaf projections are allowed to vary according to some probability distribution, which can be a function of the location of the projection. However, they found that the error of a_S from taking D constant is small, about 1% of transect length. For a uniform distribution of leaf projections over the transect and a constant D,

$$a_S = \frac{M-1}{M+1}\left(1-\frac{D}{\Lambda}\right)^{M+1} + \frac{2}{M+1}\left(1-\frac{D}{2\Lambda}\right)^{M+1}, \tag{5.29}$$

where Λ is the length of the transect.

As M increases beyond all bounds while MD is held constant, the expected value of the sunlit fraction of the transect converges rapidly to $e^{-MD/\Lambda}$, which is the standard Poisson result, equivalent to Eq. 5.21.

5.5 Clumping index

The clumping index (or nonrandomness factor) Ω was introduced into the equation describing the penetration of direct solar radiation in plant canopies (Eq. 5.21) by Black et al. (1991) to include the effect of clumping,

$$a_S(z, \vartheta_S) = \exp\left(-\frac{\Omega G(\vartheta_S)L(z)}{\cos\vartheta_S}\right); \tag{5.30}$$

Ω equals unity for a completely random foliage distribution, lower values indicate canopy clumping. The clumping index was introduced mainly to account for penetration rates differing from those predicted by the Poisson formula (Eq. 5.21) and has its origins in the parameter λ_0 of Eq. 5.28. Unlike λ_0, the clumping index Ω is not restricted to the interval $[0, 1]$, but can have any positive value, values larger than 1 indicate that the distribution of foliage is regular.

Both Eqs. 5.21 and 5.28 predict that the logarithm of canopy transmittance depends linearly on $GL/\cos\vartheta_S$ and thus require Ω to be constant. A natural extension to this is to define the clumping index Ω as a function of L by inserting Ω into Eq. 5.19:

$$\frac{\partial I_0}{\partial L} = -\frac{\Omega(L, \vartheta_S) G(\vartheta_S) I_0}{\cos\vartheta_S}, \qquad (5.31)$$

or for direct solar irradiance,

$$\frac{\partial S}{\partial L} = -\frac{\Omega(L, \vartheta_S) G(\vartheta_S) S}{\cos\vartheta_S}; \qquad (5.32)$$

direct solar irradiance at height L can hence be written as

$$S(L, \vartheta_S) = S_0 \exp\left(-\frac{G(\vartheta_S)}{\cos\vartheta_S} \int_0^L \Omega(\Lambda, \vartheta_S) d\Lambda\right), \qquad (5.33)$$

where S_0 is direct solar irradiance above the canopy.

To perform the integration, the dependence of clumping index on the downward cumulative leaf area index L, or equivalently, on the height z, must be known. Presently, no theoretical models exist for predicting the dependence of Ω on L.

Some simple general considerations can give insight into the meaning of the clumping index as defined by Eq. 5.32. For simplicity, the Sun is considered to be a point source at infinity. The total leaf area contained per unit ground area in a horizontal canopy layer of thickness dz located at the height z is $\sigma_L(z) = u_L(z)dz$. A fraction $\alpha_S(z)$ of these leaves is illuminated by the collimated beam of solar radiation; the total sunlit area of leaves per unit area in this layer is then $\sigma_{LS}(z) = \alpha_S(z)u_L(z)dz$ and assuming that the probability of being sunlit does not depend on leaf orientation, the total sunlit area per unit horizontal area projected on the plane normal to the direction of direct solar radiation equals $\hat{\sigma}_{LS}(z) = G(\vartheta_S)\sigma_{LS}(z)$.

Direct solar irradiance in a horizontal sunlit area inside the canopy equals the direct solar irradiance above the canopy S_0; direct solar irradiance on a surface perpendicular to sunrays equals $S_0/\cos\vartheta_S$. The energy absorbed by the sunlit leaves located in an area A equals the leaf area projected perpendicular to sunrays times the direct solar irradiance, $dE = A\hat{\sigma}_{LS}(z)S_0/\cos\vartheta_S$. Thus, the amount

of radiative energy scattered or absorbed by leaves in the infinitesimal layer dz per unit ground area is $S_0\hat{\sigma}_{LS}(z)/\cos\vartheta_S$. This must equal the decrease in the average direct solar irradiance in the layer dz,

$$
\begin{aligned}
-dS &= S_0\hat{\sigma}_{LS}(z)/\cos\vartheta_S \\
&= G(\vartheta_S)\sigma_{LS}(z)S_0/\cos\vartheta_S \\
&= \frac{G(\vartheta_S)S_0\alpha_S(z)u_L(z)}{\cos\vartheta_S}dz.
\end{aligned}
\tag{5.34}
$$

Using Eq. 2.4, the change in the average direct solar irradiance can be expressed as a function of L,

$$
-dS = \frac{G(\vartheta_S)S_0\alpha_S(L)}{\cos\vartheta_S}dL.
\tag{5.35}
$$

According to Eq. 5.32, the change of direct solar irradiance on a horizontal plane can also be written as

$$
\begin{aligned}
dS &= -\frac{\Omega(L)G(\vartheta_S)S}{\cos\vartheta_S}dL \\
&= -\frac{\Omega(L)G(\vartheta_S)a_S(L)S_0}{\cos\vartheta_S}dL.
\end{aligned}
\tag{5.36}
$$

Comparing Eqs. 5.35 and 5.36 gives

$$
\frac{dS}{dL} = \frac{G(\vartheta_S)S_0\alpha_S(L)}{\cos\vartheta_S} = \frac{\Omega(L)G(\vartheta_S)a_S(L)S_0}{\cos\vartheta_S},
\tag{5.37}
$$

or

$$
\Omega(L) = \frac{\alpha_S(L)}{a_S(L)}.
\tag{5.38}
$$

The clumping index $\Omega(L)$ is just the ratio of sunlit leaf fraction to canopy transmittance. Under the assumption that the Sun is a point source at infinity, canopy transmittance equals sunfleck fractional area, $a_S = k_S$. At the top of the canopy where direct solar radiation is undisturbed, $a_S = \alpha_S = 1$, and

$$
\Omega(0) = 1.
\tag{5.39}
$$

In a random canopy, $\Omega(L) = 1$, leaf locations are not correlated with sunlit areas in the canopy. If $\Omega > 1$, foliage is said to be regularly arranged as leaves tend to be in sunflecks. Inside a clumped canopy, $\Omega < 1$, and leaves are more likely to be found in the shadows of foliage elements located above them. The interpretation of Eq. 5.38 is not so straightforward in a more realistic case where the Sun has a finite angular diameter and the transition from sunfleck to umbra is

continuous. However, the view that in a clumped canopy foliage elements tend to be more in the darker areas while in a regular canopy leaves favor well-lighted locations, can be upheld.

A graphical interpretation for $\Omega(L)$ can also be given. First dividing Eq. 5.32 by S_0 and then doing some algebra gives

$$\frac{d(S/S_0)}{dL} = -\frac{\Omega(L)G(\vartheta_S)a_S(L)}{\cos\vartheta_S} \tag{5.40}$$

$$\frac{da_S}{a_S} = -\frac{\Omega(L)G(\vartheta_S)}{\cos\vartheta_S}dL = -\Omega d\left(\frac{G(\vartheta_S)L}{\cos\vartheta_S}\right) \tag{5.41}$$

$$\Omega = -\frac{d(\ln a_S)}{d\tau'}, \tag{5.42}$$

where $\tau' = \frac{G(\vartheta_S)L}{\cos\vartheta_S}$. Thus, clumping index is the slope of the logarithm of canopy beam transmittance plotted against τ'.

Although several theoretical models for Ω as a function of L can be constructed using different assumptions of the dependence of α_S on a_S, the author has not found any that would match the measured canopy beam transmittances (see Sections 6.2 and 6.3.1). It is most likely that at some depth inside the willow canopy, this dependence goes through a qualitative change caused by a transition in stand structure.

In Section 6.3.1, a method is proposed for the inclusion of the clumping index into the equation of radiative transfer. It should also be noted that the most trivial assumption for nonrandom canopies, $\Omega = $ const, does not satisfy the condition 5.39.

5.6 Leaf albedo

The albedo of a reflecting surface is defined as flux reflectance or the ratio of the reflected radiation flux to the incident flux. The albedo of a non-Lambertian surface thus depends on the directional distribution of incident radiation. For a Lambertian surface, however, the albedo is defined unambiguously.

It is customary to use the bi-Lambertian model to describe a leaf: the reflectance of a leaf is divided into the diffuse and specular parts so that the leaf BRDF consists of a Lambertian component and a delta-function describing the specular component; leaf transmission is generally considered isotropic (e.g. Ross and Nilson 1968; Ross, 1981; Shultis and Myneni, 1988; Walter-Shea and Norman, 1991). The bi-Lambertian model for leaf transmittance and reflectance

is thus given by (see Eq. 5.10)

$$r_1(\nu, \mathbf{\Omega}, \mathbf{\Omega}') \equiv \frac{1}{\pi} R_{L1}(\nu) \qquad (5.43)$$

$$r_2(\nu, \mathbf{\Omega}, \mathbf{\Omega}') \equiv \frac{1}{\pi} R_{L2}(\nu) \qquad (5.44)$$

$$t(\nu, \mathbf{\Omega}, \mathbf{\Omega}') \equiv \frac{1}{\pi} T_L(\nu), \qquad (5.45)$$

where R_{L1}, R_{L2} and T_L are the diffuse albedo of leaf adaxial side, diffuse albedo of leaf abaxial side, and leaf transmittance, respectively.

Although the albedos in Eqs. 5.43 and 5.44 can be different, a bi-Lambertian leaf has only one transmittance. The reciprocity equation (Thomas and Stamnes, 1999) can be written as

$$t_1^*(\nu, -2\pi, -\mathbf{\Omega}) = t_2^*(\nu, +\mathbf{\Omega}, +2\pi), \qquad (5.46)$$

where $-\mathbf{\Omega}$ is anti-parallel to $+\mathbf{\Omega}$ and -2π denotes the integral over all incident directions

$$t^*(\nu, -2\pi, -\mathbf{\Omega}) = \int_{2\pi-} \cos\vartheta' t(\nu, -\mathbf{\Omega}', -\mathbf{\Omega}) d(-\mathbf{\Omega}'), \qquad (5.47)$$

where ϑ' is the angle between leaf normal and $\mathbf{\Omega}'$. Thus, for a Lambertian transmitter,

$$t_1^*(\nu, -2\pi, -\mathbf{\Omega}) = \int_{2\pi-} \cos\vartheta' t_1(\nu, -\mathbf{\Omega}', -\mathbf{\Omega}) d(-\mathbf{\Omega}') \qquad (5.48)$$
$$= \frac{1}{\pi} T_{L1}(\nu) \int_{2\pi-} \cos\vartheta' d(-\mathbf{\Omega}')$$
$$= T_{L1}(\nu).$$

Similarly, as $+2\pi$ in Eq. 5.46 denotes integration over all exit directions, substituting the corresponding integral into the right hand side of Eq. 5.46 yields

$$t_2^*(\nu, +\mathbf{\Omega}, +2\pi) = T_{L2}(\nu) \qquad (5.49)$$

and using Eq. 5.46 again gives

$$T_{L1}(\nu) = T_{L2}(\nu) = T_L(\nu). \qquad (5.50)$$

The reflectance of *S. viminalis* leaves was measured in laboratory with a GER-2600 spectrometer on 2 July 2001. Measured reflectances were calibrated using a Spectralon reference. The measured reflectances for both the adaxial and abaxial
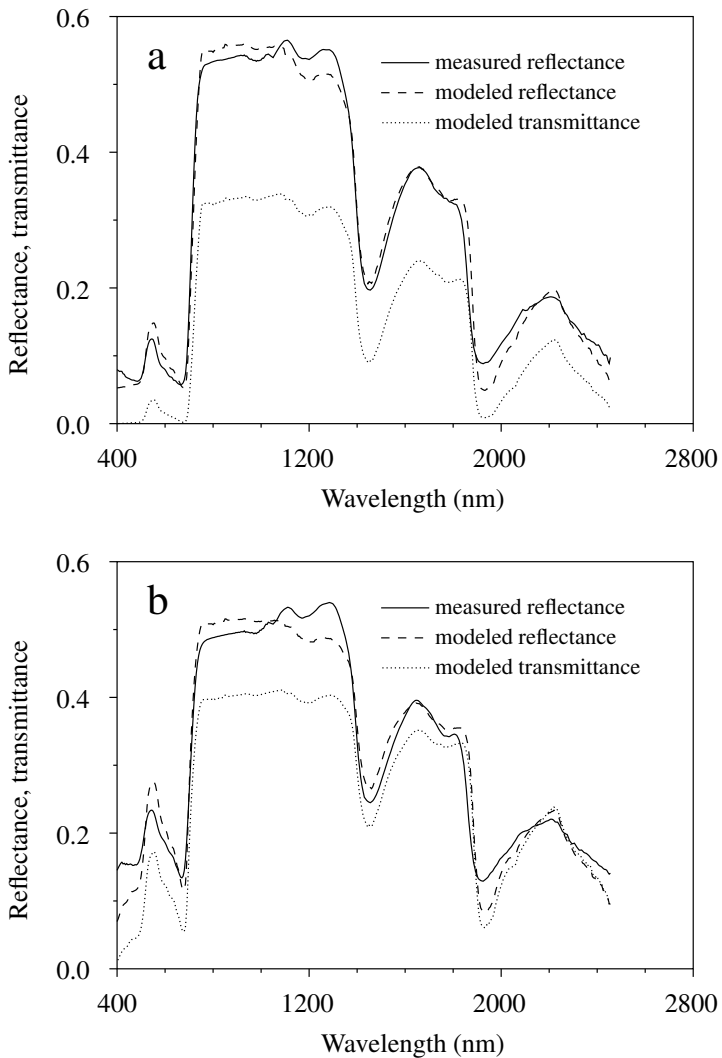
Figure 5.1: Reflectance and transmittance of a *S. viminalis* leaf. a) Adaxial side, b) abaxial side.

sides were fitted by the PROSPECT leaf model (Jacquemoud and Baret, 1990), measurements and modeling results are shown in Figure 5.1. The model was used for estimating the spectral transmittance of a *S. viminalis* leaf.

As the reflectances of the adaxial and abaxial sides in Figure 5.1 are different, the parameters of the PROSPECT model fitted to the measured reflectance data are different leading to different transmittance estimates. Thus, only transmittance calculated from the reflectance of the adaxial side is used as this side

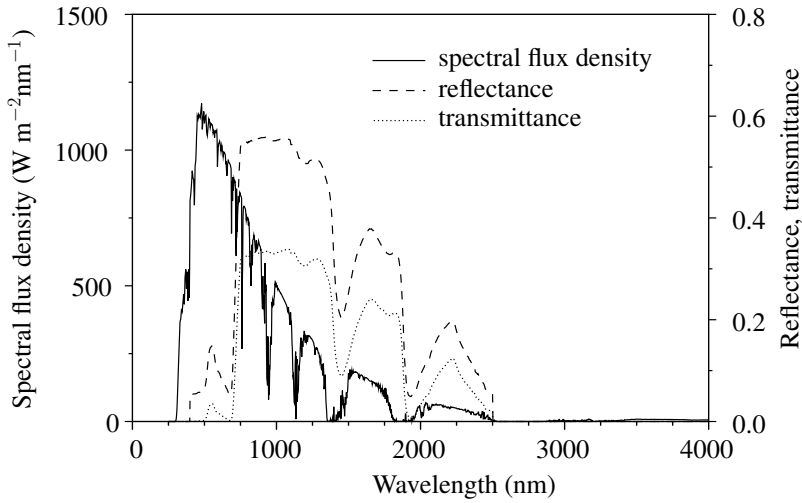**Figure 5.2:** Reflectance of the adaxial side and transmittance of a *S. viminalis* leaf compared with the spectrum of solar radiation beneath the atmosphere.

Table 5.1: Reflectances and transmittance of *S. viminalis* leaves integrated over two spectral regions, PAR and NIR.

	PAR	NIR
adaxial reflectance	0.083	0.47
abaxial reflectance	0.17	0.45
transmittance	0.011	0.28

is more smooth, has less hair and is probably better described by the leaf optics model.

The errors of the measured reflectance spectra of the adaxial and abaxial sides of leaves are quite large due to measurement inconsistencies. For measuring the spectra, leaves were laid on a black mat background with their edges overlapping. The overlapping was kept to a minimum, but still multiple reflectance in the overlapped areas may have considerably enhanced reflectance, especially in the near-infrared region.

53

In Section 6.3, leaf reflectance and transmittance in two spectral regions, PAR (wavelength = 400–700 nm) and NIR (700–2500 nm) is used for modeling radiation fluxes in the willow coppice. To calculate these quantities, the measured spectral reflectances $R_{L1}(\nu)$ and $R_{L2}(\nu)$ and the transmittance $T_L(\nu)$ were integrated over the appropriate spectral intervals weighed by the spectral composition of incident radiation. The spectral distribution of the radiation incident on a leaf was calculated using the 6S model (Vermote et al., 1997) with input parameters chosen as follows: solar zenith angle 45°, continental aerosol, aerosol optical thickness at 500 nm 0.20 (taken as the average value measured during the summers of 2002 and 2003 at Tartu Observatory with the Cimel 318 sunphotometer operated by AERONET), atmospheric conditions: subarctic summer, sensor elevation 50 m, surface type: vegetation. The calculated spectrum of solar radiation is depicted in Figure 5.2 together with the modeled reflectance of a *S. viminalis* leaf; leaf reflectances and transmittance calculated from these data are given in Table 5.1.

The amount of spectral and directional reflectance data available in literature is scarce (a recent overview was written by Jacquemoud and Ustin (2001)), but the measuring and modeling results reported here seem to be within reasonable limits.

Ross (1981) used in his book the values 0.09 and 0.06 for leaf reflectance and transmittance in the PAR region, respectively, and 0.15 for absorption in NIR. An extensive investigation was carried out by Asner et al. (1998) in Texas, USA. They measured the reflectance spectra of the leaf's adaxial side and leaf transmittance spectra for several grasses, shrubs and trees using an integrating sphere; in total, 38 different species were measured. Reflectances and transmittances were calculated for two AVHRR channels, Channel 1 (550–700 nm) and Channel 3 (700–1000 nm), approximately corresponding to the PAR and NIR regions, respectively, in the current work. They found that the variability within genera, growthform, and functional groups always exceeded that of any single species, but no single species was significantly different from these groupings; for all trees and shrubs, an average value of Channel 1 reflectance was found to be 0.09 and transmittance 0.06; for Channel 3, the corresponding numbers were 0.43 and 0.39.

5.7   Radiation field above the plant canopy

Above the atmosphere, the spectrum of solar radiation in the visible and infrared regions is quite constant and well-known, variations occur mainly due to the periodic changes in the distance between the Earth and the Sun. Extraterrestrial solar radiation approximately corresponds to that of a black body with a

temperature of 5778 K. The solar constant, or the flux density of the Sun's radiative energy at a distance of one astronomical unit ($1.5 \cdot 10^6$ km) equals about 1366 Wm^{-2} (Fröhlich, 2000).

Earth's atmosphere scatters and absorbs incident solar radiation, so only a fraction of it reaches the surface or the vegetation covering it. The radiation flux is usually divided into two components: direct solar radiation, or the flux of photons that have penetrated the atmosphere without interactions and can be described as an almost collimated beam of radiation, and diffuse sky radiation that has undergone at least one scattering interaction. Also, the atmosphere itself is a source of thermal infrared radiation, but its wavelength is outside the spectral interval under consideration in this work.

Attenuation of solar radiation most explicitly depends on the presence of clouds: low- and medium-level clouds may completely block the Sun so that no direct solar radiation will reach the surface. The description of the solar radiation illuminating the ground is most complicated under a broken cloud cover, thus most research in measuring and modeling radiative transfer in plant canopies deals only with a completely clear or an overcast sky. An example of modeled solar spectrum below the atmosphere is given in Section 5.6.

Besides clouds, the radiation field above a plant canopy is influenced by the solar zenith angle and the optical properties of the atmosphere—concentrations of water vapor, ozone, methane and other optically active gases; and the amount of and optical properties of aerosol. Most of the processes of attenuation of solar radiation by the atmosphere are spectrally selective, i.e. besides changing the amount of solar energy reaching the surface they also change the spectrum of the incident radiation. This is most evident in case of no cloud cover: due to Rayleigh scattering, the sky is blue, and in the visible part of the spectrum, the fraction of radiation reaching the vegetation as diffuse radiation is much larger than in the infrared region.

Usually, the radiation field above the canopy is used as a boundary condition for solving the radiative transfer equation inside the plant canopy. However, this is not unconditionally correct, as the radiation fields inside and above a plant canopy are coupled. This is known as the adjacency effect caused by radiation reflected by the vegetation interacting with the atmosphere above it: a photon that has been reflected by the canopy may be scattered again in the atmosphere and may therefore contribute to the diffuse flux above the canopy. Thus, the diffuse sky radiation flux is generally larger over (and next to) well-reflecting surfaces compared with darker surfaces under similar atmospheric conditions.

The number of reports on modeling radiative transfer inside the coupled vegetation-atmosphere system is small (e.g., Gerstl and Zardecki, 1985; Myneni and Asrar, 1993; Verhoef and Bach, 2003). The problem of radiative transfer in-

side plant canopies is generally separated from the larger coupled problem as the optical properties of vegetation and the atmosphere are very different. Most modern algorithms for atmospheric correction of satellite images (i.e., eliminating the effect of the atmosphere to extract the reflectance of the Earth's surface) have a mechanism to deal with the adjacency effect.

To describe the direct solar radiation flux at a given solar zenith angle, only its amplitude is needed as the spatial distribution of directions of photon travel can be described by a delta function. Also, as the measurements used in this work were made in two spectral regions, PAR and global radiation, detailed spectral characteristics of shortwave radiation field are not treated here. Thus, for the purposes of the current study, only direct solar irradance integrated over the whole spectrum, or integral direct solar irradance, and the ratio of direct PAR to integral direct radiation need to be known.

The ratio of PAR to integral solar radiation has been studied under various atmospheric conditions and in different geographic locations (e.g. Howell et al., 1983; Gueymard, 1989; Karalis, 1989; Skartveit and Olseth, 1994; Alados-Arboledas et al., 2000, Mõttus et al., 2001). However, no simple universal formulae exist for an accurate calculation of the instantaneous value of this ratio under a clear sky using just broadband radiation characteristics (Karalis, 1989; Mõttus et al., 2001).

Even such a simple treatment of the spectral characteristics of shortwave solar radiation can cause confusion. Although the definition of photosynthetically active radiation as radiation between 400 and 700 nm is well established in the scientific community, measuring and modeling results may vary according to measurement techniques and conversion factors. A detailed description of the common pitfalls when treating PAR is given by Ross and Sulev (2000).

The directional distribution of diffuse sky radiation for clear conditions can be calculated using radiative transfer models. This distribution depends generally on the azimuth angle as the scattering phase functions of atmospherical particles have a forward-scattering peak forming a brighter aureole region around the Sun. No generally accepted approximations of the directional distribution of clear sky diffuse radiation exist today.

For completely overcast conditions, the number of radiation field components is twice smaller as no direct radiation reaches the ground. Also, diffuse radiation field can be considered azimuthally symmetric. Moon and Spencer (1942) proposed an empirical formula to describe sky luminance relative to luminance at zenith:

$$\rho_L = \frac{1}{3}\left(1 + 2\cos\vartheta\right), \tag{5.51}$$

where ϑ is the zenith angle.

A set of diffuse sky models has been standardized by the International Commission on Illumination (CIE) for several cloud cover types and different atmospheric turbidities (Darula and Kittler, 2003). Although these models describe the distribution of sky luminance and are generally used for daylight modeling by architects, PAR and luminance are inconsistent by some 6–16% (Skartveit and Olseth, 1994). Two of these models are also commonly used in modeling radiation fluxes. Uniform distribution of diffuse sky radiation is the most common approximation, meaning that the intensity of diffuse sky radiation is assumed to not depend on view direction. Another common approximation, completely overcast sky, is described by the formula

$$\rho_L = \frac{1}{3}\left[1 + 4\exp\left(-\frac{0.7}{\cos\vartheta}\right)\right]. \tag{5.52}$$

5.8 Determining LAI using canopy transmittance

Direct solar radiation can be used for determining canopy gap fraction and this principle is used in both commercial instruments and experimental measuring systems for determining LAI and canopy closure. Such instruments are generally referred to as plant canopy analyzers.

The method used in canopy analyzers is based on the inversion of Eq. 5.21. As $G(\vartheta)$ is rarely known in advance, the number of unknowns requires measurements at several view angles. Solving Eq. 5.21 for $L(z)G(\vartheta_S)$,

$$-\ln\left(a_S(\vartheta_S, z)\right)\cos\vartheta_S = L(z)G(\vartheta_S) \tag{5.53}$$

multiplying by $\sin\vartheta$ and integrating over all view angles yields

$$-\int_0^{\pi/2} \ln\left(a_S(\vartheta_S, z)\right)\cos\vartheta_S \sin\vartheta_S d\vartheta_S = \int_0^{\pi/2} L(z)G(\vartheta_S)\sin\vartheta_S d\vartheta_S. \tag{5.54}$$

Considering Miller's theorem (Miller, 1967),

$$\int_0^{\pi/2} G(\vartheta)\sin\vartheta d\vartheta = 0.5, \tag{5.55}$$

Eq. 5.54 becomes

$$L(z) = -2\int_0^{\pi/2} \ln\left(a_S(\vartheta_S, z)\right)\cos\vartheta_S \sin\vartheta_S d\vartheta_S. \tag{5.56}$$

Thus, $L(z)$ can be calculated from canopy beam transmittance regardless of the knowledge of $G(\vartheta)$ if transmittance is known for $\vartheta \in [0, \frac{\pi}{2}]$.

Examples of instruments that use sunrays as probes are DEMON (CSIRO, Canberra, Australia) and TRAC (3rd Wave Engineering, Ontario, Canada). As instantaneous measurement of penetration of direct solar radiation at multiple view angles is impossible and obtaining measurements at several solar altitudes is thus time-consuming, canopy transmittance is sometimes measured using the diffuse radiation of a clear sky. The instruments using diffuse sky radiation include LAI-2000 (Licor Inc., Nebraska) and Sunfleck Ceptometer (Decagon Devices Inc., Pullman, WA, USA). Hemispherical photography makes also use of diffuse sky radiation, due to its versatility and the ongoing increase of computing power that can be used for image processing, this method is gaining popularity. Still, radiometric calibration of digital cameras and image analysis algorithms have a lot of room for improvement.

As Eq. 5.21 is only valid under a random canopy, several attempts have been made to include canopy clumping; clumping index described in Section 5.5 is one of the most frequently used corrections, other methods include utilizing sunfleck length distribution or some specific assumptions about canopy structure. Also, the inversion of a single measurement, even if it is a digital photo containing millions of pixels, does not describe the (usually quite significant) natural inhomogeneity. Reports on inverting canopy transmittance in almost all vegetation types are abundant, recent reviews include those by Gower et al. (1999) and Jonckheere et al. (2004).

In real canopies with finite-dimensional scatterers, a_S measured at some single point underneath a canopy can be zero and inversion of Eq. 5.21 gives infinite LAI. To have a finite LAI, a_S has to be averaged over some area (the case of a special spatial leaf arrangement where the transmittance a_S is zero everywhere underneath the canopy is unnatural and is not discussed here). Lang and Xiang (1986) studied the effect of different averaging lengths for calculating the mean transmittance, assuming the canopy to be random for each averaging path. They found that for distances of about ten times the average size of the canopy element, a canopy can be considered random and Eq. 5.21 can be inverted; this principle is used in the DEMON instrument. However, according to model calculations performed by Chen et al. (1993), the use of a penetration value averaged over a horizontal surface to invert the stand foliage-area index (LAI) can cause a large underestimation of LAI, especially in the case of large LAI; thus, this approach must be used with care.

In coniferous stands, the method of indirect determination of LAI from canopy transmittance data, if the effects of canopy clumping are included, is more accurate than using destructive sampling (Chen, 1996). The use of generalized allometric relations available in literature can lead to even larger errors—according

to Grier et al. (1984), generalized allometric relations for Douglas fir stands produced errors ranging from -8% to $+93\%$.

According to Gower et al. (1999), direct and indirect estimates of LAI compare to within 25–30% in most canopies. However, relationships between canopy clumping calculated from canopy transmittance and the geometric structure of the stand still need more clarification. Also, canopy transmittance tends to saturate at LAI > 5. At about the same LAI value, the canopy's ability to absorb photons saturates (Asner and Wessman, 1997). Using different radiation models, Anisimov and Fuchansky (1997) found that the PAR and NIR spectral albedos do not change noticeably with the total LAI already for LAI ≥ 3.

Knowledge of the G-function (Eq. 2.6) that can be calculated from the measured or modeled distribution of leaf normals (Section 3.3) can be of help in inverting Eq. 5.21. Canopy transmittance, even if multi-angular measurements are available and canopy clumping is taken into account, can not be reliably used for determining $G(\vartheta)$: even for a uniform distribution of leaf azimuth, Lang et al. (1985) showed that in many cases, the distribution of leaf inclination angles obtained by inverting $G(\vartheta_S)$ is imprecise and the method should only be used for calculating the mean leaf inclination angle.

A review of traditional methods and recent advances in determining leaf area using canopy transmittance is given in (Weiss et al., 2004).

5.9   Sunfleck, penumbra and umbra

As the Sun is not a point source, the edges of shadows cast by leaves are not sharp: when moving from direct sunlight into a shadow, an observer passes through a strip of penumbra, where irradiance depends on the visible fraction of the solar disc. Due to penumbra, the radiation field in an actual canopy is very variable and shadows of single leaves are rarely distinguishable. The distribution of irradiance in penumbra at various levels has been studied by Oker-Blom (1984), Stenberg (1995), Kucharik et al. (1998), Palmroth et al. (1999), and Mõttus (2004).

Several definitions exist for sunfleck and umbra, but when the finite dimensions of the solar disc are taken into account, penumbral effects have to be considered and also the distinctions between umbra and penumbra and between penumbra and sunfleck have to be made. The criterion for identifying umbra, penumbra and sunfleck is based on the comparison of the measured direct solar irradiance S with the direct solar irradiance above the canopy S_0; in accordance with Oker-Blom (1984), Myneni and Impens (1985) and Ross and Mõttus (2000a,b), the following definitions are used in this work:

- umbra is an area inside the plant canopy where the Sun is totally shaded by leaves, i.e. $S = 0$;

- penumbra is an area inside the plant canopy where the Sun's disc is partly covered by leaves, i.e. $0 < S < S_0$;

- sunfleck is an area inside the plant canopy where the Sun's disc is not shaded, i.e. $S = S_0$.

The fractional areas of sunfleck (k_S), penumbra (k), and umbra (k_U) are defined as fractions of a horizontal area inside the willow coppice where the sensor reading would indicate sunfleck, penumbra, or umbra, respectively.

Due to electrical noise and other causes of measurement uncertainty, the value of $S/S_0 = 0.007$ is used as umbra threshold: areas with irradiances below this value are considered to be in umbra. Analogously, areas where $S/S_0 > 0.95$ are referred to as sunflecks. The main causes of fluctuation of direct solar irradiance in sunfleck as measured with the sunfleck indicator are the bending of the aluminium bar and thus shifting the solar disc from the center of the view; continuous changes in direct solar irradiation due to changes in solar zenith angle; and fluctuations in atmospheric conditions.

Sunfleck and umbra thresholds were chosen using Figure 5.3 where sunfleck and umbra areas are plotted as functions of the respective thresholds. On one hand, the location of sunfleck threshold should be at the edge of the area where the change of sunfleck fractional area with sunfleck threshold is small, so the discrimination between sunfleck and penumbra is stable; on the other hand, it has to be at as high values of direct solar irradiance as possible. Similar considerations apply to selecting umbra threshold.

Miller and Norman (1971b) developed a geometrical model for predicting direct solar irradiance in penumbra. Leaf edges were approximated by straight lines crossing the transect at different angles and direct solar irradiance along the transect was calculated.

This theory was improved by Denholm (1981). Two new concepts, augmented and diminished leaf area, were introduced. Additional umbra due to overlapping penumbral strips and shading due to curved edges (with a constant radius of curvature for any finite segment) was calculated.

Monte-Carlo methods have also been used in estimating direct solar irradiation in penumbra (e.g., Oker-Blom, 1984), but they require the construction of a geometric model of the plant canopy and are not invertible.

5.10   Sunfleck length distribution

Miller and Norman (1971a) developed a theory for sunfleck length distribution, assuming the Sun to be vertically overhead and have zero angular size, and the
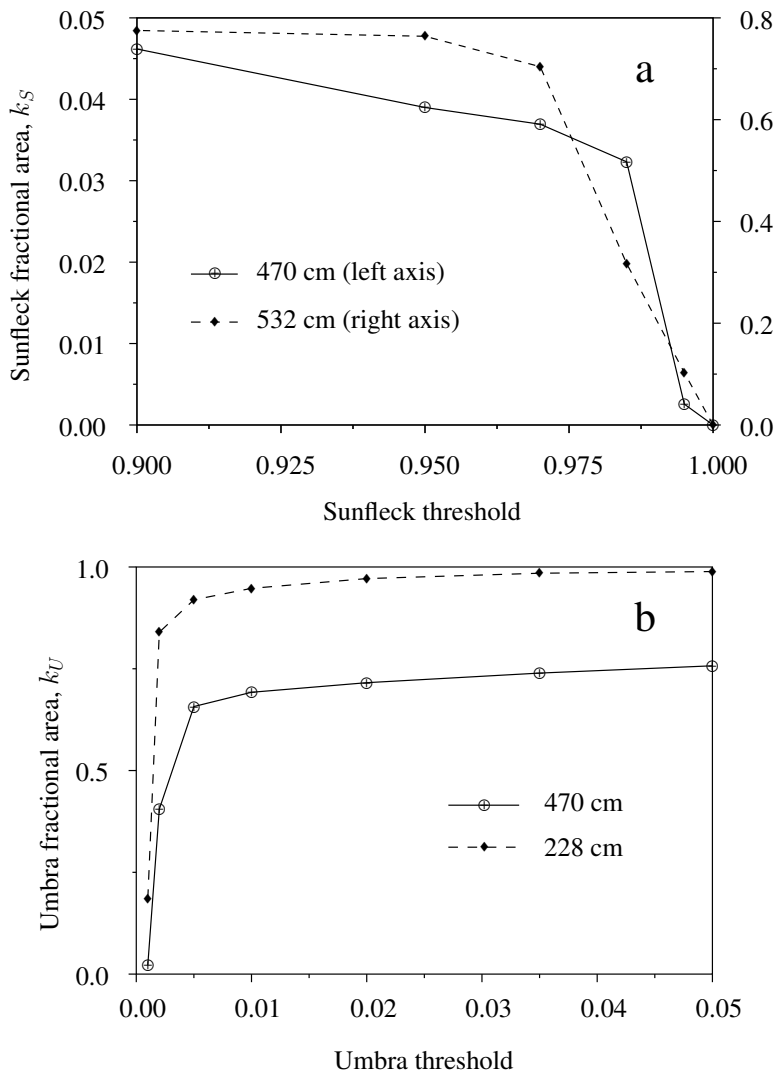
Figure 5.3: Sunfleck and umbra fractional areas as functions of the respective thresholds at two measurement heights inside the willow coppice. Thresholds are given as fractions of direct solar irradiance above the canopy.

canopy to consist of leaves that are identical in shape, size, azimuthal orientation, and height above the (flat) ground; all leaves must be horizontal, flat and located at random.

They arrived at the formula

$$F_S(l) = (1 + \rho wl)e^{-(\rho\sigma + \rho wl)}, \tag{5.57}$$

where $F_S(l)$ is cumulative sunfleck fractional area, or the length of a transect that is contributed by sunflecks that are longer than l, ρ is the average number of leaves per unit area, σ is the area of a leaf, and w is the span of a leaf in the direction perpendicular to the transect.

A more general theory was developed by Mann and Curry (1977). As the limiting case when the length of the transect is increased beyond all bounds, their formula for the expected fraction of the transect that is covered by sunflecks each of length exceeding l, $F_S(l)$, coincides with Eq. 5.57.

Eq. 5.57 has been used in estimating leaf area index and clumping in coniferous forests by Chen and Cihlar (1995a,b). They used a "gap removal" process, eliminating large sunflecks by approximating the measured gap size distribution F_S with the theoretical function (Eq. 5.57).

Eq. 5.57, derived by Miller and Norman (1971a), gives a theoretical distribution of sunfleck length. Calculating the first derivative with respect to l gives the theoretical leaf number distribution per unit scan length,

$$n_S(l, \rho, w, \sigma) = (\rho w)^2 l e^{-\rho(\sigma + wl)}. \tag{5.58}$$

Eq. 5.58 indicates that the distribution of sunfleck length is exponential, i.e. under all circumstances, the number of short sunflecks is much larger than the number of longer ones. Integrating Eq. 5.58 over all possible sunfleck lengths gives the number of sunflecks per 1 m:

$$N_S(\rho, w, \sigma) = \int_0^\infty (\rho w)^2 e^{-\rho(\sigma + wl)} dl = \rho w e^{-\rho\sigma}. \tag{5.59}$$

Dividing sunfleck fractional area calculated as $F_S(0)$ (Eq. 5.57) by N_S gives the theoretical mean sunfleck length:

$$< l > = \frac{e^{-\rho\sigma}}{\rho w e^{-\rho\sigma}} = \frac{1}{\rho w}. \tag{5.60}$$

However, this equation cannot be applied directly to describe a discretely sampled sunfleck length. If direct solar irradiance is sampled at discrete intervals of length Δ, the number of registered sunflecks has to be smaller than that predicted by Eq. 5.59 as most sunflecks with lengths below Δ are not registered.
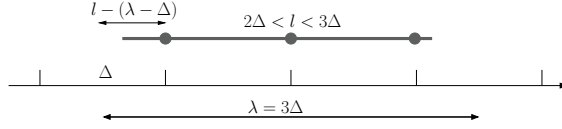
Figure 5.4: A sunfleck with the length $2\Delta < l < 3\Delta$ being registered as having length $\lambda = 3\Delta$, Δ is the sampling interval.

A sunfleck that was registered as having the minimum length (Δ) can actually have a length of $0\ldots2\Delta$, if a sunfleck was registered to have the length $l = 2\Delta$, its actual length has to be between 1Δ and 3Δ. More exactly, when measuring a sunfleck with length $l \in (\lambda - \Delta, \lambda)$, it will be registered as having length λ if its beginning lies in a part the sampling interval Δ with a length $l - (\lambda - \Delta)$ (Figure 5.4). For the same sunfleck to be registered with a length $\lambda - \Delta$, its beginning has to lie in the part of the sampling interval with a length $\Delta - (l - (\lambda - \Delta)) = \lambda - l$.

Thus, λ will be the recorded length of a sunfleck with the length

- $l \in (\lambda - \Delta, \lambda)$ with the probability $\frac{1}{\Delta}\left[l - (\lambda - \Delta)\right]$,

- $l \in (\lambda, \lambda + \Delta)$ with the probability $\frac{1}{\Delta}\left[(\lambda + \Delta) - l\right]$,

where $\lambda = n\Delta$, $n = 1, 2\ldots$

The possibility that two consecutive sunfleck recordings can be caused by two separate sunflecks is ignored here as it depends on the time constant and the field of view of the actual sensor and also on the number of sunflecks and the distribution of their length.

The theoretical distribution of sunfleck length in case of a discrete sampling interval can be written as

$$n_S^\Delta(i, \rho, w) = \int_{(i-1)\Delta}^{i\Delta} n(l, \rho, w)\frac{l - (i-1)\Delta}{\Delta}dl \qquad (5.61)$$

$$+ \int_{i\Delta}^{(i+1)\Delta} n(l, \rho, w)\frac{(i+1)\Delta - l}{\Delta}dl.$$

Substituting Eq. 5.58 into Eq. 5.61 and integrating yields after some simplifications

$$n_S^\Delta(i, \rho, w) = \frac{e^{-\rho(\sigma + w\Delta i)}\left(-2 + e^{-\rho w\Delta} + e^{\rho w\Delta}\right)}{\Delta}. \qquad (5.62)$$

This equation can be viewed as a geometric progression and its sum (i.e. the total number of registered sunflecks per unit scan length) can readily be calculated:

$$N_S^\Delta(\rho, w) = \sum_{i=1}^{\infty} n_S^\Delta(i, \rho, w) = \frac{1 - e^{-\rho w\Delta}}{\Delta}e^{-\rho\sigma}. \qquad (5.63)$$

63

Eq. 5.63 is similar to Eq. 5.59 for continuous measurement if the factor $\frac{1-e^{-\rho w \Delta}}{\Delta}$ is substituted with ρw.

The discrete analogue of Eq. 5.57 for calculating the measured cumulative sunfleck fractional area can be derived by summing the lengths of all sunflecks longer than l multiplied by their number calculated from Eq. 5.62:

$$F_S^\Delta = \left(1 - i + i e^{\Delta \rho w}\right) e^{-\rho(\sigma + w\Delta i)}. \tag{5.64}$$

As expected, the sunfleck fractional areas calculated for discrete and continuous measurement coincide,

$$k_S^\Delta = F_S^\Delta(0) = e^{-\rho \sigma} = k_S.$$

The mean sunfleck length $< l >^\Delta$ measured with a finite sampling step Δ can now be calculated as

$$< l >^\Delta = \frac{k_S}{N_S^\Delta} = \frac{e^{-\rho\sigma}}{\frac{1-e^{-\rho w \Delta}}{\Delta} e^{-\rho\sigma}} = \frac{\Delta}{1 - e^{-\rho w \Delta}}. \tag{5.65}$$

When going to the limit $\Delta \to 0$, Eqs. 5.62, 5.63, 5.64 and 5.65 converge to their continuous analogues: Eqs. 5.58, 5.59, 5.57 and 5.60, respectively.

6 MODELING RADIATION FIELD INSIDE THE CANOPY

Radiation field both above and underneath a plant canopy is frequently measured using electromagnetic radiation of several wavelengths. Above vegetation, various space- and airborne instruments look down at the surface of our planet, for both scientific and commercial purposes. Much less information is gathered by looking up through the plant cover, as recording the shortwave solar radiation penetrating a plant canopy is more laborious and requires human involvement in the measuring process. Still, scientific reports describing various aspects of the shortwave radiation field below a plant canopy are far too numerous to be listed here, recent reviews include those by Gower et al. (1999) and Jonckheere et al. (2004). The variation of the radiation field with height inside a plant canopy is studied even less frequently, although from the scientific point of view, this problem is no less interesting.

If a fast retrieval of canopy parameters from measured canopy brightness is required and ground measurements are available, a statistical method can be used without looking into the mechanisms producing the observed canopy reflectance. However, in the long run, radiative transfer models based on universal physical laws may provide a more efficient solution (Asner and Wessman, 1997).

When a model of penetration of solar radiation inside a plant canopy is constructed, it is most logical to verify it by measuring transmitted radiation below the canopy, reflected radiation above the canopy, and both transmitted and reflected radiation at various heights inside the canopy. Depending on the type of vegetation under observation, this can include measurements at both very large scales, like inside a rainforest, or at a relatively small scale, like in grasslands.

The number of radiative transfer models inside plant canopies is substantial, especially of those describing canopy reflectance. But not all works use solid validation by comparison with accurate measurements of the radiation field either inside or above the canopy, like (Kimes and Smith, 1980; Kimes et al.,1985; Verhoef, 1985; Myneni, 1991; Nilson and Peterson, 1991 ; Gobron et al., 1997; Liang et al., 1997; Myneni et al., 1997; Demarez et al., 2000; Kuusk and Nilson, 2000; Panferov et al., 2001). More commonly, models are compared with other models, approximate analytical solutions, or Monte Carlo simulations (Li and Strahler, 1986, 1992; Myneni et al., 1986, 1988; Shultis and Myneni, 1988; Knyazikhin et al., 1992; Chen et al., 1993, 1994; Asner and Wessman, 1997; Chelle and Andrieu, 1998; España et al., 1999b; Ganapol et al., 1999; Shabanov et al., 2000; Kuusk, 2001; Kimes et al., 2002; Liangcrocapart and Petrou, 2002; Ahmad et al., 2003).

Besides radiative transfer models, Monte Carlo simulations have been used for describing the radiation field inside a plant canopy (Kimes et al., 1980; Oker-Blom, 1984; Gerstl et al., 1986; Ross and Marshak, 1988; Antyufeev and Marshak, 1990a,b; North, 1996). These calculations are more laborious and generally require a geometric reconstruction of the plant canopy, thus making comparisons with measurements more difficult. Also, Monte Carlo models can not be easily inverted.

This section deals directly with the radiation field inside the *S. viminalis* canopy. Several approaches are used to describe the various aspects of penetration of shortwave solar radiation in the plant stand: sunfleck and umbra length are described as functions of depth inside the canopy; distribution of direct solar irradiance in penumbra is compared to Monte Carlo modeling results; canopy transmittance and clumping are studied as functions of solar zenith angle and height inside the canopy; and measured fluxes of PAR and integral solar radiation are compared with both a model based on the radiative transfer equation and a Monte Carlo simulation.

A large fraction of this work deals with the penetration of direct solar radiation. Direct solar radiation is the most variable component of radiation balance, and besides being a major contributor to the shortwave radiation flux inside a plant canopy, it is also a useful indicator of the correctness of our understanding of the radiation field inside a plant canopy. Direct solar radiation depends mostly on the structure of the canopy, the effect of "external" influences, like cloud cover and solar height, can be easily eliminated.

6.1 Sunfleck and umbra length

To describe the distribution of sunfleck and umbra length inside the willow stand, sunfleck sensor readings at various heights inside the coppice were used. Readings were converted to direct solar irradiance values using an approximate calibration, and using background measurements, sunfleck and umbra thresholds were calculated as described in Section 5.9.

In Figure 6.1, four recordings of the sunfleck sensor made on the same day at different heights in *S. viminalis* coppice are presented. The height of the coppice was 6.10 m and leaf area index was 5.20. More information about the measurements is given in Table 6.1.

As can be seen in Figure 6.1, at small relative heights, most of the transect is covered by umbrae, no sunflecks exist. Sunflecks emerge only at $z/z_{max} > 0.7$ and their share increases very rapidly with height. At the top of the canopy, large sunflecks are interrupted by short umbrae, when the sensor moves from a sunfleck into a shadow of a leaf located not far from the sensor.
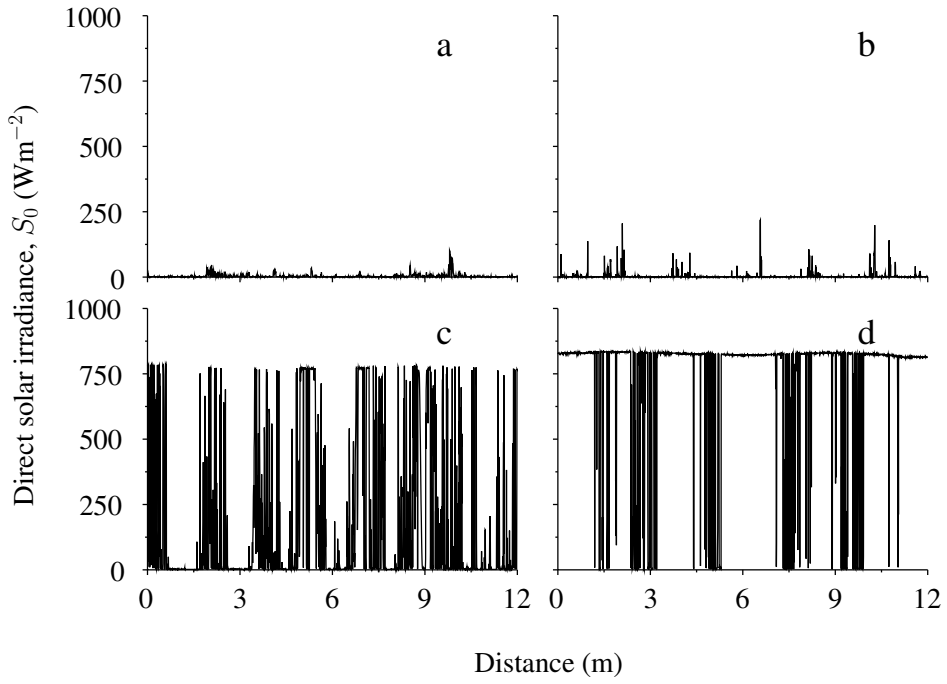
66

Figure 6.1: Sunfleck sensor's recordings at different heights within the *S. viminalis* canopy. Relative height z/z_{max}: a) 0.10; b) 0.54; c) 0.77; d) 0.87. See Table 6.1 for more details.

Table 6.1: Additional data for Figure 6.1.

subfigure		a	b	c	d
height	z (m)	0.62	3.30	4.70	5.32
downward cumulative LAI	$L(z)$	5.20	4.75	1.65	0.55
relative height	z/z_{max}	0.10	0.54	0.77	0.87
sunfleck fractional area	k_S	0	0	0.12	0.84
umbra fractional area	k_U	0.87	0.92	0.53	0.07
solar zenith angle	ϑ_S (deg)	52	50	48	39

This picture is typical for the dense willow coppice. Even at the end of the first growing year, the gaps in the canopy are so small that no sunflecks exist on the ground.

Analysis of experimental data shows that umbra and sunfleck length characteristics are largely determined by three factors: solar zenith angle ϑ_S, depth of the measurement level characterized by $L(z)$, and leaf, plant and canopy architectural characteristics. The first two factors determine the pathlength of the direct solar radiation beam in coppice, $\tau = L/\cos\vartheta_S$, expressed in the units of L. Hereafter umbra and sunfleck length characteristics will be considered as functions of the pathlength τ, assuming that it is the key factor determining the absorption pattern of direct sunlight.

As penumbra characteristics depend on the distance between the sensor and leaves, it might be expected that the geometric pathlength of a photon inside the canopy is also an important predictor of sunfleck and umbra characteristics. However, according to experimental data, the effective geometrical distance is dominated by the distance measured in units L, i.e. the optical pathlength τ. This is most likely due to the high density of the willow canopy and its relative compactness.

6.1.1 Sunfleck length distribution

As sunflecks were present only in upper canopy layers, the dataset for *S. dasyclados* was too small for yielding a reliable statistical description of sunfleck length. Thus, only measurements inside the *S. viminalis* stand are used for characterizing the distribution of sunfleck and umbra characteristics.

For analysis of sunfleck length variability, the number of sunflecks with length l per 1 m of scan, $n_S(l)$, and the cumulative sunfleck fractional area $F_S(l)$ are used. $F_S(l)$ denotes the fraction of the transect occupied by sunflecks larger than l, or the fractional area of sunflecks with lengths from l to the maximum sunfleck length l_{Smax}:

$$F_S(l) = \sum_{\lambda_i=l}^{l_{Smax}} \lambda_i\, n_S(\lambda_i), \tag{6.1}$$

or in the integral form

$$F_S(l) = \int_{l_S}^{l_{Smax}} \lambda\, n_S^*(\lambda)d\lambda, \tag{6.2}$$

where

$$n_S^*(l) = \lim_{\Delta l \to 0} \frac{n_S(l)}{\Delta l}. \tag{6.3}$$
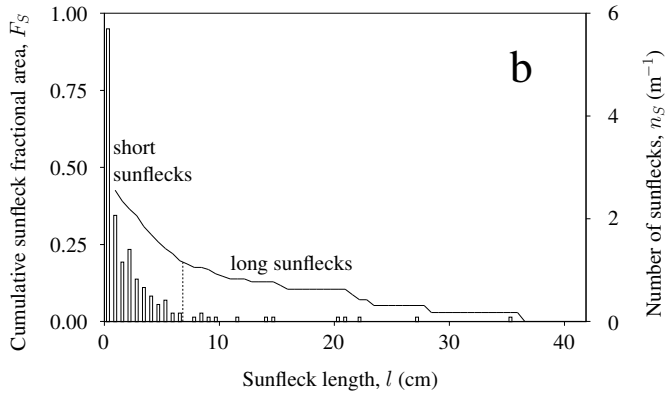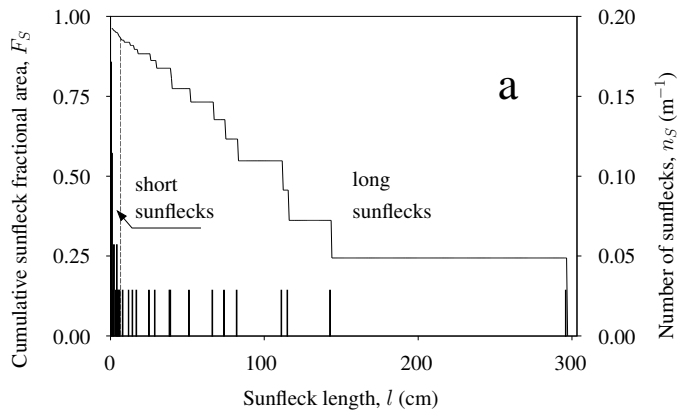
Figure 6.2: Examples of the number of sunflecks with length l per 1 m of scan, or the sunfleck length distribution function $n_S(l)$ (histogram), and the cumulative sunfleck fractional area function F_S (solid line) inside the *S. viminalis* stand.

subfigure	a	b
height z, m	2.60	2.00
relative height z/z_U	0.84	0.65

The sum of $n_S(l)$ equals the total number of sunflecks per 1 m of scan,

$$N_S = \sum_{l=0}^{l_{Smax}} n_S(l). \qquad (6.4)$$

From Eq. 6.1 it follows that

$$F_S(0) = k_S, \quad F_S(l_{Smax}) = 0, \qquad (6.5)$$

where k_S is sunfleck fractional area.

As an example, Figure 6.2 expresses two sunfleck length distribution functions $n_S(l)$ and cumulative sunfleck fractional area functions $F_S(l)$ for 14 September 1998 at relative heights a) $z/z_{max} = 0.84$ and b) $z/z_{max} = 0.65$, when the coppice height was $z_{max} = 310$ cm.

In the dense lower layers, the number of sunflecks per scan may be so small that determination of $n_S(l)$ and $F_S(l)$ proves impossible; below a canopy with $L > 4$, direct solar radiation penetrates only in penumbra, no sunflecks exist.

Analysis of $F_S(l)$ and $n_S(l)$ shows that for upper layers it is reasonable to divide the interval between 0 and l_{Smax} into two parts (Figure 6.2): short and long sunflecks. It should be noted that the location of the point separating the intervals and, consequently, the fractional areas of short and long sunflecks are somewhat arbitrary and subjective.

It is appropriate to assume that short sunflecks are caused by the gaps between individual leaves at least in upper canopy layers and are hence determined by the distance between leaves, while the length of long sunflecks is determined by the distance between shoot cylinders. Large sunflecks occur only in upper canopy layers, where the distance between neighboring shoots is large.

Figures 6.3a and b express two sunfleck length characteristics: a) mean sunfleck length $\langle l_S \rangle$ and b) maximum sunfleck length l_{Smax} as functions of the pathlength τ.

$\langle l_S \rangle$ and l_{Smax} decrease with τ exponentially. In the S. viminalis coppice, the maximum length of sunflecks in the upper cylindrical layer takes the values of 2–3 m, the length of short sunflecks in lower layers, only 0.01–0.03 m. The maximum sunfleck length l_{Smax} and the mean sunfleck length $\langle l_S \rangle$ are statistically interdependent (Figures 6.3a and b): the mean length $\langle l_S \rangle$ increases logarithmically with increasing l_{Smax}.

Theoretically: if $\tau \to 0$, $\langle l_S \rangle \to \infty$; if $\tau \to \infty$, $\langle l_S \rangle \to 0$.

Figure 6.4 shows the number of sunflecks N_S per unit scan length (a), and the share of short sunflecks in the total number of sunflecks X_{SS} (b) versus the pathlength τ.
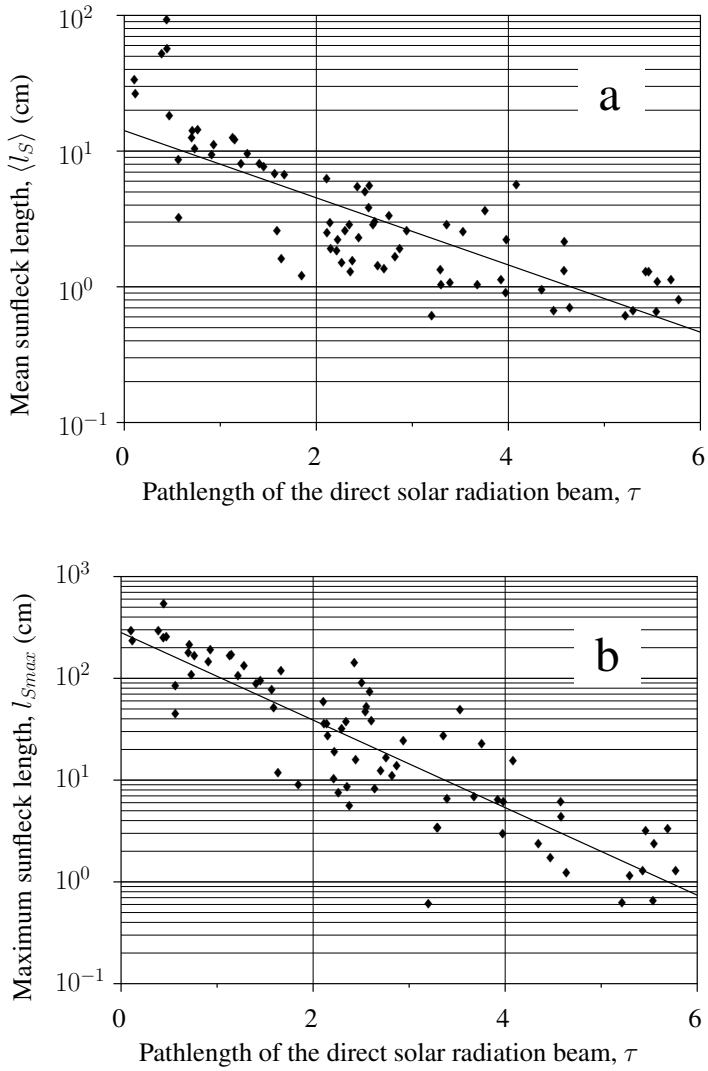
Figure 6.3: Two sunfleck length characteristics: the mean sunfleck length $\langle l_S \rangle$ and the maximum sunfleck length l_{Smax} inside the *S. viminalis* stand with the approximation formulae $\ln \langle l_S \rangle = -0.57\tau + 2.65$ and $\ln l_{Smax} = -0.99\tau + 5.64$.

Figure 6.4: a) Vertical distribution of the number of sunflecks, N_S, and b) the number-fraction of short sunflecks, X_{SS}, inside the *S. viminalis* stand with the approximation formulae $N_S = 11.5\tau \exp(-0.13\tau^2)$ and $X_{SS} = 1 - 0.53 \exp(-0.84\tau)$.

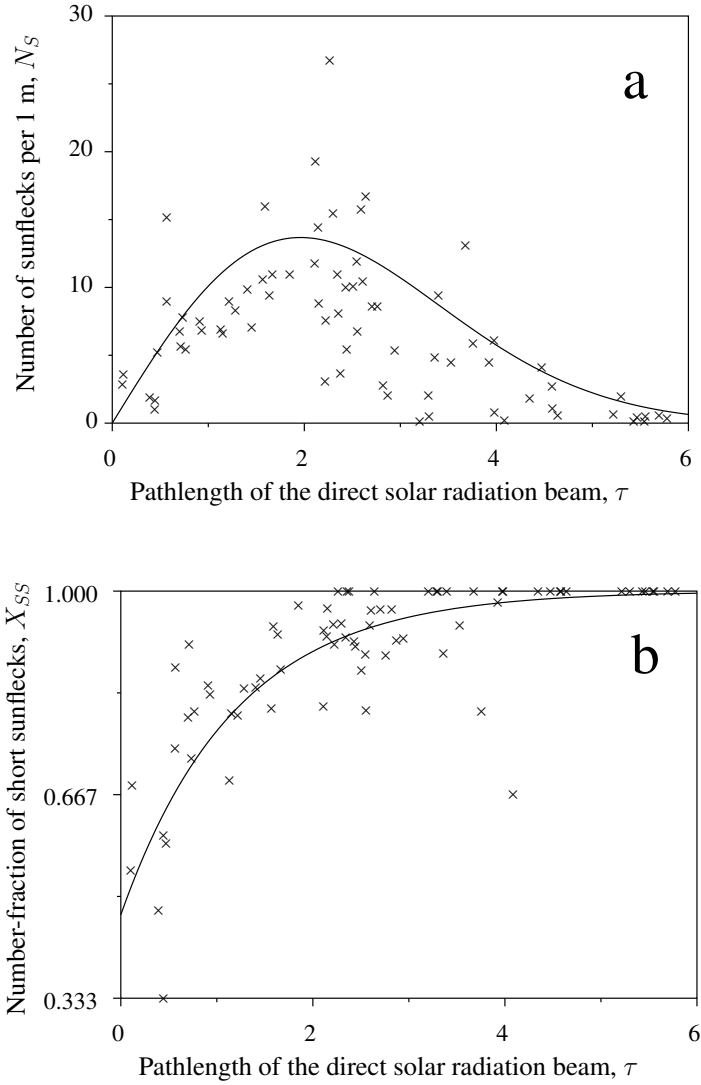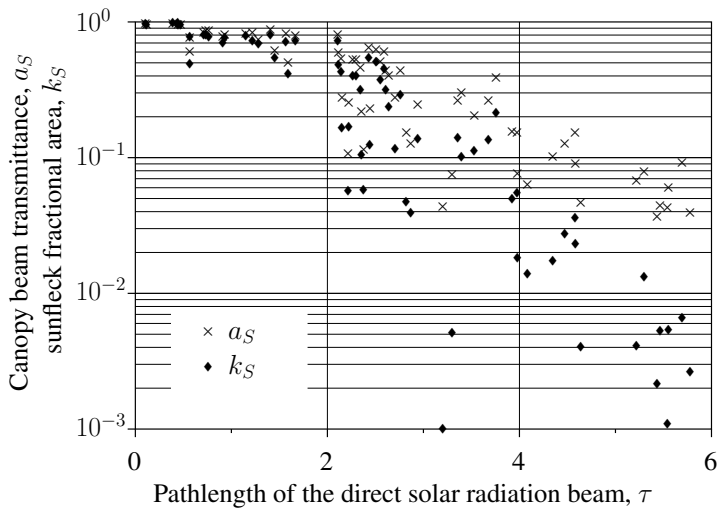**Figure 6.5:** The sunfleck fractional area k_S and the canopy beam transmittance a_S versus the pathlength of the direct solar radiation beam, $\tau = L/\cos\vartheta_S$ inside the *S. viminalis* stand.

The total number of sunflecks as well as the number of short sunflecks increases with τ, reaches a maximum value of 10 to 12 sunflecks per meter at $\tau = 2.5$ and then decreases slowly to zero at $\tau = 6$.

Figure 6.4b demonstrates that the number of short sunflecks dominates in all layers, while in lower layers, starting from $\tau = 2.5$, practically all sunflecks are "short" ($l \leq 6$ cm).

The function $N_S(\tau)$ is different for the one-year-old (1998) and for the several-years-old coppice (1995–1996). The number of sunflecks is greater in the former, which is evidently due to its better expressed cylindrical vertical structure that enhances penetration of direct solar radiation. Large deviations from the mean value indicate the existence of specific random configurations in willow coppice where the number of sunflecks is extremely large.

The sunfleck fractional area k_S together with the canopy beam transmittance a_S, i.e. the fraction of direct sunlight reaching the sensor during the scan, is plotted against the pathlength of the direct solar radiation beam, $\tau = L/\cos\vartheta_S$ in Figure 6.5. Canopy beam transmittance includes besides transmittance in sunflecks also transmittance in penumbra and therefore always $a_S \geq k_S$.

Theoretical values can be calculated for the measured sunfleck characteristics (Section 5.10), however, these values are not directly comparable with measure-
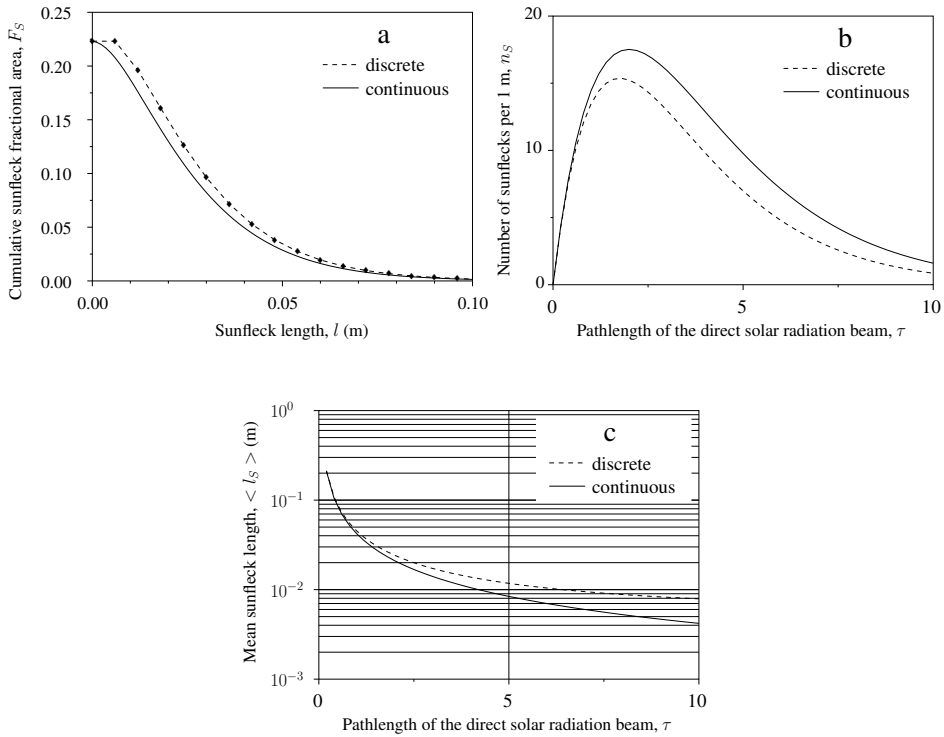
Figure 6.6: Theoretical cumulative sunfleck fractional area and other sunfleck characteristics calculated for both continuous and discrete measurement. Canopy parameters are approximated using the measured properties of the *S. viminalis* coppice: measurement step, $\Delta = 0.6$ cm, $\tau = L/\cos\vartheta_S = 2$, projected area of a leaf, $\sigma = 2.1$ cm^2, span of a leaf in the direction perpendicular to the transect, $w = 1$ cm.

ment results as the role of penumbra is of utmost importance in the dense willow coppice with long and narrow leaves. .

If all leaves are of the same size and isotropically oriented, the mean projected area of a leaf $\sigma = S_L/2$ and LAI $= 2\rho\sigma$, where ρ is the number of leaves per unit ground area. Using this to include the pathlength τ into the theoretical equations, some theoretical sunfleck characteristics are calculated using the measured characteristics of the willow coppice (Figure 6.6).

Eq. 5.57 assumes spatial homogeneity and requires many input parameters: the average number of leaves per unit area, the (projected) area of a leaf, and the span of a leaf in the direction perpendicular to the transect. To use it for a natural canopy, Eq. 5.57 has to be integrated over all leaf shapes, sizes and orientations.

74

It also excludes penumbra, and as the number of short sunflecks is very large, most of them pass by undetected even in a perfectly homogeneous canopy.

6.1.2 Umbra length distribution

The measured area of an umbra caused by the shadow of a single leaf depends on the following factors:

1. angular diameter of the solar disc (32"),

2. leaf shape and area characterized by its effective diameter,

3. projected area of a leaf.

Analogously to sunfleck statistics, for analysis of umbra length variability, the umbra length distribution function n_U and the cumulative umbra fractional area function F_U are used. $F_U(l)$ denotes the fraction of the transect occupied by umbrae larger than l, or the fractional area of umbrae with lengths from l to l_{Umax}:

$$F_U(l) = \sum_{\lambda=l}^{l_{Umax}} \lambda n_U(\lambda), \qquad (6.6)$$

or in the integral form

$$F_U(l) = \int_l^{l_{Umax}} \lambda n_U^*(\lambda) d\lambda, \qquad (6.7)$$

where

$$n_U^*(l) = \lim_{\Delta l \to 0} \frac{n_U(l)}{\Delta l}. \qquad (6.8)$$

The total number of umbrae per 1 m, N_U, can be calculated as the sum of $n_U(l)$:

$$N_U = \sum_{l=0}^{l_{Umax}} n_U(l). \qquad (6.9)$$

From Eq. 6.7 it follows that

$$F_U(0) = k_U, \quad F_U(l_{Umax}) = 0. \qquad (6.10)$$

Analysis of F_U and n_U shows that it is reasonable to divide the interval between 0 and l_{Umax} into three parts (Figure 6.7): short, medium-length, and long umbra intervals. It should be noted that the location of points separating the intervals and, consequently, the fractional areas of short, medium-length and long umbrae are somewhat arbitrary and subjective.
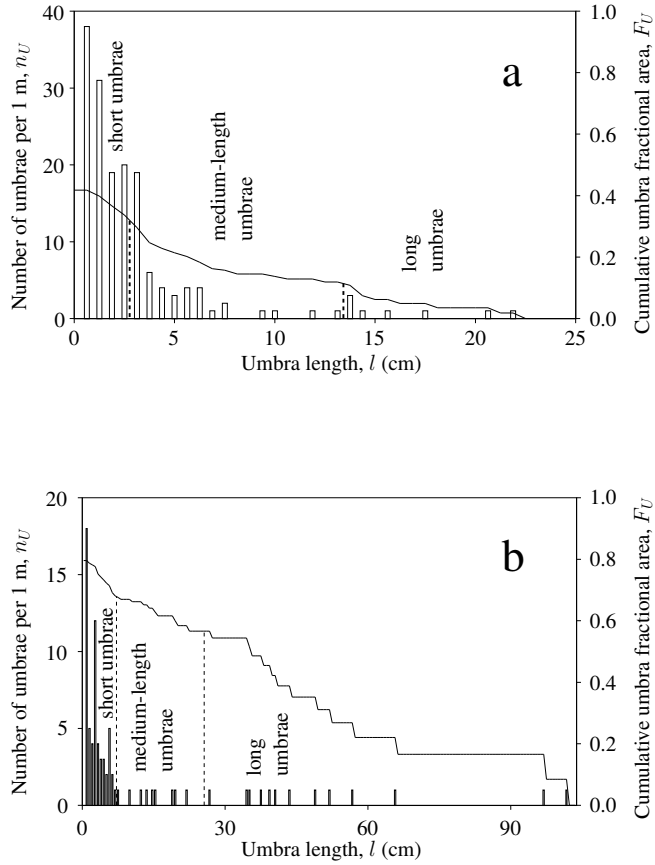
Figure 6.7: Examples of the number of umbrae with length l per 1 m of scan, or the umbra length distribution function $n_U(l)$ (histogram), and the cumulative umbra fractional area function F_U (solid line); *S. dasyclados*.

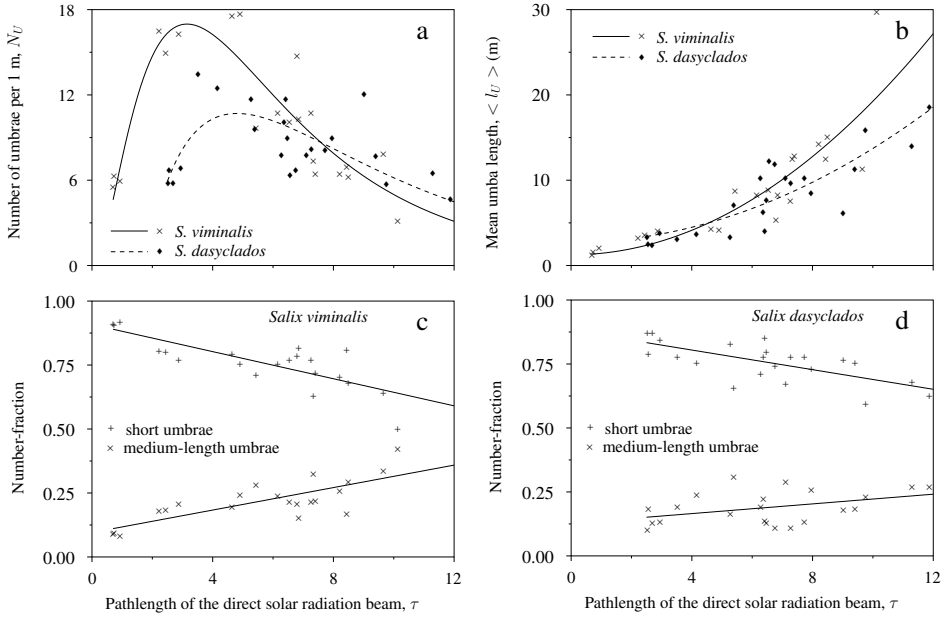| subfigure	a	b
measurement height z (m)	3.50	0.45
relative height z/z_{max}	0.74	0.09

Figure 6.8: a) Number of umbrae per 1 m scan length, N_U, fitted by the regression curve $N_U = a(\tau^3 + b)\exp(c\sqrt{\tau})$ (see the table below for the parameters a, b and c); b) mean umbra length and fitted regression curves $\langle l_U \rangle = p + q\tau^2$; c,d) number-fractions of small and medium-length umbrae versus pathlength τ, linear regression.

	a	b	c	p	q
S. viminalis	218.9	0.014	-3.38	1.25	0.18
S. dasyclados	56.0	-5.57	-2.28	2.72	0.11

Small umbrae dominate in all layers and the maximum of n_U corresponds to $l \approx 0$. In the short umbra interval, $F_U(l)$ decreases rapidly with increasing l and is approximated by a straight line. Further down, overlapping shadows from different shoots lead to reduction in the number of small umbrae. In deeper layers, large umbrae dominate and n_U decreases more slowly with τ, slowing down the decrease in F_U.

The number of umbrae increases rapidly at small τ and has a maximum at $\tau \approx 3$ for *S. viminalis* and at $\tau = 4 \dots 5$ for *S. dasyclados* (Figure 6.8a).

It is obvious that when $\tau = 0$, no phytoelements can occur between the Sun and the sensor, and the number of umbrae as well as umbra fractional area must be zero. However, as in the upper canopy layer the leaf area density $u_L(z)$ is very

small and leaf dimensions are finite, the number of leaves that can shade the Sun is small, and statistical methods prove unreliable. So the regression functions used in this study were chosen keeping in mind the asymptotic case where $\tau \to 0$, but are applicable only when $\tau > 0.5$ for *S. viminalis* and $\tau > 3$ for *S. dasyclados*.

The smaller and narrower leaves of *S. viminalis* generate more small umbrae compared with the larger and wider leaves of *S. dasyclados* (Figure 6.8c,d). The difference becomes less significant in deeper canopy layers where the overlapping shadows of separate shoots generate large umbra areas. For both species, the number-fraction of short umbrae (i.e. the fraction of short umbrae in the total number of umbrae) is larger than 80% in all coppice layers, and short umbrae dominate in upper layers where long umbrae do not exist. The number-fraction of short umbrae decreases linearly for both species, $R^2 = 0.53$ and $R^2 = 0.43$ for *S. viminalis* and *S. dasyclados*, respectively. For *S. viminalis*, the number-fraction of medium-length umbrae increases noticeably with τ, $R^2 = 0.53$ (Figure 6.8c); for *S. dasyclados*, the number-fraction of medium-length umbrae depends weakly on τ; the square of the correlation coefficient of the linear regression shown in Figure 6.8d, $R^2 = 0.15$.

The maximum length of umbrae in the uppermost layers ($\tau = 0.5$) is about 5 cm and increases linearly up to 140 cm at ground level. For mean umbra length, there is no major difference between *S. viminalis* and *S. dasyclados* (Figure 6.8b).

Division of umbrae into three length intervals is somewhat unreliable in upper coppice layers where mutual shadowing by shoot cylinders is not present.

The umbra fractional area k_U, i.e. the total length of umbra per unit scan distance, increases rapidly with τ until $\tau \approx 6$ (Figure 6.9). In deeper layers, umbra makes up from 80% to 90% of total area. In middle layers ($\tau = 3 \ldots 5$) k_U for *S. viminalis* is twice as large as for *S. dasyclados*, probably due to a different leaf area density distribution, whereas in upper layers the difference almost disappears. However, the fraction of umbra is smaller in *S. dasyclados*, indicating more pronounced clumping.

Fast increase in umbra fractional area with increasing τ in middle and deeper layers is caused by cooperative shadowing, as a result of which large areas are created where the Sun is completely shaded by phytoelements.

6.1.3   Penumbra

The mean direct solar irradiance registered during one scan by the sunfleck sensor is

$$\langle S_F \rangle = S_0 k_S + \langle S_{FU} \rangle \, k_U + \langle S_{FP} \rangle \, k_P, \qquad (6.11)$$

where $\langle S_{FU} \rangle$ and $\langle S_{FP} \rangle$ are the mean values of direct solar irradiance, measured in shade and penumbra, respectively; k_S, k_U and k_P are the fractional areas of
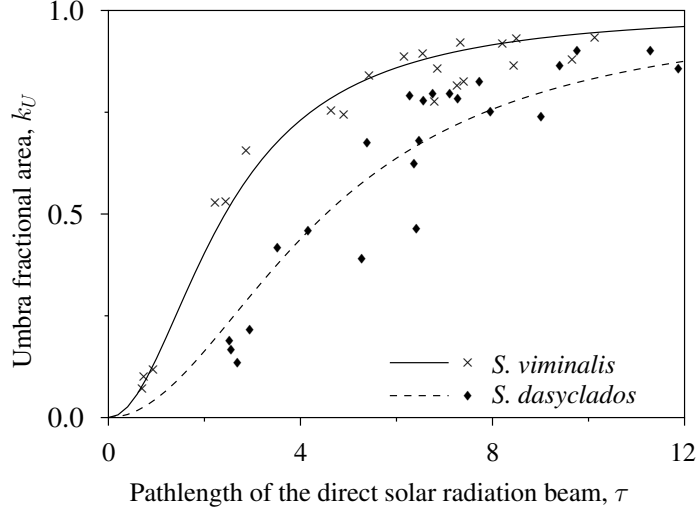
Figure 6.9: Umbra fractional area, k_U, inside the willow coppice as a function of the pathlength τ for *S. viminalis* and *S. dasyclados* together with fitted regression curves $k_U(\tau) = \frac{\tau^2}{a+\tau^2}$, $a = 5.90$ for *S. viminalis* and $a = 20.5$ for *S. dasyclados*.

sunflecks, shade and penumbra, respectively, with the condition

$$k_S + k_U + k_P = 1. \tag{6.12}$$

Irradiance in umbra area is practically zero, $\langle S_{FU} \rangle < 0.007 S_0$. So, neglecting the umbral irradiance, the mean value of direct solar irradiance in penumbra area in Eq. 6.11 is

$$\langle S_{FP} \rangle = \frac{\langle S_F \rangle - k_S S_0}{k_P}, \tag{6.13}$$

and the penetration function of direct solar radiation in penumbra area, $a_P(\tau) = \langle S_{FP} \rangle / S_0$, in accordance with Eq. 6.13, is

$$a_{SP} = \frac{a_S(\tau) - k_S(\tau)}{k_P(\tau)}. \tag{6.14}$$

Thus, the total mean penetration of direct solar radiation in the canopy at the pathlength τ consists of two parts:

$$a_S(\tau) = k_S(\tau) + k_P(\tau) a_P(\tau). \tag{6.15}$$

The first term determines the mean penetration in sunflecks and the latter, penetration in penumbra. Measurements with the sunfleck sensor allow calculation of all terms of Eq. 6.15.
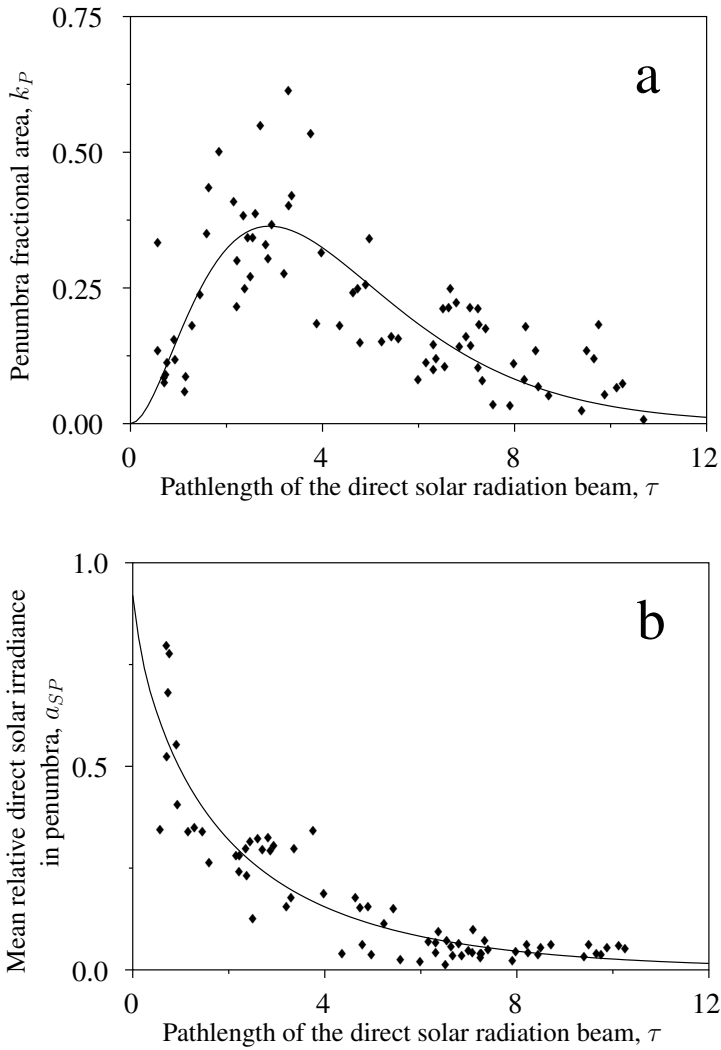
Figure 6.10: a) The penumbra fractional area k_P fitted by the function $k_P = 0.32\tau^2 e^{-0.69\tau}$ and b) the penetration function for direct solar radiation in penumbra a_{SP} inside the *S. viminalis* stand fitted by the function $a_{SP} = 0.92\exp(-0.63\tau^{3/4})$ as functions of the pathlength of the direct solar radiation beam in coppice, τ.
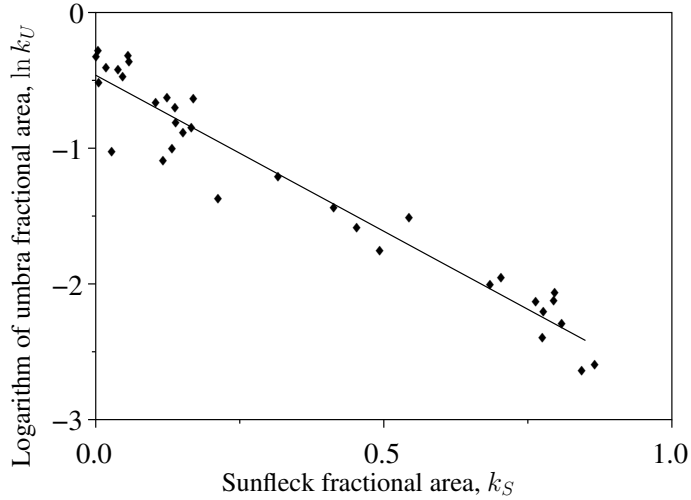
Figure 6.11: Relation between the sunfleck fractional area k_S and the umbra fractional area k_U and the regression function $k_U = 0.63e^{-2.30k_S}$, *S. viminalis*.

The fractional area of penumbra k_P as a function of the pathlength τ (Figure 6.10a) shows that the role of penumbra is greatest in the medium layer where τ is between 2 and 4. The maximum value of k_P is about 0.35. The function $k_P(\tau)$ was approximated by the formula

$$k_P(\tau) = 0.32\tau^2 \exp(-0.69\tau), \ R^2 = 0.60. \tag{6.16}$$

Figure 6.10b expresses the penetration function $a_P(\tau)$ in penumbra area as a function of the pathlength τ and shows that $a_P(\tau)$ decreases exponentially not with τ, but with $\tau^{3/4}$. In the upper canopy layer, penetration in the penumbral area may increase total penetration by about $0.3\ldots0.6$. Penetration in penumbral area reaches the deeper layers (until $\tau = 8\ldots9$) while penetration in sunfleck reaches the depth $\tau \approx 4$ only.

6.1.4 Relation between sunfleck and umbra areas

Calculation shows that there is no correlation between sunfleck length and umbra length, and between the number of sunflecks and umbrae. However, there exists a quite good correlation with $R^2 = 0.94$ between their products: sunfleck fractional area $k_S = N_S \langle l_S \rangle$ and umbra fractional area $k_U = N_U \langle l_U \rangle$ (Figure 6.11). This correlation was fitted by the exponential formula

$$k_U = 0.63 \exp(-2.30k_S\tau), \ R^2 = 0.94, \tag{6.17}$$

81

which shows that sunfleck fractional area increases exponentially with decreasing umbra fractional area.

There exists a specific layer inside the *S. viminalis* coppice ($\tau = 2 \ldots 4$) where the number of sunflecks, penumbra fractional area as well as the number of umbrae (Figures 6.4a,6.8a, 6.10a) reach their maxima. In this layer the maximum number of sunflecks reaches 17 m^{-1}, while the maximum number of umbrae is 18 m^{-1}, i.e. in this layer, the number of umbrae and sunflecks is equal. Penumbrae (Figure 6.10a) too exert the maximum effect in this layer. While sunflecks dominate above this layer, then umbrae together with penumbrae dominate below it.

6.2 Penetration of direct solar radiation

Direct solar radiation is an important component of all radiant energy a plant receives and inside a plant canopy it is also the most variable component of radiation balance: besides dependence on solar height, cloud cover, atmospheric transparency, and other "external" influences, direct solar irradiance depends directly on canopy architecture. As the dependence of photosynthesis on photon flux density is not linear, a good knowledge of penetration of direct radiation is required for an adequate description of productivity of plant stands.

Although the theory of radiative transfer briefly described in Section 5.3 has proved to be very fruitful, the structure inherent in all real plant canopies has a noticeable effect on canopy beam transmittance: clumping tends to increase canopy transmittance while some regular arrangements of leaves can have the opposite effect (Nilson, 1971). Therefore, parameters describing the spatial distribution of foliage or models of plant structure have to be introduced.

The main goals of this subsection are: i) using the distribution of direct solar irradiance, to test whether a quite simple 3D model of willow coppice, describing the coppice as consisting of vertical shoots, can be used to adequately describe the radiation regime of a real-life canopy; and ii) to find the main differences between a 3D model and a simpler random model.

6.2.1 Shoot model

The shoot model describes the willow coppice on 9 September 1998 (first grwing year) as consisting of randomly located vertical shoots. The shoots were divided into height classes using the measured distribution of shoot height (Section 3.6, Figure 3.11b), and the distribution of the intensity of direct solar radiation was calculated inside the shadow of the "average" tree of each class together with the

Table 6.2: Shoot height, maximum diameter, leaf area, and the number of shoots per square meter for the six shoot height classes used for calculations.

no.	height m	max. diameter m	leaf area m^2	shoots per sq. meter m^{-2}
1	1.17	0.28	0.065	2.75
2	1.50	0.33	0.113	4.42
3	1.83	0.37	0.175	3.00
4	2.17	0.41	0.250	3.00
5	2.50	0.44	0.338	5.17
6	2.83	0.47	0.440	2.58

area of the shadow. The locations of the shoots were considered random and independent of each other, and the probability that the sensor lies in the shadow of a shoot or in a manifold shadow of several shoots from the same or different classes was calculated. Thus, the distribution of direct solar radiation for the whole coppice was calculated by superimposing the radiation distributions of single shoots. Shoot height, maximum diameter, leaf area, and the number of shoots per square meter for the six height classes used for calculations are given in Table 6.2.

The shoot was modeled as a vertical stem with flat leaves at a constant inclination angle (Section 3.3). The shape of the shoot was determined from phytometrical measurements: the leaves were attached to the stem at constant intervals starting at relative height $z'_{\min}$ that was determined from measurements (Section 3.4); the size of leaves was chosen such that both the modeled total leaf area and the distribution of leaf area density along the shoot stem would match the measured quantities. The azimuths of leaf midribs were determined from a slightly modified genetic spiral: a small random number was added to the number of leaves per one step of the spiral so the leaves' midribs would not be located in vertical planes. Sinoquet et al. (1991) studied the direction of leaf azimuths and its influence on transmission of modeled maize canopies and found that placing the modeled leaves in vertical planes does not reflect the actual canopy.

The concept of the shoot model is very similar to the forest gap fraction model proposed by Nilson (1999).

6.2.2   Reference model

A second model, called the reference model, was used for simulating a random canopy. In principle, it was a turbid plate medium model with the distributions of

leaf size and orientation taken from the shoot model. The locations of leaves in horizontal directions were random, the vertical coordinates of leaves were generated randomly and transformed to match the measured variation of leaf area with height. Again, the shoot stems were ignored.

The canopies created with the shoot and reference models were very similar, with a certain degree of clumping introduced into the shoot model by the special arrangement of horizontal leaf coordinates; also, a correlation between leaf height and leaf area exists in the shoot model.

For both models, the method of modeling the penetration of direct solar irradiance consisted in calculating whether a foliage element would intercept a line connecting the sensor with a random point inside the solar disk. The number of these points (the number of sunrays) determines the accuracy of the calculation of the distribution of the intensity of direct solar radiation. Leaves were considered opaque and for the calculation of the distribution of direct solar irradiance, the luminosity of the Sun was considered uniform.

Additionally, the following approximations were made in the models: the size of the sensor was not taken into account, and measurements were instantaneous, i.e. the time constant of the imaginary sensor was zero. The effect of these approximations is much more difficult to assess, because besides spatial variation, an unestimated temporal variation of direct solar irradiance existed in the coppice. The overall effect of ignoring the characteristics of the sensor should be towards an underestimation in penumbra fractional area, as using finite sensor dimensions or time constant means averaging the signal over some area or time period.

For both models, the sensor was located at the points of a regularly spaced grid on the horizontal measurement plane at specified height. For the shoot model, the size of the grid was determined from the dimensions of the projection of the cylinder totally encompassing the shoot onto the horizontal plane; for the reference model, it was chosen by evaluating the possible error of modeled radiation characteristics. The number of grid points and the number of points in the solar disc used for calculating the distribution of radiation intensity were also taken large enough to keep model errors reasonable.

To estimate the errors arising from statistical fluctuations due to the limited number of data points, grid size, etc., repeated test runs of the reference model were made. During these test runs, the parameters describing the simulated situation (LAI, solar height, leaf size distribution, etc.) were kept constant and the uncertainty of radiation field characteristics and their standard deviations were calculated at 0.1 significance level. Using the upper confidence limit of the standard deviation, a maximum error estimate was calculated.

These test runs were made with the reference model at the solar zenith angle $\vartheta_S = 45°$ and measurement height $z = 2$ m using the coppice characteristics

Table 6.3: Error estimates of modeled sunfleck and umbra fractional areas (k_S and k_U, respectively) and canopy beam transmittance (a_S) at 0.1 significance level.

quantity	mean	max. error	max. relative error
K_S	0.115	0.017	0.15
K_U	0.650	0.036	0.06
a_S	0.219	0.019	0.08

of the selected day, 9 September 1998. At this height, both umbra and sunflecks exist and radiation field is most variable. The most reasonable model parameters were found to be the following: simulated canopy area (grid size) 1×1 m, the number of grid points 2000, and the number of sunrays 50. Maximum and relative errors for the sunfleck and umbra fractional areas (k_S and k_U, respectively) and canopy beam transmittance a_S are given in Table 6.3. The number of sunrays has an effect on umbra, penumbra and sunfleck fractional areas: the larger the number of sunrays, the smaller are both umbra and sunfleck fractional areas. However, considering the results of the test runs, using 50 sunrays results in an underestimation of umbra, smaller than 5%, and an overestimation of sunflecks of a similar magnitude. At lower canopy levels, the relative errors of a_S and k_S will most likely be higher as these quantities decrease exponentially with the pathlength of solar rays inside the canopy.

Such calculations were not carried out for the shoot model since it involves a second stage of superposing shadows and input parameters were selected considering the reference model's error estimates. In the shoot model, the number of sunrays was 50, the number of grid points 3000, and the number of shoot height classes 6. The size of the grid depended on the dimensions of the shoot's projection onto the measurement plane. As can be seen from Figure 6.14, the results from shoot model, probably due to its more statistical character, are more smooth than the results from the reference model. Thus, the errors from statistical fluctuations are not larger for the shoot model than they are for the reference model.

Umbra and sunfleck thresholds are described in more detail in Section 5.9. As measurement uncertainties are not present in models, the following approach is used here: if all sunrays reach the imaginary sensor, the sensor is in sunfleck; if all rays are intercepted, the sensor is in umbra; otherwise the sensor is in penumbra.

The model's umbra threshold can be calculated from the number of sunrays as follows. Let the probability that n sunrays are transmitted through the canopy and $n_R - n$ are intercepted, where n_R is the number of sunrays used in the model, be $p(n)$. The value of $p(n)$ can be considered to be the probability that the direct

solar irradiance is

$$\left(n - \frac{1}{2}\right)\frac{1}{n_R}S_0 < S < \left(n + \frac{1}{2}\right)\frac{1}{n_R}S_0. \tag{6.18}$$

Thus, taking $n = 0$, $S < \frac{1}{2n_R}$ and

$$\frac{S}{S_0} = \frac{1}{2n_R} \tag{6.19}$$

is the umbra threshold for modeled penetration of radiation. Analogously, taking $n = n_R - 1$ yields $\left(1 - \frac{3}{2n_R}\right)S_0 < S < \left(1 - \frac{1}{2n_R}\right)S_0$ and

$$\frac{S}{S_0} = 1 - \frac{1}{2n_R} \tag{6.20}$$

is the model's sunfleck threshold.

Using $n_R = 50$, Eq. 6.19 yields 0.01 for umbra threshold and Eq. 6.20 yields 0.99 for sunfleck threshold. Comparing these numbers with the thresholds used for measurements (Section 6.2), the following conclusions can be made: i) according to Figure 5.3, the difference between the umbra fractional areas calculated with the thresholds is small; and ii) the use of 0.99 instead of 0.95 for sunfleck threshold for calculating k_S from measurement data would cause significant differences, but these are mainly due to the change in solar height during a scan and the bending of the aluminium bar under the weight of the carriage.

Thus, together with the thresholds given in Section 6.2 of this work, the following thresholds are used:

- umbra threshold $S/S_0 = 0.007$ for measured irradiances, and $S/S_0 = 0.01$ for modeled irradiances;

- sunfleck threshold $S/S_0 = 0.95$ for measured irradiances, and $S/S_0 = 0.99$ for modeled irradiances.

6.2.3   Results

In 1998, there were few days with low cloud, and 9 September was the only completely cloudless day when radiation measurements were carried out in the willow coppice. A total of 36 scans were made during that day inside *S. viminalis* stand between 8 a.m. and 3 p.m. apparent solar time at solar zenith angles $\vartheta_S = 53\ldots68°$. Twenty-one scans were used to test the model, ten scans were discarded due to data logging problems, and five scans were made above the coppice.
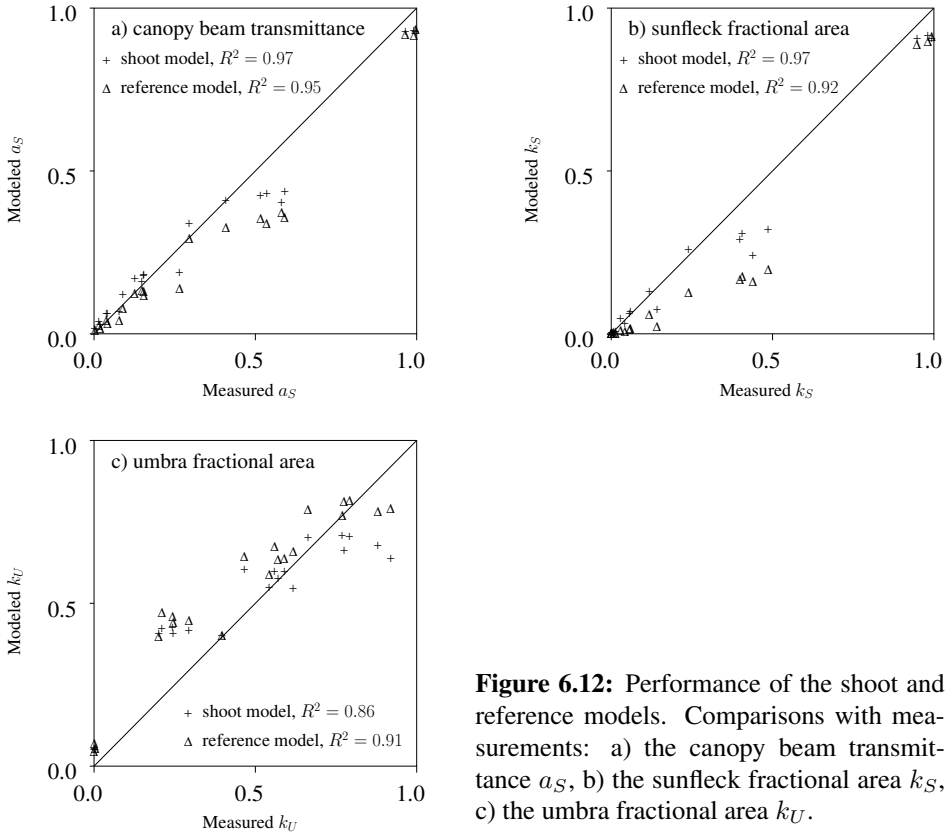
Figure 6.12: Performance of the shoot and reference models. Comparisons with measurements: a) the canopy beam transmittance a_S, b) the sunfleck fractional area k_S, c) the umbra fractional area k_U.

To illustrate the performance of the shoot and reference models, the modeled canopy beam transmittance, and sunfleck and umbra fractional areas are plotted against the measured values in Figure 6.12. The R^2 of the reference model is almost equal to that of the more complex shoot model with the shoot model performing only marginally better, and a better insight into the model's performance is given with the analysis of the intensity distribution histograms presented below. Also, the range of the solar zenith angles that could be used is unfortunately very small.

Despite the large correlation coefficients, Figure 6.12 demonstrates quite a large scatter. The largest differences in the modeled and measured values for a_S and k_S are for $a_S \gtrsim 0.5$ and $k_S \approx 0.5$, respectively. For k_U, the difference is large at $k_U \approx 0.3$. This group of data points in all three figures corresponds to the measurements made at $z = 2.0$ m. This indicates a departure from the mathematical description of the willow coppice: the differences can be due to a discrepancy between the real and predicted shape of a few shoots located between
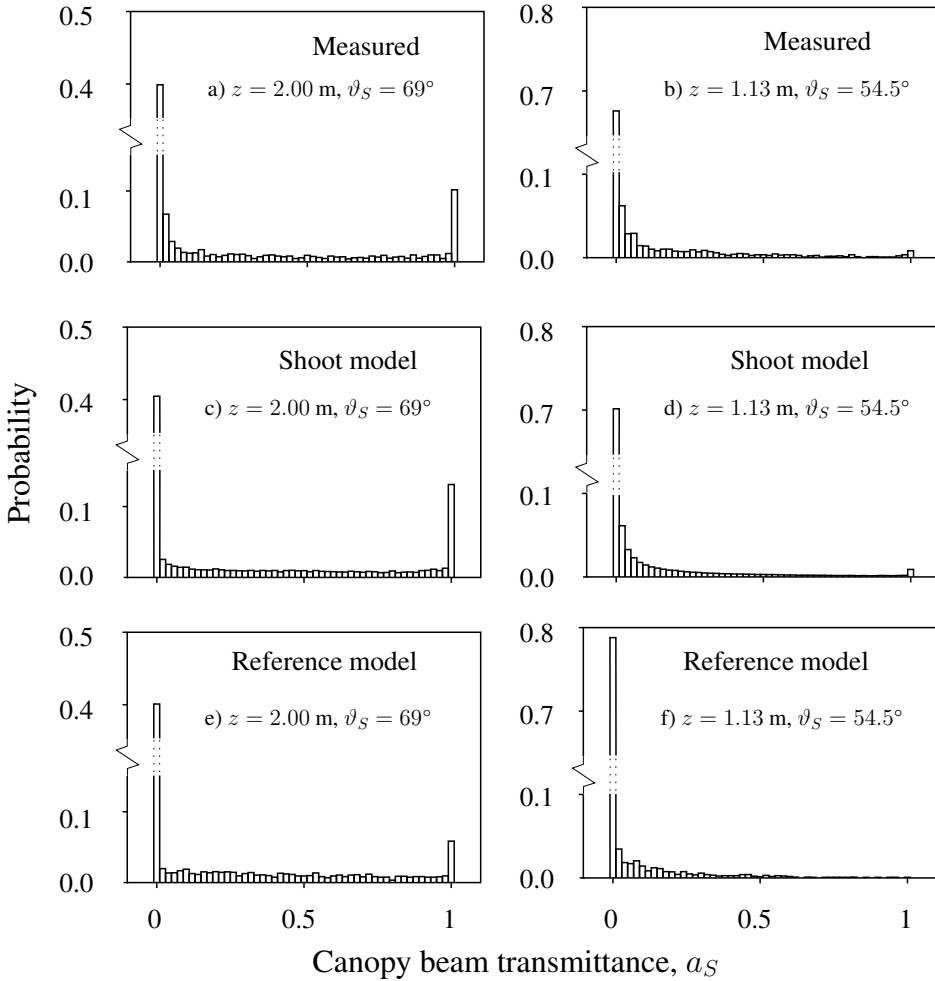
Figure 6.13: Distribution of the canopy beam transmittance a_S inside willow coppice. The left-hand sub-figures show results for a height, $z = 2.0$ m and solar zenith angle, $\vartheta_S = 69°$ and the right-hand sub-figures for $z = 1.13$ m and $\vartheta_S = 54.5°$.

the sensor and the Sun or a non-uniform distribution of shoots in some area close to the measurement system. Also, the length of the bar (6 m) may be inadequate for a good statistical picture of the radiation field, especially at large z, where the number of leaves between the sensor and the Sun is small.

Two measured distributions of direct solar irradiance inside the willow coppice out of the total of 21 are shown in Figure 6.13 together with model results; additional data for the scans shown in Figure 6.13 and four scans made at small solar zenith angles are given in Table 6.4. In Figure 6.13, the normalized value of

Table 6.4: Modeled and measured radiation characteristics for selected scans: solar zenith angle ϑ_S, measurement height z, downward cumulative leaf area index $L(z)$, canopy beam transmittance a_S, and sunfleck fractional area k_S. The measured and modeled canopy transmittance distributions of the first and third scan are shown in Figure 6.13.

			measured		reference model		shoot model	
ϑ_S	z (m)	$L(z)$	a_S	k_S	a_S	k_S	a_S	k_S
69.0°	2.00	1.17	0.295	0.12	0.293	0.058	0.338	0.13
54.3°	0.37	4.97	0.0191	0	0.0157	0	0.0304	0.0003
54.5°	1.13	3.78	0.0780	0.013	0.0388	0.0003	0.0687	0.009
54.2°	1.60	2.34	0.265	0.14	0.137	0.022	0.188	0.077
53.9°	2.00	1.17	0.591	0.49	0.358	0.20	0.437	0.32
55.1°	2.60	0.09	0.991	0.98	0.915	0.90	0.932	0.92

direct solar irradiance, or the canopy beam transmittance a_S, is used; the number of bins in the histograms is 51.

As can be seen from Figure 6.13 and Table 6.4, the shoot model's transmittance is close to the measured values and to the value produced by the reference model, also, the shapes of all three irradiance distribution histograms are similar. However, the shoot model seems to give slightly better results, especially in the darker end of penumbra. The distribution generated by the reference model has a more uniform distribution of irradiance in penumbra compared with both the measured and the shoot model's distributions. Also, the fraction of sunflecks is better estimated by the shoot model for both scans.

The distribution of irradiance inside the coppice simulated by the shoot model is quite similar to that of the reference model. Close to the top of the canopy where the number of leaves between the Sun and the sensor is small, the sensor is mainly in full sunshine. At small solar zenith angles, almost no penumbra exists as the leaves are close to the sensor the change from sunfleck to umbra occurs over very short distances. When the Sun is closer to the horizon, penumbra fractional area increases and the radiation distribution in penumbra has a maximum at high irradiances.

The distribution of irradiance in penumbra, calculated using the reference model, tends to be more uniform compared with the distributions with well-defined maxima produced by the shoot model.

While the shape of the irradiance distribution in penumbra is similar, the predictions for the canopy beam transmittance a_S and the fractional areas of sunfleck k_S, penumbra k_P, and umbra k_U can be quite different.
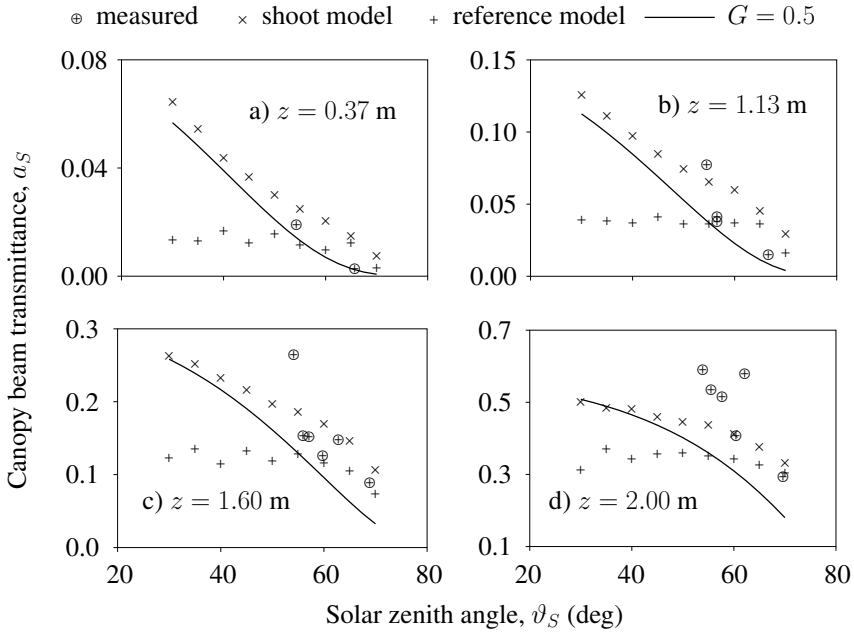
Figure 6.14: Dependence of the canopy beam transmittance a_S on the solar zenith angle ϑ_S for four heights, z, inside the canopy. $G = 0.5$ is the theoretical curve for a random canopy.

The dependence of the canopy beam transmittance a_S on solar zenith angle at four levels inside the coppice is depicted in Figure 6.14. Together with the modeled results, the measured transmittances and a theoretical curve, calculated from Eq. 5.21, are shown. The theoretical curve corresponds to a totally random canopy with no preferred leaf directions or positions.

The shoot model predicts that the canopy beam transmittance a_S decreases with increasing solar zenith angle, while the reference model predicts that it remains almost constant until $\vartheta_S \approx 60°$. The theoretical G-function of the model canopy described by Eq. 3.12 is inversely proportional to $\cos\vartheta_S$ for $0 < \vartheta_S < 59.7°$, and thus the transmittance, calculated from Eq. 5.21, does not depend on ϑ_S at small zenith angles. As is expected, when calculating transmittance, the reference model behaves like a spatially random canopy. The transmittance of the shoot model, on the other hand, depends also on the clumping of the foliage. The difference between the two models is relevant only at $\vartheta_S < 65°$ and can be ignored at larger solar zenith angles. Also, the difference is larger in lower canopy layers. As can be seen from Figure 6.14, the minimum ϑ_S for 9 Septem-

ber is larger than 55° and the measurements are in the range where the difference between the two models is small.

The simplest way to estimate leaf area index from radiation measurements is by solving Eq. 5.21 for $L(z)$. Eq. 5.21 is based on the assumption of spatially uniform distribution of foliage that is used as a simplification when no information is available about the actual canopy. For a single measurement, inverting Eq. 5.21 requires the knowledge of $G(\vartheta_S)$. A natural choice would be $G = 0.5$ that is valid for a random canopy, although several other empirical distributions have been described (Ross, 1981). When measurements under various solar zenith angles are available, it is possible to retrieve an estimate of the distribution of leaf normals, calculate $G(\vartheta_S)$ and use that for calculating $L(z)$ (e.g., van Gardingen et al., 1999).

If such measurements of canopy transmittance were carried out under (or inside, at height z) the theoretical canopy described by the shoot model and canopy transmittance were inverted to obtain $L(z)$, the results could be deceptive. E.g., for $z = 0.37$ m (Figure 6.14a), measured $L(z) = 4.97$; taking $G = 0.5$ and fitting Eq. 5.21 to the modeled data using the least squares method yields $L(z) = 4.69$, $R^2 = 0.98$.

As the difference between the transmittances of the shoot model and a random canopy is small, if the leaves of the canopy were harvested and the true LAI determined, the index determined from radiation measurements using $G = 0.5$ would be corroborated. However, the dependence of the shoot model's a_S on ϑ_S at $\vartheta_S < 59.7°$ is a result of clumping, not leaf orientation, and cannot be modeled using Eq. 5.21. The similarity of the transmittance of a random canopy and that of the shoot model is a coincidence that demonstrates the effects of 3D canopy structure on beam transmittance. Although results coincide for this special foliage arrangement, another foliage distribution could result in a considerable error: for the shoot and reference models, at $z = 0.37$ m and $\vartheta_S = 30°$, the transmittance of the shoot model is about four times higher than the transmittance of the reference model.

According to the shoot model, the effect of clumping depends on both the height inside the coppice z (or $L(z)$) and the solar zenith angle ϑ_S. As can be seen from Figure 6.14, the relative difference between the shoot and reference models is largest at small ϑ_S and small z. At small solar zenith angles, the lower leaves are shaded by higher leaves of the same shoot and radiation is less effectively attenuated. At larger zenith angles, the shoot is illuminated from the side and clumping is less evident. As the pathlength of rays in the coppice increases with increasing ϑ_S, the average number of shoots a ray has to pass through rises and the probability of passing through none decreases. As the difference between the
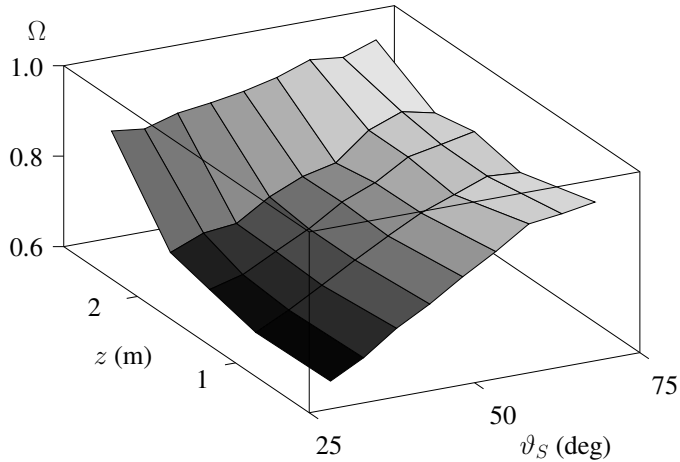
Figure 6.15: The clumping index Ω as a function of the solar zenith angle ϑ_S and the height z calculated from the shoot model.

models decreases also with z, a decrease in the probability of a photon passing through a gap between the shoots results in a decrease in clumping.

The dependence of the clumping index Ω (Section 5.5) on the solar zenith angle ϑ_S and the height z calculated with the shoot model is depicted in Figure 6.15. Ω varies from 0.63 to 0.96 with lower values obtained in deeper canopy layers at small ϑ_S and large values at both large z and large ϑ_S. Considering that for a random canopy, $\Omega = 1$, this result is consistent with conclusions from the analysis of Figure 6.14.

For the shoot model, the increase in canopy transmittance is caused by the aggregation of leaves into vertical structures, which is not uncommon for natural canopies. But in many cases the preferred orientation of such "foliage containers" may be different, e.g. for leaves attached to branches, or non-existent, e.g. for the shoots of conifers. According to Chen and Black (1991), branch structure has a significant effect in broadleaved forests.

As Ω depends substantially on both ϑ_S and z, it cannot be considered a fundamental parameter of canopy architecture that can be used to relate leaf area density to the attenuation of radiation. Instead, it has to be treated as a function of more basic canopy parameters, related to the arrangement of foliage elements.

Although the statistical analysis presented above does not favor one model over the other, the shoot model seems to perform better than the reference model: in Figure 6.14, for smaller solar zenith angles ($\vartheta_S \approx 53°$), the shoot model can predict canopy beam transmittance better than the reference model. At larger ϑ_S, the difference between the models is small or nonexistent. Use of measure-

ments made at smaller solar zenith angles, i.e. for the middle of days nearer mid-summer, is required for making the final conclusion; unfortunately, no such measurements were carried out in 1998.

6.3 Vertical profile of radiation fluxes

The work described in this section was done to compare the results of measurements with two models, a solution of the radiative transfer equation (Eq. 5.17) using the exact kernel discrete ordinates method, and a Monte Carlo model. Also, an attempt was made to include the effect of clumping on the penetration of direct solar radiation into the radiative transfer model.

For this purpose, radiation measurements carried out under clear conditions during two periods with a sufficient number of measurement scans were used: 21 and 22 July 1997, and 9 September 1998.

On 21 and 22 July 1997, canopy height was 6 m and LAI was 8.0, measurements were carried out at the following fixed levels inside the coppice: 0.62, 2.28, 3.30, 3.92, and 5.32 m above the ground. On 9 September 1998, the height of the willow coppice was 3 m and its leaf area index was 5.0, measurement heights were 0.37, 1.13, 1.60, 2.00, and 2.60 m. The total number of measurements was 41 on 21 and 22 July 1997, and 25 scans were made on 9 September 1998.

Varying the model parameters resulted in six different modeling results for each measurement. The solar spectrum was divided into two regions, photosynthetically active radiation (PAR, 400–700 nm) and near-infrared radiation (NIR, 700–2500 nm). The flux densities measured by the quantum PAR sensors were modeled in a single model run; flux densities measured by the pyranometers were modeled as sums of radiative energy in the PAR and NIR regions.

Models were used to simulate every measurement situation—measured data was used for solar zenith angle, ratios of diffuse to direct radiation flux above the canopy and surface albedos for PAR and NIR regions. The ground was modeled as a Lambertian surface, i.e. radiation was scattered isotropically.

The influence of different diffuse sky conditions on downward diffuse PAR flux is represented in Figure 6.16. The different distributions of diffuse sky irradiance were calculated using the CIE models briefly described in Section 5.7.

Sky luminance approximately corresponds to radiation intensity in the PAR region, in the infrared region, sky is darker and the distribution of diffuse intensity less important. Thus, only calculations using the PAR reflectance and transmittance values are used in Figure 6.16. The values of diffuse fluxes are normalized to unity, i.e diffuse fluxes are compared with those above the canopy.

According to Figure 6.16, the effect of changing the modeled situation from completely overcast to low turbidity diffuse sky with large intensity gradients
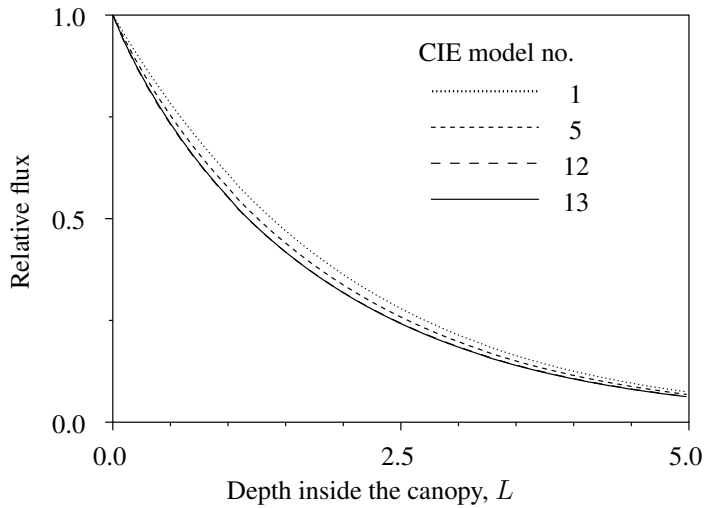
Figure 6.16: Dependence of downward diffuse PAR flux (diffuse sky + scattered inside the canopy) as a function of the downward cumulative leaf area index L for different distributions of diffuse sky radiation. Calculations were made with the discrete ordinates method ($\vartheta_S = 50°$, $G \equiv 0.5$, surface albedo 0.2). Modeled fluxes for models 12 and 13 practically coincide.

CIE model	description
1	CIE Standard Overcast Sky. Steep luminance gradation towards zenith, azimuthal uniformity
5	Sky of uniform luminance
12	CIE Standard Clear Sky, low illuminance turbidity
13	CIE Standard Clear Sky, polluted atmosphere

has a minimal influence on the modeled fluxes and are ignored in the current study; in both PAR and NIR, the intensity of diffuse sky radiation is considered independent of view direction. Diffuse radiation inside the willow stand is much more influenced by the ratio of diffuse to direct radiation, the value of which is taken from measurements for each model run.

In July 1997 and September 1998, the ratio of diffuse to direct radiation flux above the canopy varied between 0.3 and 0.6 for PAR and between 0.03 and 0.18 for NIR; surface albedos were 0.05–0.25 and 0.1–0.4 for PAR and NIR, respectively; the solar zenith angle ϑ_S varied from 38° to 60° on 21 and 22 July 1997 and from 53° to 68° on 9 September 1998.

Both models were written in the C++ programming language.

6.3.1   Discrete ordinates model

The radiation field in a homogeneous plant canopy as a function of the downward cumulative leaf area index L (Eq. 2.2) is given by Eq. 5.17. As L is monotonously decreasing with the height z, the dependence of any quantity on L is described as its dependence on height.

The mean projection of unit foliage area on the plane normal to the direction of photon travel $G(\mathbf{\Omega})$ can be calculated from the measured distribution of leaf normals (Section 3.3); the leaf area scattering phase function $\Gamma(\mathbf{\Omega}' \rightarrow \mathbf{\Omega})$ depends on leaf transmittance and reflectance (Section 5.6), and also on the distribution of leaf normals. Thus, both G and Γ can be calculated from the measured characteristics of the willow canopy.

The discrete ordinates method of solving Eq. 5.17 is based on using discrete directions $\mathbf{\Omega}_i$ and solving the obtained system of coupled differential equations. In plant canopies where scattering and absorption depend on the direction $\mathbf{\Omega}$, no analytical solutions exist and thus iterative methods are commonly used and the canopy is divided into a number of layers. A good description of the method and the problems involved is given by Myneni et al. (1991).

As direct solar radiation arrives from a very small solid angle often approximated by a delta-function, its intensity is much larger than that of radiation arriving from other directions; also, the direction of direct solar radiation need not coincide with any direction of the cubature chosen for solving Eq. 5.17. It is common to separate direct radiation (and often also first order scattering of diffuse sky radiation) and to add a source term to Eq. 5.17:

$$-\mu_i \frac{\partial I(L, \mathbf{\Omega}_i)}{\partial L} + G(\mathbf{\Omega}_i) I(L, \mathbf{\Omega}_i) =$$

$$= \frac{1}{\pi} \sum_{j=1}^{N} w_j I(L, \mathbf{\Omega}_J) \Gamma(\mathbf{\Omega}_j \rightarrow \mathbf{\Omega}_i) + Q(L, \mathbf{\Omega}_i),$$

$$i = 1 \ldots N. \quad (6.21)$$

The equation of radiative transfer is now given for the discrete directions (or cubature) $\mathbf{\Omega}_i$, N is the number of directions in the cubature, w_j are the weights of the cubature, and I denotes only the intensity of diffuse radiation. If only direct solar radiation is separated (ie., I in Eq. 6.21 denotes the sum of diffuse sky radiation and radiation scattered by foliage elements), the source term can be written as

$$Q(L, \mathbf{\Omega}_i) = \frac{1}{\pi} I_0(L) \Gamma(\mathbf{\Omega}_0 \rightarrow \mathbf{\Omega}_i), \qquad (6.22)$$
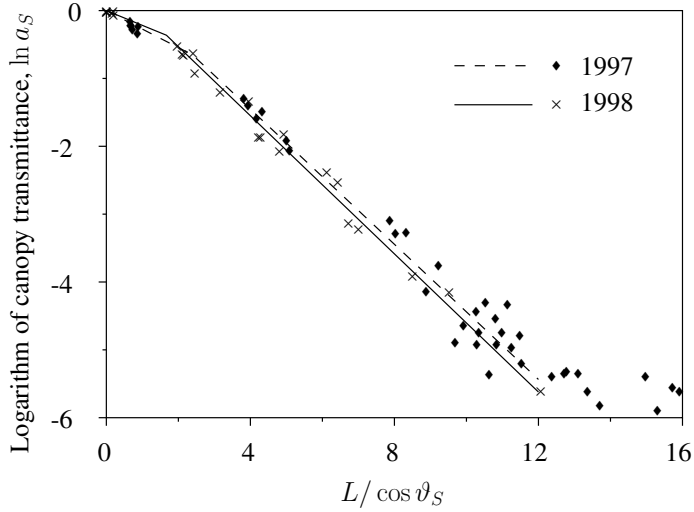
Figure 6.17: Effect of clumping on canopy transmittance: logarithm of the canopy beam transmittance $\ln a_S$ as a function of $L/\cos\vartheta_S$, where L is downward cumulative leaf area index and ϑ_S is solar zenith angle, on 21 & 22 July 1997 and 9 September 1998 measured inside the *S. viminalis* coppice. See text for approximation formulae.

where $I_0(L)$ is the intensity of direct solar radiation at height L and $\mathbf{\Omega}_0$ is the direction of sunrays.

Several formulae for calculating the intensity of direct solar radiation $I_0(L)$ are given in Section 6.2. Two approximations were used in the discrete ordinates model:

1. The most simple case of homogeneous canopy, where direct solar radiation can be calculated from the equation of radiative transfer, Eq. 5.20.

2. Clumped canopy, canopy clumping is described by the clumping index $\Omega(L)$ (Eq. 5.31).

The clumping index is basically an *ad hoc* correction factor for matching the measured and calculated transmittances. For the willow canopy, it can be calculated using measured canopy transmittance. Graphically, $\Omega(L)$ is the slope of $\ln a_S$ plotted against $G(\vartheta_S)L/\cos\vartheta_S$.

In Figure 6.17, $\ln a_S$ is plotted against $L/\cos\vartheta_S$, the slope of the line gives $G(\vartheta_S)\Omega(L,\vartheta_S)$. As the dependence is clearly non-linear, the following approximations were used:

$$\begin{cases} \ln a_S = -0.277L/\cos\vartheta_S, & L/\cos\vartheta_S < 2.40 \\ \ln a_S = 0.539 - 0.498L/\cos\vartheta_S, & L/\cos\vartheta_S > 2.40 \end{cases} \qquad (6.23)$$

for July 1997, and

$$\begin{cases} \ln a_S = -0.0917L/\cos\vartheta_S, & L/\cos\vartheta_S < 1.17 \\ \ln a_S = 0.487 - 0.509L/\cos\vartheta_S, & L/\cos\vartheta_S > 1.17 \end{cases} \quad (6.24)$$

for September 1998. Although the dependence of $\ln a_S$ on $L/\cos\vartheta_S$ is remarkably similar for the two days, different formulae were used as no explanation can be given for the change of $\Omega(L, \vartheta_S)$ at small values of L. This change has to be a consequence of canopy structure, which was not similar for the two years. Using a mean solar zenith angle, the location of the in-continuity in canopy structure can be specified: $L \simeq 1.6$ for July 1997 and $L \simeq 0.6$ for September 1998.

The effect of saturation evident in Figure 6.17 at large values of LAI in July 1997 was ignored in fitting the regression line (Eq. 6.23); thus this equation is only valid up to $L/\cos\vartheta_S \simeq 12$. Such saturation at large values of L has been noted before as described in Section 5.8. However, in the saturated region, canopy transmittance is about 0.3% and the saturation effect in Figure 6.17 may be due to measurement uncertainties or the view configuration of the sunfleck sensor.

The clumping index $\Omega(L, \vartheta_S)$ can be incorporated into the equation of radiative transfer. Using the principle of conservation of intensity (or, equivalently, energy), if the attenuation of radiation changes by the factor $\Omega(L, \vartheta)$ (Eq. 5.31), the area scattering phase function has to be multiplied by the same factor, $\Gamma_C(\boldsymbol{\Omega} \rightarrow \boldsymbol{\Omega}') = \Omega(L, \vartheta_S)\Gamma(\boldsymbol{\Omega} \rightarrow \boldsymbol{\Omega}')$. The source function (Eq. 6.22) now becomes

$$Q(L, \boldsymbol{\Omega}_i) = \frac{1}{\pi}I_0(L)\Gamma_C(\boldsymbol{\Omega}_0 \rightarrow \boldsymbol{\Omega}_i) = \frac{1}{\pi}I_0(L)\Omega(L, \vartheta_S)\Gamma(\boldsymbol{\Omega}_0 \rightarrow \boldsymbol{\Omega}_i). \quad (6.25)$$

Naturally, clumping has a similar effect on the right hand side of the radiative transfer equation (Eq. 5.17), but the effect of clumping is difficult to measure for other values of the zenith angle ϑ; also, the intensity of diffuse radiation is generally much smaller than that of direct solar radiation, and the effect of clumping on diffuse radiation is ignored here.

The weights w_i in Eq. 5.17 depend on the chosen cubature. In the current work, the cubature is chosen to have equal weights, i.e. the directions of the cubature are evenly distributed on the sphere (Fliege and Maier, 1996).

Four different parameter sets were used to model the radiation field inside the willow stand with the radiative transfer approach:

1. Canopy clumping was taken into account for direct solar radiation (Eqs. 5.33 and 6.25), distribution of leaf inclinations was approximated by the normal distribution (see Section 3.3).

2. Canopy clumping was taken into account for direct solar radiation, distribution of leaf normals was spherical ($G(\vartheta) \equiv 0.5$).

3. No clumping ($\Omega(L, \vartheta_S) \equiv 1$), distribution of leaf inclinations approximated by the normal distribution.

4. No clumping, spherical distribution of leaf normals.

For all four cases, the radiative transfer equation (Eq. 5.17) was solved iteratively using the exact kernel discrete ordinates method with 240 directions and 50 canopy levels (see Myneni et al., 1991 for a description of the method).

6.3.2   Monte Carlo model

The Monte Carlo method is based on calculating the fluxes by tracing photons in a simulated *S. viminalis* canopy. The canopy was constructed using measurements of canopy structure and allometric relations valid for that period. First, the shoots were counted and their heights were measured. As 1998 was the first growing year, all shoots started from the ground. In 1997, shoots started from previous-year stems; so their base heights were also measured. Approximations were used to simulate the measured distributions in the model; allometric relations were then used to calculate the leaf area and its distribution for each computer-generated shoot. The locations of leaves on the stem were calculated and the areas of leaves were taken such as to match the measured leaf area distribution. The shape of the leaf was described using Eq. 3.6, shoots were considered vertical.

Although in 1997, shoots were attached to previous-year stems, this structure is extremely difficult to model with sufficient variability, so the horizontal components of shoot locations were calculated using a random number calculator. The number of shoots per square meter was 46 in 1997 and 22 in 1998. The modeled leaf area density resembled closely that shown in Figure 3.12.

Photons were then traced as they entered the canopy from both the direction of the Sun (direct photons) or from randomly generated directions in the upper hemisphere (diffuse photons). Reflections and transmissions from leaves were calculated using the bi-Lambertian model (Section 5.6) using a random number generator, each photon was traced until it was either absorbed by the canopy or the soil, or exited the canopy as reflected radiation. Photons exiting through the sides of the modeled coppice reentered from the opposite side at the same height and in the same direction with the reentry point randomly shifted in the horizontal direction. To calculate flux densities, photons passing through predetermined horizontal surfaces inside the canopy corresponding to measurement heights were counted.

The simulation area was a 4 by 4 m square with an appropriate buffer zone for eliminating edge effects, containing more than 740 shoots when modeling the stand in 1997 or more than 360 shoots when modeling the canopy in 1998. To keep model errors within reasonable limits (see next section), the number of stand configurations generated for modeling PAR and NIR fluxes varied between 8 and 16, the total number of photons used for each spectral interval varied between 40,000 and 60,000.

Similarly to the radiative transfer model, two parameter sets were used:

5. Distribution of leaf inclinations was approximated by the normal distribution.

6. Distribution of leaf normals was spherical.

6.3.3   Model error

The error of the radiative transfer model arises from discretizations. The number of directions and canopy levels is sufficient to consider this model exact, uncertainties of determining the $L(z)$ values of measurement heights have a considerably larger effect on modeling results compared with discretization errors.

The same can not be said about the Monte Carlo model. Here, two types of uncertainties exist. Firstly, an uncertainty in modeled flux densities is due to the small number of photons reaching the bottom of the canopy, especially in 1997 when LAI was 8. Secondly, a specific realization of canopy structure may not be similar to the natural situation at the radiation measurement site despite a similar dependence of u_L on z; again, this uncertainty was larger for 1997 when an additional parameter, the distribution of shoot base height, was used.

To estimate these uncertainties, several model runs were made with different number of photons using the same modeled stand structure, and using a fixed number of photons for a large number of computer-generated canopies. The relative errors of the models depended linearly on the logarithm of the modeled quantity, the larger the measured quantity, the smaller the relative error. This is due to the fact that if the modeled fluxes were small, the number of modeled photons was also small and random variations were thus relatively large. The standard deviation of the canopy beam transmittance a_S was estimated to be 1.5–9%, the standard errors of the flux densities were 1–9%, 1–4%, 5–25% and 5–25% for the downward global flux density Q, the downward PAR flux density PAR(Q), the upward global flux density R, and the upward PAR flux densityPAR(R), respectively.

6.3.4 Results and discussion

The modeled values of the canopy transmittance a_S and the densities of the global downward flux Q, the downward PAR flux $\text{PAR}(Q)$, the upward global flux R, and the upward PAR flux $\text{PAR}(R)$ are plotted against the measured values in Figures 6.18 to 6.22. The numbers of the models correspond to the descriptions in Sections 6.3.1 and 6.3.2. Each figure has four subfigures:

a) 21 and 22 July 1997, radiative transfer models (models 1–4).

b) 21 and 22 July 1997, Monte Carlo models (models 5,6).

c) 9 September 1998, radiative transfer models (models 1–4).

d) 9 September 1998, Monte Carlo models (models 5,6).

At a fixed solar zenith angle, all the measured and modeled quantities are decreasing monotonic functions of L and increasing monotonic functions of z. Thus, 'at small values of the modeled quantity' is equivalent to saying 'in deep canopy layers.'

Root mean squared errors were calculated for all models using the equation

$$\text{RMSE}(x) = \sqrt{\frac{\sum_{i=1}^{N}(x_{\text{model}} - x_{\text{measured}})^2}{N}}, \qquad (6.26)$$

where N is the number of modeled measurement scans and x is the modeled quantity (a_S, Q, R, $\text{PAR}(Q)$ or $\text{PAR}(R)$); RMSE values are given in Table 6.5.

Figure 6.18 describes canopy transmittance, the measured values are the same as in Figure 6.17. The models 1 and 2 that include canopy clumping produce the same transmittance values as model transmittance is given as an input parameter. Due to the scatter in Figure 6.17, the results are not perfect but as expected, these two models outperform others.

As expected, the radiative transfer models without clumping, models number 3 and 4, underestimate transmittance due to clumping. The Monte Carlo models 5 and 6 generally do a better job, as is also evident from RMSE values (Table 6.5).

The effect of clumping is not very large in the *S. viminalis* canopy. In the middle and deeper canopy layers, both in July 1997 and September 1998, the slope of $\ln a_S$ plotted against $L/\cos\vartheta_S$ is almost equal to 0.5 (Figure 6.17, Eqs. 6.23 and 6.24) corresponding to a non-clumped canopy with uniformly distributed leaf normals. If the distribution of leaf normals is approximated by the normal distribution as described in Section 2.2, $G > 0.5$ for $\vartheta_S \lesssim 60°$, as is the case for most measured transmittances, and the slope of 0.5 can indicate minimal clumping.
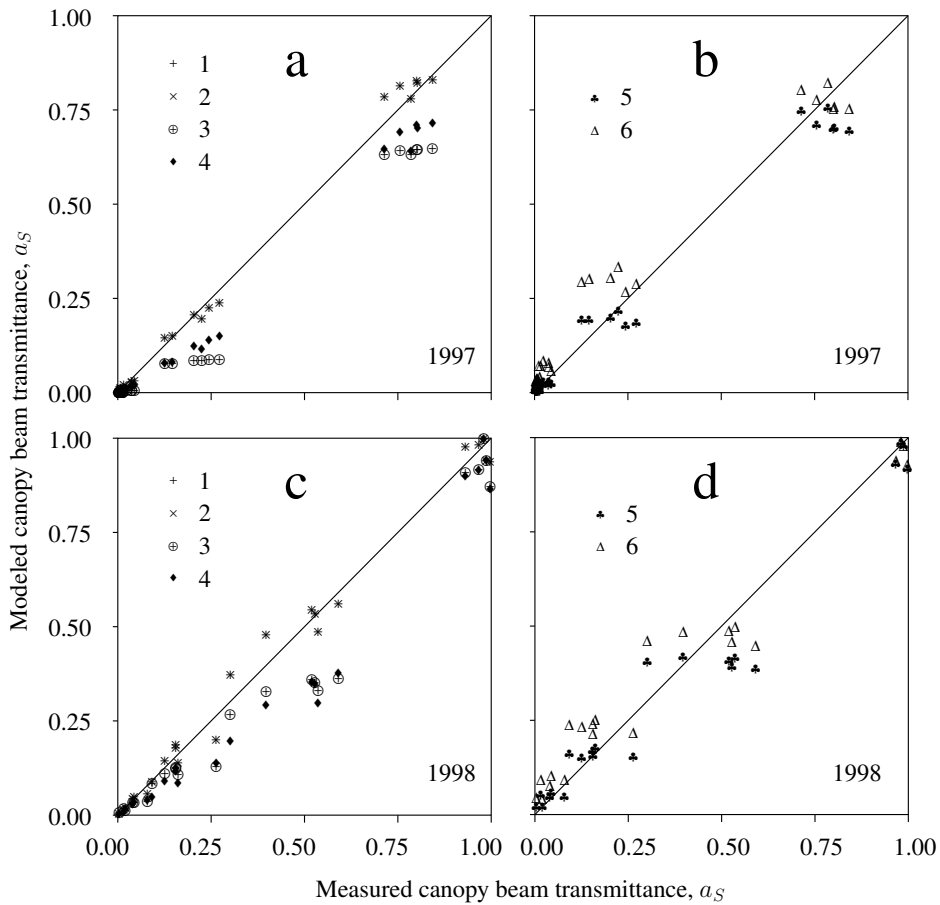
Figure 6.18: Direct solar transmittance of the *S. viminalis* canopy modeled using discrete ordinates (1–4) and Monte Carlo (5,6) models for mid-July 1997 (a,b) and mid-September 1998 (c,d). See article text for model descriptions.

However, in upper canopy layers, the effect of clumping is clearly evident. It may be due to the large number of young leaves located at the tip of the shoot as this phenomenon can also be seen in other measurements inside the willow coppice made at various times during the foliated season. Clearly, at the top of the canopy, only a few shoots extend above the measurement system and the variation in L along the transect is large. Still, the author could not construct any canopy models describing the coppice as consisting of vertical shoots that could describe such a change in stand structure.

Therefore, there is a possibility that this change is a result of variations in the specific leaf area (or leaf area per unit mass) or other undetected variations in similar parameters at the tip of the shoot.

Some uncertainties in the measurements of radiation flux densities are also evident in Figure 6.18: in Figures 6.18c and d, the dispersion near $a_S = 1$ is partially caused by the differences in the readings of the sensors on the carriage and those used for background measurements. As the carriage moved along the aluminium bar, the bar bent under its weight and the sensors were not strictly horizontal any more.

On the other hand, as measurements were made at the same heights each day, the models simulate quite similar situations more than once. As can be seen in Figures 6.18b and d (and also in later figures), the scatter of the Monte Carlo modeling results is not much larger than that of the radiative transfer models; thus the modeling errors are within reasonable limits. This claim may not be valid in deeper canopy layers, but as the fluxes are small there, the absolute values of errors remain small despite the large relative errors and have a small effect on the RMSE values in Table 6.5.

Figure 6.19 describes the measured and modeled downward flux densities of global radiation Q. As the contribution of direct solar radiation is large for downward fluxes, especially at upper canopy layers, the results are quite analogous to those of a_S: models 1 and 2 produce very similar, although not identical results; models 3 and 4 underestimate global downward flux at $Q < 0.3$ Wm^{-2}; in July 1997, the underestimation is quite large (Figure 6.19a). The Monte Carlo models 5 and 6 (Figure 6.19b,d) perform better, especially in September 1998, when the results are spread evenly around the 1:1 line. The underestimation, especially at smaller heights, is partly due to the saturation of canopy transmittance evident in Figure 6.17, but the effect of clumping is also clearly present.

The modeled vs. measured downward PAR flux densities are shown in Figure 6.20. Here, the most surprising fact is that while the global flux and canopy transmittance were modeled quite well for July 1997, all models underestimate the downward PAR flux in the upper part of the canopy (Figure 6.20a,b). In the lower part, the Monte Carlo models (Figure 6.20b) produce better results, but radiative transfer models underestimate PAR in the whole canopy (Figure 6.20a). Theoretically, PAR(Q) depends more on direct transmittance than Q as scattered radiation should be small in this spectral interval—as is the case in September 1998, when models 1 and 2 (Figure 6.20c) produce almost identical results and both perform very well. Again, in the lower part of the canopy, models 3 and 4 underestimate the PAR flux (Figure 6.20c).

The modeled upward global flux densities R are plotted against the measured values in Figure 6.21. Near the bottom of the canopy, the reflected flux density
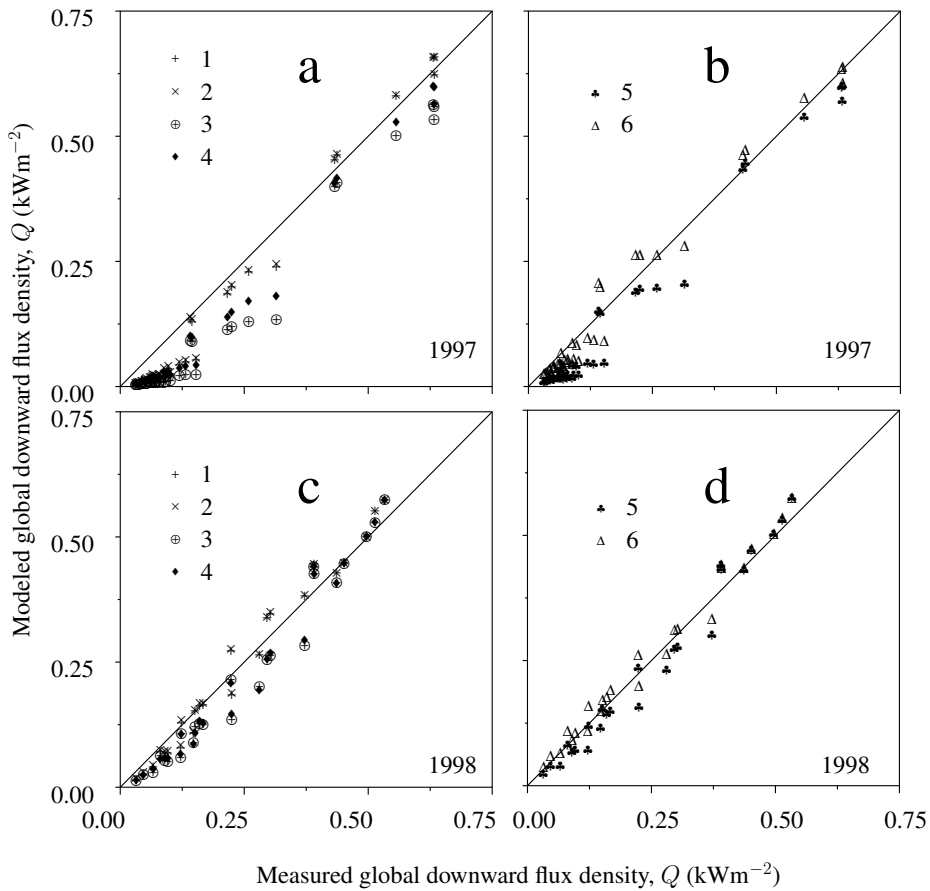
Figure 6.19: Downward global radiation flux densities inside the *S. viminalis* canopy modeled using discrete ordinates (1–4) and Monte Carlo (5,6) models for mid-July 1997 (a,b) and mid-September 1998 (c,d). See article text for model descriptions.

R is related to the downward flux density Q as the underestimation of the latter evidently led to the underestimation of the former (Figure 6.21a,b). Again, Monte Carlo models seem to perform better. For modeling the upward flux, the inclusion of the clumping index into the equation of radiative transfer improves the estimate in 1997, but in 1998, radiative transfer models without clumping perform generally better; thus, the effect of clumping on upward fluxes remains unclear.

A significant difference between the two leaf inclination approximations used in the radiative transfer model is evident in the upward PAR flux density, PAR(R)

Figure 6.20: Downward PAR flux densities inside the *S. viminalis* canopy modeled using discrete ordinates (1–4) and Monte Carlo (5,6) models for mid-July 1997 (a,b) and mid-September 1998 (c,d). See article text for model descriptions.

(Figure 6.22a,c). However, in the Monte Carlo simulations, the two inclination models give similar results (Figure 6.22b,d). Generally, the predictions for the PAR fluxes are more inaccurate than estimations of other fluxes. Although the downward PAR fluxes for July 1997 are underestimated, the upward PAR fluxes are predicted quite accurately. For September 1998, Monte Carlo models underestimate the upward PAR flux while the predictions of radiative transfer models stray to both sides of the 1:1 line.

The RMSE values given in Table 6.5 give a quantitative measure of the model's performance, but this number should be handled with care as it does
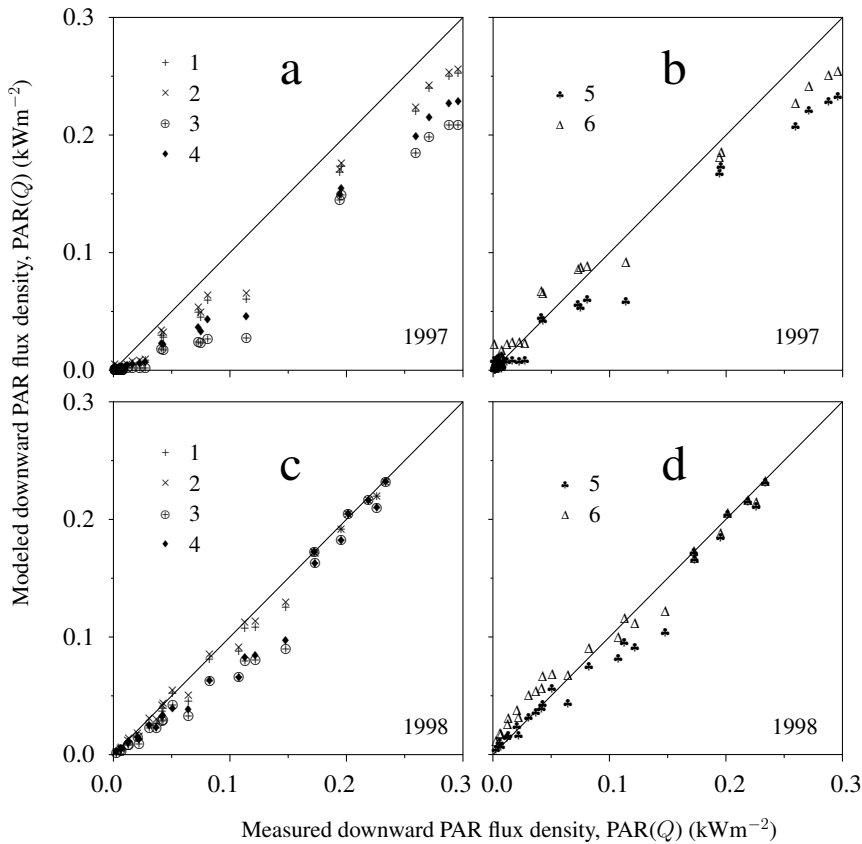
Figure 6.21: Upward global flux densities inside the *S. viminalis* canopy modeled using discrete ordinates (1–4) and Monte Carlo (5,6) models for mid-July 1997 (a,b) and mid-September 1998 (c,d). See article text for model descriptions.

describe the type of disagreement between the measured and modeled values. However, as expected, the RMSE values for canopy transmittance are the smallest for models 1 and 2; also, inclusion of clumping (models 1,2) improves the estimates of downward global radiation and PAR fluxes. There is no single model type that outperformed others when modeling upward radiation. For modeling global downward radiation, the Monte Carlo model with uniform leaf inclination (6) had the smallest RMSE value, but in modeling downward PAR flux, there was no clear winner.

Generally, the Monte Carlo models 5 and 6 that included explicit information of canopy structure tended to give slightly better results; the introduction of the
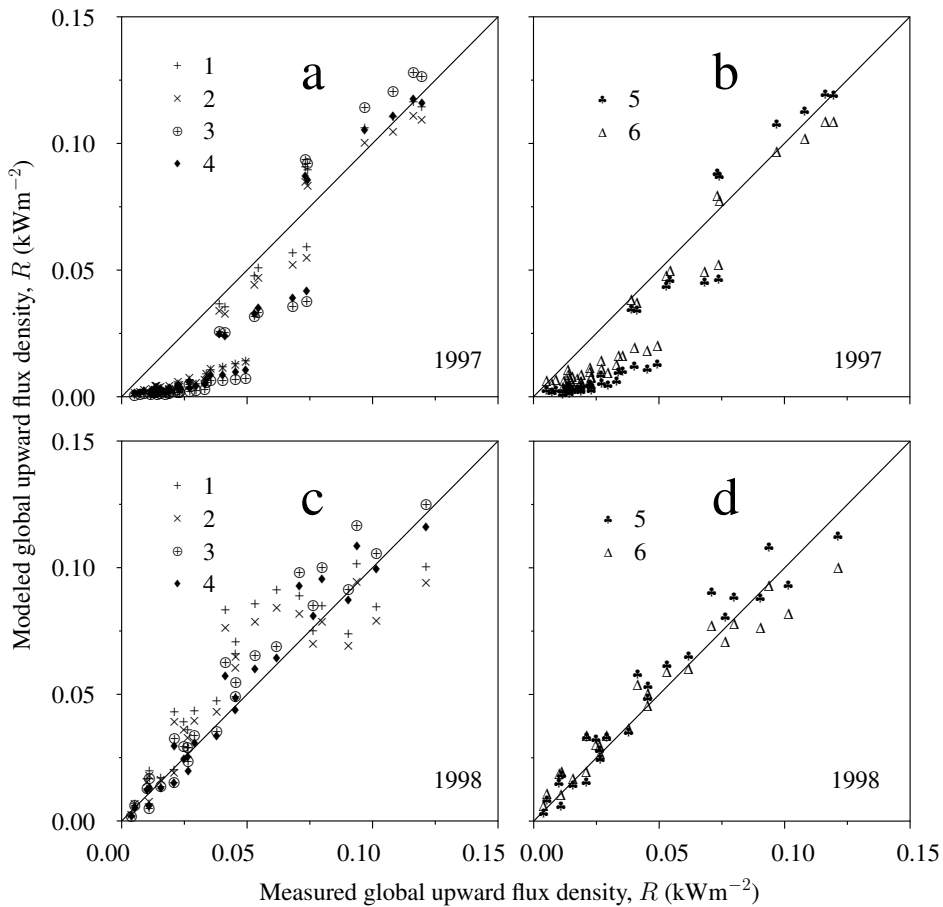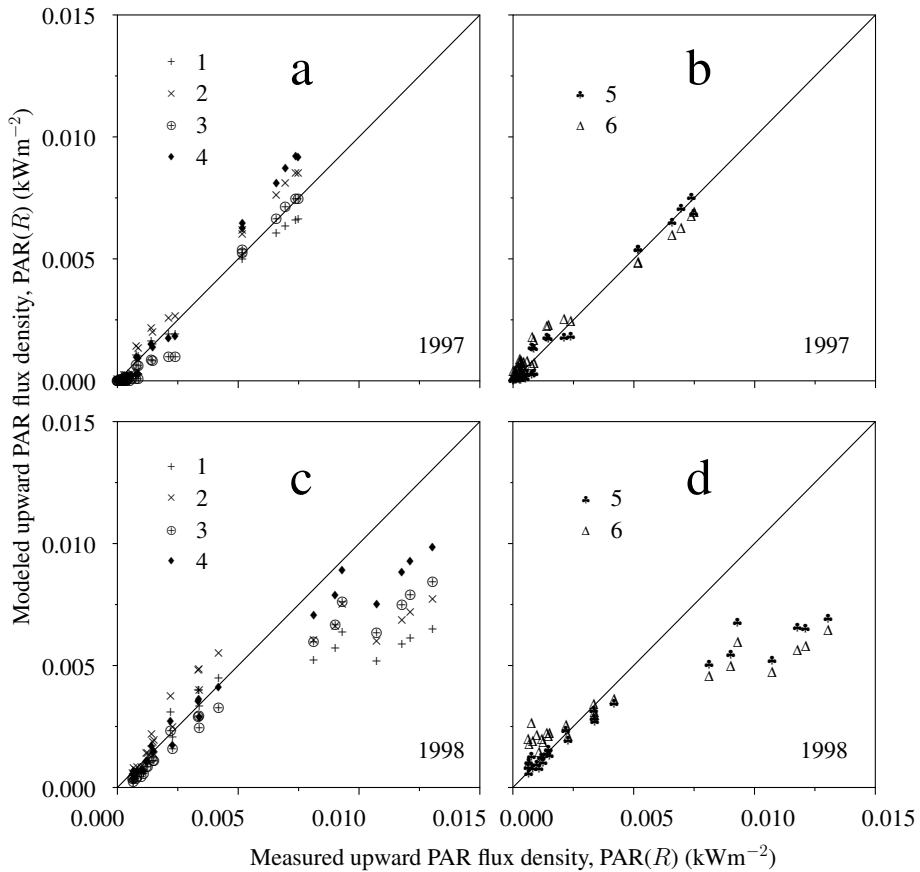
Figure 6.22: Upward PAR flux densities inside the *S. viminalis* canopy modeled using discrete ordinates (1–4) and Monte Carlo (5,6) models for mid-July 1997 (a,b) and mid-September 1998 (c,d). See article text for model descriptions.

clumping index into the radiative transfer model also improved performance at the cost of having some prior knowledge of the radiation field.

The effect of leaf orientation is small and it is difficult to prefer one model of leaf inclination over the other; an unexpected exception is the upward PAR flux (Figure 6.22) modeled using the four radiative transfer models.

The models' predictions for the upward flux densities R and PAR(R) were not as good as predictions for downward fluxes. This may be partly due to inaccuracies in determining leaf transmittance and reflectance as these fluxes consist of scattered radiation, but as the modeled fluxes err in both directions, this is not

Table 6.5: Model root mean square errors (RMSE) for measurements in July 1997 and September 1998. See article text for explanation of model numbers. a_S is canopy transmittance, Q global downward flux density, PAR(Q) downward PAR flux density, R global upward flux density, PAR(R) upward PAR flux density.

model	a_S	Q kW m^{-2}	PAR(Q) kW m^{-2}	R kW m^{-2}	PAR(R) kW m^{-2}
			21 & 22 July 1997		
1	0.0180	0.0481	0.0177	0.0166	0.0003
2	0.0180	0.0445	0.0159	0.0164	0.0005
3	0.0755	0.0736	0.0341	0.0211	0.0004
4	0.0537	0.0588	0.0271	0.0192	0.0006
5	0.0400	0.0494	0.0213	0.0171	0.0003
6	0.0542	0.0283	0.0145	0.0131	0.0004
			9 September 1998		
1	0.0361	0.0305	0.0084	0.0173	0.0026
2	0.0361	0.0300	0.0063	0.0149	0.0022
3	0.0905	0.0442	0.0207	0.0107	0.0019
4	0.0978	0.0427	0.0188	0.0079	0.0013
5	0.0784	0.0320	0.0137	0.0082	0.0025
6	0.0804	0.0247	0.0128	0.0084	0.0029

the major factor. Clearly, not every detail of the radiation field or fluctuation in canopy structure can be described by any of these models.

7   CONCLUSIONS

The willow coppice whose structure and radiation regime was under investigation in this thesis is a compact and, both optically and physically, a dense medium. Although the extinction of direct solar radiation is similar to that inside a completely random canopy, ignoring the structure of the canopy can lead to wrong estimations of the regime of photosynthetically active radiation and misinterpretations of both transmitted and reflected radiation fluxes. The role of canopy structure is evident in the distribution of direct solar irradiance in penumbra, the differences in umbra length distributions between the two willow species, *S. viminalis* and *S. dasyclados*, and in the influence of clumping on canopy transmittance.

Modeling canopy structure

Generally, the measured canopy transmittance (Figure 6.17) agrees well with the measured $u_L(z)$, but the origin of large clumping at small $L(z)$ evident in this figure is unclear. Also, the shoot structure of the willow coppice can be modeled using the measured characteristics of the canopy. During the first growing year, the method is quite straight-forward, but as shoots are attached to previous-year stems from the second year on, the model becomes more complicated.

The effect of stand structure is evident in both Monte-Carlo models and models based on the equation of radiative transfer. Although the simplifying assumptions used may decrease the accuracy of the canopy model, the results obtained corroborate the correctness of the basis of the stand model. Whether adding more variables, like shoot inclination angle, would improve the model, is open for discussion, but it would clearly make the interpretation of the effects of stand structure on radiation field more complex.

Sunfleck and umbra length

Because of the extreme complexity of natural canopies, analytical models fail to give the distribution of solar radiation in plant canopies with sufficient accuracy.

In upper canopy layers, the total number of umbrae is larger for *S. viminalis* than for *S. dasyclados*. The initially large number of short umbrae inside the *S. viminalis* coppice decreases more rapidly with $L/\cos\vartheta_S$ than inside the *S. dasyclados* coppice. At the same time, starting from $L/\cos\vartheta_S = 5\ldots6$, about 60% of total umbra in *S. dasyclados* is contributed by long umbrae, about 10% by short umbrae and only 30% by medium-length umbrae. On the ground under the *S. dasyclados* coppice, large umbra areas appear to be separated by intervals of short penumbrae, where radiation density changes rapidly. In the four-years-old

S. viminalis coppice, the amount of umbra contributed by medium-length umbrae is larger, since individual shoots allow sunrays to penetrate among them.

It is surprising that at the same pathlength $L/\cos\vartheta_S$, the wider leaves of *S. dasyclados*, located closer to the ground, allow more penumbra to fall onto the transect than do the narrow leaves of *S. viminalis*. This is a certain evidence of a major difference in the stand architecture of the two species. Differences in the number of umbrae and in the fraction of medium-length umbrae suggest that umbra distribution at ground surface can be used for estimation of the geometrical characteristics of a plant stand. However, as the two species with relatively similar characteristics demonstrate quite a different behavior, the correlation between umbra fraction and plant architecture is not a simple one.

An important methodological problem is how to perform the statistical data processing. The measurement system enables to use a maximum averaging length of 12 m. However, Figure 6.2 shows that the obtained sample size is too small for sufficiently exact determination of probability density distribution characteristics. Calculations (not given here) show that for willow coppice an averaging length of about 50–70 m would be required.

Penetration of direct solar radiation

Considering the modeled and measured distributions of direct solar irradiance inside the willow coppice (Figure 6.13), the modeling approach used to describe the structure of willow coppice gave good results. Although the measurements were carried out under a restricted range of solar zenith angles, the following conclusions drawn from the models should hold for real canopies under a wider range of solar zenith angles.

The shoot model, introduced to describe the structure of the coppice canopy, alters the fractional areas of penumbra, umbra and sunfleck. The effect of the different descriptions of the canopy structure is clearly seen by comparing the transmittances of the shoot and reference models in Figure 6.14.

In the dense *S. viminalis* canopy, the fractional area of sunflecks diminishes rapidly after solar radiation enters the canopy and the role of penumbra as the region where direct solar irradiance is above zero is important in most canopy layers.

While the shape of the simulated distribution of irradiance in penumbra is realistic in both the shoot model and the simpler reference model, considering the different fractional areas, the radiation regime of a leaf is quite different in the two models. The effect of clumping as introduced by attaching the leaves to an imaginary shoot stem cannot be described by a constant clumping index—the clumping index depends on solar zenith angle and measurement height.

Vertical profile of radiation fluxes

Although below the topmost canopy layer the attenuation of direct solar radiation by the willow coppice is similar to that of a random canopy, clumping is evident also in deeper canopy layers as homogeneous models underestimate downward fluxes.

It can be concluded that to some extent, the Monte Carlo models do describe clumping inside the willow canopy. This improvement comes at the cost of a much larger computation time, and Monte Carlo models are also generally non-invertible. Most likely, the use of Monte Carlo models will be restricted to scientific research aimed at a better understanding of the radiation field inside a plant canopy and also to evaluation of other canopy radiative transfer models.

Inclusion of the clumping index Ω (Eq. 5.32) into the equation of radiative transfer (Eq. 5.17), although improving model estimates, is difficult to justify theoretically. However, if measured data on canopy transmittance are available, it should be used, but the *ad hoc* nature of this approach should be kept in mind.

Although the models performed reasonably well, several unexpected results were obtained for different components of the radiation field. Despite the fact that the theory of radiative transfer is quite well-known and its application straightforward, small changes may give unexpected differences in some measurable quantities. Whether these differences are important or not, depends on the problem, but they should at least be considered for each particular case.

REFERENCES

Ahmad, F., Oppenheimer, S., Razzaghi, M., 2003. A discrete bidirectional reflectance model in remote sensing. J. Quant. Spectrosc. Radiat. Transfer 77, 335–343.

Alados-Arboledas, L., Olmo, F. J., Pérez, M., 2000. Parametric models to estimate photosynthetically active radiation in Spain. Agric. For. Meteorol. 101, 187–201.

Andrieu, B., Ivanov, N., Boissard, P., 1995. Simulation of light interception from a maize canopy model constructed by stereo plotting. Agric. For. Meteorol. 75, 103–119.

Anisimov, O., Fuchansky, L., 1997. Optics of vegetation: implications for the radiation balance and photosynthetic performance. Agric. For. Meteorol. 85, 33–49.

Antyufeev, V. S., Marshak, A. L., 1990a. Monte Carlo method and transport equation in plant canopies. Remote Sens. Environ. 31, 183–189.

Antyufeev, V. S., Marshak, A. L., 1990b. Inversion of Monte Carlo model for estimating vegetation canopy parameters. Remote Sens. Environ. 33, 201–209.

Asner, G. P., 1998. Biophysical and biochemical sources of variability in canopy reflectance. Remote Sens. Environ. 64, 234–253.

Asner, G. P., Wessman, C. A., 1997. Scaling PAR absorption from the leaf to landscape level in spatially heterogeneous ecosystems. Ecol. Model. 103, 81–97.

Asner, G. P., Wessman, C. A., Schimle, D. S., Archer, S., 1998. Variability in leaf and litter optical properties: implications for BRDF model inversions using AVHRR, MODIS, and MISR. Remote Sens. Environ. 63, 243–257.

Beyschlag, W., Ryel, R. J., Caldwell, M. M., 1995. Photosynthesis of vascular plants: assessing canopy photosynthesis by means of simulation models. In: Schulze, E.-D., Caldwell, M. M. (Eds.), Ecophysiology of Photosynthesis. Springer-Verlag, Berlin Heidelberg, 409–430.

Björkman, O., Demmig-Adams, B., 1995. Regulation of photosynthetic light energy capture, conversion, and dissipation in leaves of higher plants. In: Schulze, E.-D., Caldwell, M. M. (Eds.), Ecophysiology of Photosynthesis. Springer-Verlag, Berlin Heidelberg, 17–48.

Black, T. A., Chen, J.-M., Lee, X., Sagar, M., 1991. Characteristics of shortwave and longwave irradiances under a Douglas-fir forest stand. Can. J. For. Res 21, 1020–1028.

Bonhomme, R. Varlet-Grancher, C., 1978. Estimation of the gramineous crop geometry by plant profiles including leaf width variations. Photosynthetica 12, 193–196.

Campbell, G. S., Norman, J. M., 1998. Introduction to Environmental Biophysics. 2nd ed. Springer-Verlag, New York.

Castro, F., Fetcher, N., 1999. The effect of leaf clustering in the interception of light in vegetal canopies: theoretical considerations. Ecol. Model. 116, 125–134.

Chandrasekhar, S., 1960. Radiative Transfer. Dover Publications, New York.

Chelle, M., Andrieu, B., 1998. The nested radiosity model for the distribution of light within plant canopies. Ecol. Model. 111, 75–91.

Chen, J. M., 1996. Optically-based methods for measuring seasonal variation of leaf area index in boreal conifer stands. Agric. For. Meteorol. 80, 135–163.

Chen, J. M., Black, T. A., 1991. Measuring leaf-area index of plant canopies with branch architecture. Agric. For. Meteorol. 57, 1–12.

Chen, J. M, Black, T. A., 1992. Defining leaf area index for non-flat leaves. Plant Cell Environ. 15, 421–429.

Chen, S. G., Ceulemans, R., Impens I., 1994. A fractal-based Populus canopy structure model for the calculation of light interception. For. Ecol. Manage. 69, 97–110.

Chen, J. M., Cihlar, J., 1995a. Plant canopy gap-size analysis theory for improving optical measurements of leaf-area index. Appl. Optics 34, 6211–6222.

Chen, J. M., Cihlar, J., 1995b. Quantifying the effect of canopy architecture on optical measurements of leaf area index using two gap size analysis methods. IEEE Trans. Geosci. Remote Sens. 33, 777–787.

Chen, S. G., Shao, B. Y., Impens, I., 1993. A computerised numerical experimental study of average solar radiation penetration in plant stands. J. Quant. Spectrosc. Radiat. Transfer 49, 651–658.

Chen, S. G., Shao, B. Y., Impens, I., Ceulemans, R., 1994. Effects of plant canopy structure on light interception and photosynthesis. J. Quant. Spectrosc. Radiat. Transfer 52, 115–123.

Darula, S., Kittler, R., 2003. CIE general sky standard defining luminance distributions. The Canadian conference on building energy simulation, Montreal, September 11th - 13th, 2002.

Denholm, J. V., 1981. The influence of penumbra on canopy photosynthesis. I Theoretical considerations. Agric. Meteorol. 25, 145–166.

Demarez, V., Gastellu-Etchegorry, J.-P., Mordelet, P., Tosca, C., Marty, G., Guillevic, P., 2000. Modeling of the radiation regime and photosynthesis of a finite canopy using the DART model. Influence of canopy architecture assumptions and border effects. Agronomie 20, 259–270.

España M., Baret, F., Chelle, M., Aries, F., Andrieu, B., 1998. A dynamic model of maize 3D architecture: an application to the parameterisation of the clumpiness of the canopy. Agronomie 18, 609–627.

España M., Baret, F., Aries F., Andrieu B., Chelle, M., 1999a. Radiative transfer sensitivity to the accuracy of canopy structure description. The case of a maize canopy. Agronomie 19, 241–254.

España M., Baret, F., Aries, F., Chelle, M., Andrieu, B., Prévot, L., 1999b. Modeling maize canopy 3D architecture. Application to reflectance simulation. Ecol. Model. 122, 25–43.

Falster, D. S., Westoby, M., 2003. Leaf size and angle vary widely across species: what consequences for light interception? New Phytol. 158, 509–525.

Fournier, R. A., Landry, R., August, N. M., Fedosejevs, G., Gauthier, R. P., 1996. Modelling light obstruction in three conifer forests using hemispherical photography and fine tree architecture. Agric. For. Meteorol. 82, 47–72.

Fournier, C., Andrieu, B., 1998. A 3D architecture and process-based model of maize development. Ann. Bot. 81, 233-250.

Fröhlich, C., 2000. Observations of irradiance variations. Space Sci. Rev. 94, 15–24.

Ganapol, B. D., Johnson, L. F, Hlavka, C. A., Peterson, D. L., Bond, B., 1999. LCM2: a coupled leaf/canopy radiative transfer model. Remote Sens. Environ. 70, 153–166.

van Gardingen, P. R., Jackson, G. E., Hernandez-Daumaz, S., Russell, G., Sharp, L., 1999. Leaf area index estimates obtained for clumped canopies using hemispherical photography. Agric. For. Meteorol. 99, 243–257.

Génard, M., Baret, F., Simon, D., 2000. A 3D peach canopy model used to evaluate the effect of tree architecture and density on photosynthesis at a range of scales. Ecol. Model. 128, 197–209.

Gerstl, S. A. W., Zardecki, A., 1985. Coupled atmosphere/canopy model for remote sensing of plant reflectance features. Appl. Optics 24, 94–103.

Gerstl, S. A. W., Simmer, C., Powers, B. J., 1986. The canopy hot-spot as crop identifier. In: Damen, M. S. J., Sicco Smit G., Verstappen, H. T. (Eds.), Remote Sensing for Resources Development and Environmental Management. Proceedings of the 7th International Symposium, Enschede, 25–29 August 1986. A. A. Balkema, Rotterdam.

Gobron, N., Pinty, B., Verstraete, M. M., Govaerts, Y., 1997. A semidiscrete model for the scattering of light by vegetation. J. Geophys. Res. Atmosph. 102(D8), 9431–9446.

Gower, S. T, Kucharik, C. J., Norman, J. M., 1999. Direct and indirect estimation of leaf area index, f_{APAR}, and net primary production of terrestrial ecosystems. Remote Sens. Environ. 70, 29–51.

Grier, C. C., Lee, K. M., Archibald, R. M., 1984. Effect of urea fertilization on allometric relations in young Douglas-fir trees. Can. J. For. Res. 14, 900–904.

Gueymard, C., 1989. A two-band model for the calculation of clear sky solar irradiance, illuminance, and photosynthetically active radiation at the Earth's surface. Solar Energy 43, 253–265.

Howell, T. A., Meck, D. W., Hatfield, J. L., 1983. Relationship of photosynthetically active radiation to shortwave radiation in the San Joaquin Valley. Agric. Meteorol. 28, 157–175.

Ivanov, N., Boissard, P., Chapron, M., Andrieu, B., 1995. Computer stereo plotting for 3-D reconstruction of a maize canopy. Agric. For. Meteorol. 75, 85–102.

Jacquemoud, S., Baret, F., 1990. PROSPECT: a model of leaf optical properties spectra. Remote Sens. Environ. 34, 75–91.

Jacquemoud, S., Ustin, S.L., 2001. Leaf optical properties: a state of the art. Proc. 8th International Symposium Physical Measurements & Signatures in Remote Sensing. Aussois (France), 8–12 January 2001, CNES, 223–232.

Jonckheere, I., Fleck, S., Nackaerts, K., Muys, B., Coppin, P., Weiss, M., Baret, F., 2004. Review of methods for in situ leaf area index determination. Part I. Theories, sensors and hemispherical photography. Agric. For. Meteorol. 121, 19–35.

Karalis, J. D., 1989. Characteristics of direct photosynthetically active radiation. Agric. For. Meteorol. 48, 225–234.

Kimes, D., Gastellu-Etchegorry, J., Estève, P., 2002. Recovery of forest canopy characteristics through inversion of a complex 3D model. Remote Sens. Environ. 79, 320–328.

Kimes, D. S., Norman, J. M., Walthall, C. L., 1985. Modeling the radiant transfers of sparse vegetation canopies. IEEE Trans. Geosci. Remote Sens. GE-23, 695–704.

Kimes, D. S, Ranson, K. J., Smith, J. A., 1980. A Monte Carlo calculation of the effects of canopy geometry on PhAR Absorption. Photosynthetica 14, 55–64.

Kimes, D. S., Smith, J. A., 1980. Simulation of solar radiation absorption in vegetation canopies. Appl. Optics 19, 2801–2811.

Knyazikhin, Y., Marshak, A., 1991. Fundamental equations of radiative transfer in leaf canopies, and iterative methods for their solution. In: Myneni, R. B., Ross, J. (Eds.), Photon-Vegetation Interactions: Applications in Optical Remote Sensing and Plant Ecology. Springer-Verlag, Berlin, 11–43.

Knyazikhin, Y., Marshak, A., Myneni, R. B., 1992. Interactions of photons in a canopy of finite-dimensional leaves. Remote Sens. Environ. 39, 61–74.

Kucharik, C. J., Norman, J. M., Gower, S. T., 1998. Measurements of leaf orientation, light distribution and sunlit leaf area in a boreal aspen forest. Agric. For. Meteorol. 91, 127–148.

114

Kuusk, A., 2001. A two-layer canopy reflectance model. J. Quant. Spectrosc. Radiat. Transfer 71, 1–9.

Kuusk, A., Nilson, T., 2000. A directional multispectral forest reflectance model. Remote Sens. Environ. 72, 244–252.

Kvet, J., Marshall, J. K., 1971. Assessment of leaf area and other assimilating plant surfaces. In: Šestak, Z., Čatsky, J., Jarvis, P. G. (Eds.), Plant Photosynthetic Production, Manual and Methods. Dr. W. Junk N. V. Publishers, The Hague, 517–555.

Lang, A. R. G., 1991. Application of some of Cauchy's theorems to estimation of surface areas of leaves, needles and branches of plants, and light transmittance. Agric. For. Meteorol 57, 157–170.

Lang, A. R. G. and Xiang, Y., 1986. Estimation of leaf area index from transmission of direct sunlight in discontinuous canopies. Agric. For. Meteorol. 55, 191–212

Lang, A. R. G., Xiang, Y., Norman, J. M., 1985. Crop structure and the penetration of direct sunlight. Agric. For. Meteorol. 35, 83–101.

Larcher, W., 1995. Physiological Plant Ecology. 3rd ed. Springer-Verlag, Berlin Heidelberg.

Lewis P., 1999. Three-dimensional plant modelling for remote sensing simulation studies using the Botanical Plant Modelling System. Agronomie 19, 185–210.

Li, X., Strahler, A. H., 1986. Geometric-optical bidirectional reflectance modeling of a conifer forest canopy. IEEE Trans. Geosci. Remote Sens. GE-24, 906–919.

Li, X., Strahler, A. H., 1992. Geometric-optical bidirectional reflectance modeling of the discrete crown vegetation canopy: Effect of crown shape and mutual shadowing. IEEE Trans. Geosci. Remote Sens. 30, 276–292.

Liang, S., Strahler, A. H., Jin, X., Zhut, Q., 1997. Comparisons of radiative transfer models of vegetation canopies and laboratory measurements. Remote Sens. Environ. 61,129–138.

Liangrocapart, S., Petrou, M., 2002. A two-layer model of the bidirectional reflectance of homogeneous vegetation canopies. Remote Sens. Environ. 80, 17–35.

Mann, J. E., Curry, G. L., 1977. A sunfleck theory for general foliage location distributions. J. Math. Biol. 5, 87–97.

Mann, J. E., Curry, G. L., Hartfiel, D. J., Demichele, D. W., 1977. A general law for direct sunlight penetration. Math. Biosci. 34, 63–78.

Miller, E. E., Norman, J. M., 1971a. A sunfleck theory for plant canopies. I. Lengths of sunlit segments along a transect. Agron. J. 63, 735–738.

Miller, E. E., Norman, J. M., 1971b. A sunfleck theory for plant canopies. II. Penumbra effect: intensity distributions along sunfleck segments. Agron. J. 63, 739–743.

Miller, J. B., 1967. A formula for average foliage density. Aust. J. Bot. 15, 141–144.

Moon, P., Spencer, D. E., 1942. Illumination from a non-uniform sky. Trans. Illum. Engng Soc., N. Y. 37, 707–712.

Mõttus, M., 2004. Measurement and modelling of the vertical distribution of sunflecks, penumbra and umbra in willow coppice. Agric. For. Meteorol. 121, 79–91.

Mõttus, M., Ross, J., Ross, V., 2002. Shape and area of simple narrow leaves. Proc. Estonian Acad. Sci. Biol. Ecol. 51, 147–62.

Mõttus, M., Ross, J., Sulev, M., 2001. Experimental study of ratio of PAR to direct integral solar radiation under cloudless conditions. Agric. For. Meteorol. 109, 161–170.

Myneni, R. B., 1991. Modeling radiative transfer and photosynthesis in three dimensional vegetation canopies. Agric. For. Meteorol. 55, 323–344.

Myneni, R. B., Asrar, G., 1993. Radiative transfer in three-dimensional atmosphere-vegetation media. J. Quant. Spectrosc. Radiat. Transfer 6, 585–598.

Myneni, R. B., Asrar, G., Kanemasu, E. T., 1988. Finite element discrete ordinates method for radiative transfer in non-rotationally invariant scattering media: application to the leaf canopy problem. J. Quant. Spectrosc. Radiat. Transfer 40, 147–155.

Myneni, R. B., Asrar, G., Kanemasu, E. T., Lawlor, D. J., Impens, I., 1986. Canopy architecture, irradiance distribution on leaf surfaces and consequent photosynthetic efficiencies in heterogeneous plant canopies. Part 1. Theoretical considerations. Agric. For. Meteorol. 37, 189–204.

Myneni, R. B., Impens, I., 1985. A procedural approach for studying the radiation regime of infinite and truncated foliage spaces. Part II. Results and discussion. Agric. For. Meteorol. 34, 3–16.

Myneni, R. B, Marshak, A., Knyazikhin, Y., Asrar, G., 1991. Discrete ordinates method for photon transport in leaf canopies. In: Myneni, R. B., Ross, J. (Eds.), Photon-Vegetation Interactions: Applications in Optical Remote Sensing and Plant Ecology. Springer-Verlag, Berlin, 45–109.

Myneni, R. B., Nemani, R. R., Running, S. W., 1997. Estimation of global leaf area index and absorbed PAR using radiative transfer models. IEEE Trans. Geosci. Remote Sens. 35, 1380–1393.

Niinemets, Ü., Cescatti, A., Christian, R., 2004. Constraints on light intercep-
tion efficiency due to shoot architecture in broad-leaved *Nothofagus* species.
Tree Physiol. 24, 617–630.

Nilson, T., 1971. A theoretical analysis of the frequency of gaps in plant stands.
Agric. Meteorol. 8, 25–38.

Nilson, T., 1999. Inversion of gap frequency data in forest stands. Agric. For.
Meteorol. 98–99, 437–448.

Nilson, T., Peterson, U., 1991. A forest canopy reflectance model and a test case.
Remote Sens. Environ. 37, 131–142.

Nilson, T., Ross, J., 1997. Modeling radiative transfer trough forest canopies:
implications for canopy photosynthesis and remote sensing. In: Gholz, H. L.,
Nakane, K., Shimoda, H. (Eds.), The Use of Remote Sensing in the Modeling
of Forest Productivity. Kluwer Academic Publishing, Dordrecht, 23–60.

North, P. R. J., 1996. Three-dimensional forest light interaction model using a
Monte Carlo method. IEEE Trans. Geosci. Remote Sens. 34, 946–956.

Oker-Blom, P., 1984. Penumbral effects of within-plant and between-plant shad-
ing on radiation distribution and leaf photosynthesis: a Monte Carlo simula-
tion. Photosynthetica 18, 522–528.

Oker-Blom, P., 1985. Photosynthesis of a Scots pine shoot: simulation of the ir-
radiance distribution and photosynthesis of a shoot in different radiation fields.
Agric. For. Meteorol. 34, 31–40.

Palmroth, S., Palva, L., Stenberg, P., Kotisaari, A., 1999. Fine scale measure-
ment and simulation of penumbral radiation formed by a pine shoot. Agric.
For. Meteorol 95, 15–25.

Palva, L., Garam., E., Siivola, E., Sepponen, R., Hari, P., 1998. Quantifying
spatial variability of photosynthetically active radiation within canopies using
a multipoint measuring system. Agric. For. Meteorol. 92, 163–171.

**Panferov, O., Knyazikhin, Y., Myneni, R. B., Szarzynski, J., Engwald, S.,
Schnitzler, K. G., Gravenhorst, G., 2001.** The role of canopy structure in
the spectral variation of transmission and absorption of solar radiation in veg-
etation canopies. IEEE Trans. Geosci. Remote Sens. 39, 241–253.

Pearcy, R. W., Pfitsch, W. A., 1995. The consequences of sunflecks for photo-
synthesis and growth of forest understory plants. In: Schulze, E.-D., Caldwell,
M. M. (Eds.), Ecophysiology of Photosynthesis. Springer-Verlag, Berlin Hei-
delberg, 343–360.

Pommel, B., Sohbi, Y., Andrieu, B., 2001. Use of virtual 3D maize canopies to
assess the effect of plot heterogeneity on radiation interception. Agric. For.
Meteorol. 110, 55–67.

Prevot, L., Brunet, Y., 1993. Estimating vertical profile of the leaf inclination
distribution function: the silhouette method. In Varlet-Grancher, C., Bon-

homme, R., Sinoquet, H. (Eds.)., Crop Structure and Light Microclimate, Characterization and Application. Paris, INRA Editions, 195–200.

Ross, J., 1981. The Radiation Regime and Architecture of Plant Stands. Dr. W. Junk Publishers, The Hague – Boston – London.

Ross, K. J, Marshak, A. L., 1988. Calculation of canopy bidirectional reflectance using the Monte Carlo method. Remote Sens. Environ. 24, 213–225.

Ross, J., Mõttus, M., 2000a. Statistical treatment of umbra length inside willow coppice. Agric. For. Meteorol. 100, 89–102.

Ross, J., Mõttus, M., 2000b. Statistical treatment of sunfleck length inside willow coppice. Agric. For. Meteorol. 104, 215–231.

Ross, J., Nilson, T., 1968. A mathematical model of radiation regime of plant cover. In: Actinometry and Atmospheric Optics. Valgus, Tallinn, pp 263–281 (in Russian).

Ross, J., Ross, V., 1998. Statistical description of the architecture of a fast growing willow coppice. Agric. For. Meteorol. 91, 23–37.

Ross, J., Sulev, M., 2000. Sources of errors in measurements of PAR. Agric. For. Meteorol. 100, 103–125.

Ross, J., Sulev, M., Saarelaid, P., 1998. Statistical treatment of the PAR variability and its application to willow coppice. Agric. For. Meteorol. 91, 1–21.

Shabanov, N. V., Knyazikhin, Y., Baret, F., Myneni, R. B, 2000. Stochastic modeling of radiation regime in discontinuous vegetation canopies. Remote Sens. Environ. 74, 125–144.

Shultis, J. K., Myneni, R. B., 1988. Radiative transfer in vegetation canopies with anisotropic scattering. J. Quant. Spectrosc. Radiat. Transfer 39, 115–129.

Sinoquet, H., Andrieu, B., 1993. The geometrical structure of plant canopies: characterization and direct measurement methods. In: Varlet-Grancher, C., Bonhomme, R., Sinoquet, H. (Eds.), Crop Structure and Light Microclimate, Characterization and Application. INRA Edition, Paris, 131–158.

Sinoquet, H., Moulia, B., Bonhomme, R. 1991. Estimating the three-dimensional geometry of a maize crop as an input of radiation models: comparison between three-dimensional digitizing and plant profiles. Agric. For. Meteorol. 55, 233–249.

Sinoquet, H., Thanisawanyangkura, S., Mabrouk, H., Kasemsap, P., 1998. Characterization of the light environment in canopies using 3D digitising and image processing. Ann. Bot. 82, 203–212.

Skartveit, A., Olseth, J. A., 1994. Luminous efficacy models and their application for calculation of photosynthetically active radiation. Solar Energy 52, 391–399.

Stenberg, P., 1995. Penumbra in within-shoot and between-shoot shading in conifers and its significance for photosynthesis. Ecol. Model. 77, 215–231.

Stenberg, P., 1998. Implications of shoot structure on the rate of photosynthesis at different levels in a coniferous canopy using a model incorporating grouping and penumbra. Funct. Ecol. 12, 82–91.

Stenberg, P., Kangas, T., Smolander, H., Linder, S., 1999. Shoot structure, canopy openness, and light interception in Norway spruce. Plant Cell Environ. 22, 1133–1142.

Stenberg, P., Linder, S., Smolander, H., Flower-Ellis, J., 1994. Performance of the LAI-2000 plant canopy analyzer in estimating leaf area index of some Scots pine stands. Tree Physiol. 14, 981–995.

Thomas, G. E., Stamnes, K., 1999. Radiative Transfer in the Atmosphere and Ocean. Cambridge University Press.

Valladares, F., Pugnaire, F. I., 1999. Tradeoffs between irradiance capture and avoidance in semi-arid environments assessed with a crown architecture model. Ann. Bot. 83, 459–469.

Verhoef, W., 1985. Earth observation modeling based on layer scattering matrices. Remote Sens. Environ. 17, 165–178.

Verhoef, W., Bach, H., 2003. Remote sensing data assimilation using coupled radiative transfer models. Phys. Chem. Earth 28, 3–13.

Vermote, E., Tanré, D., Deuzé, J. L., Herman, M., Morcrette, J. J., 1997. Second simulation of the satellite signal in the solar spectrum, 6S — An overview. IEEE Trans. Geosci. Remote Sens. 35, 675–686.

Verwijst, T., Wen, D., 1996. Leaf allometry of *Salix viminalis* during the first growing season. Tree Physiol. 16, 655–660.

Vierling, L. A., Wessman, C. A., 2000. Photosynthetically active radiation heterogeneity within a monodominant Congolese rain forest canopy. Agric. For. Meteorol. 103, 265–278.

Walter-Shea, E. A., Norman, J. M., 1991. Leaf optical properties. In: Myneni, R. B., Ross, J. (Eds.), Photon-Vegetation Interactions: Applications in Optical Remote Sensing and Plant Ecology. Springer-Verlag, Berlin, 229–251.

Weiss, M.,Baret F., Smith, G. J., Jonckheere, I., Coppin, P., 2004. Review of methods for in situ leaf area index (LAI) determination. Part II. Estimation of LAI, errors and sampling. Agic. For. Meteorol. 121, 37–53.

Zhang, X., Xu, D., 2002. Modeling radiative transfer within the canopy of a Chinese fir plantation. For. Ecol. Manage. 170, 107–116.

ABSTRACT

Shortwave (400–2500 nm) solar radiation field inside a plant canopy is a major contributor to canopy microclimate determining the biochemical processes in plant organs. It determines plant growth, has a large effect on the energy budget and is the driving force behind photosynthesis.

Different plants have different adaptation mechanisms to their radiation environment and react differently to varying levels of incident solar radiation. The variability of the radiation regime of a plant canopy thus describes various biological, physical and chemical characteristics of the ecosystem.

Besides being essential to understanding the ecosystem and its functioning, the knowledge of the shortwave radiation field has another somewhat related application. Determining how the radiation field depends on the various elements of the plant canopy—branches, leaves, flowers, etc.—is a key issue in interpreting remote sensing data obtained over vegetated areas.

Radiation measurements were carried out inside a short-rotation willow plantation at Tartu Observatory, Tõravere, Estonia. The plantation was divided between two willow species: *Salix viminalis* and *Salix dasyclados*.

The radiation measurement system consisted of a sensor carriage moving along a 6-m-long horizontal aluminium bar at different heights inside and above the willow stand. Two pyranometers for measuring downward and upward flux densities of global radiation, two quantum sensors for measuring downward and upward flux densities of photosynthetically active radiation, a miniature net radiometer for measuring net radiation, and a miniature actinometer for detecting sunflecks were mounted on the carriage. Background measurements of the same radiation field characteristics were carried out above or beside the coppice.

The plantation was established in 1994 and cut in 1997; in the spring of 1998, new shoots sprouted from the stools and it was the first growing year of a new coppice. The measurements used in this thesis were carried out on cloudless days in the foliated periods of 1995 to 1999 with most of the work concentrating on the years 1997 and 1998 that were the fourth and first growing year, respectively.

During the first year, the foliage could be described as a single 'cylindrical foliage layer', a layer of almost vertically oriented stem foliage cylinders. The second-year stems sprouting from the apex of the first-year stem elongated and formed lateral branches; the uppermost parts of the most vigorous stems and branches formed the new upper cylindrical foliage layer. The layer below the cylindrical layer that formed at the beginning of the second foliated season consisted of leaves and small branches located on the stems and can be described as a turbid medium.

Allometric formulae were constructed to describe the distribution of leaf area within the willow canopy. These formulae, valid for a short period around the

biometrical measurements, were used for the calculation of the downward cumulative leaf area index that was used as the vertical coordinate, and other canopy parameters. A 3D model of the willow canopy was constructed, describing the stand as consisting of vertical shoots. The characteristics of the shoots were determined from the detailed measurements of canopy structure.

A leaf shape formula was proposed to describe a simple narrow leaf using three parameters: leaf length, leaf width, and leaf form factor (the ratio of leaf area to the product of leaf length and leaf width). These parameters can be determined from quite simple geometrical measurements of leaves. The leaf shape function was compared with the measured shape of the leaves of *S. viminalis* and *S. dasyclados.*

Using the leaf form factor determined for *S. viminalis*, the shape function was included in the 3D model.

The distribution of umbra length was studied for both *S. viminalis* and *S. dasyclados*; due the small number of radiation measurements in the *S. dasyclados* stand, sunfleck length characteristics were investigated only inside the *S. viminalis* canopy. The optical pathlength $\tau = L/\cos\vartheta_S$, where L is the downward cumulative leaf area index and ϑ_S is the solar zenith angle, was found to be the key factor determining the absorption pattern of direct sunlight, not the average geometrical distance between the leaves and the sensor.

Evidence of differences in the stand architecture of the two species was found during the analysis of sunfleck and umbra statistics. At the same values of τ, the wider leaves of *S. dasyclados*, located closer to the ground, allowed more penumbra to fall onto the transect than did the narrow leaves of *S. viminalis*. Differences in the number of umbrae and in the fraction of medium-length umbrae suggested that umbra distribution at ground surface can be used to estimate the geometrical characteristics of a plant stand.

Several attempts were made to describe the effects of the geometric structure of the willow canopy on the shortwave radiation field. Using the 3D model of canopy structure, distribution of direct solar radiation intensity was modeled inside the *S. viminalis* stand, taking into account the finite dimensions of the Sun. Modeling results were compared with a simpler model, describing the canopy as a volume filled with randomly oriented leaves, and also with measurement data.

The shape of the simulated distribution of irradiance in penumbra is realistic in both the shoot model and the simpler reference model. Considering the different fractional areas of umbra, penumbra and sunfleck, the direct radiation regime of a leaf is quite different for the two models. The effect of clumping evident in the 3D model cannot be described by a constant clumping index—clumping depends on solar zenith angle and measurement height.

To introduce the effect of clumping into the equation of radiative transfer, the clumping index, mainly used as a correction factor to match measured canopy transmittance with that calculated by the exponential formula, was included in the source term of the radiative transfer equation to modify the attenuation of direct solar radiation. Radiation fluxes inside the *S. viminalis* stand were modeled by dividing shortwave radiation into two spectral regions, photosynthetically active radiation and near-infrared radiation. The Monte Carlo technique was applied to the 3D canopy model; and the equation of radiative transfer was solved using the discrete ordinates method for both with (clumped canopy) and without (horizontally homogeneous canopy) the inclusion of the clumping index.

All models performed reasonably well when predicting downward fluxes, reflected fluxes were modeled less accurately. The Monte Carlo model was found to describe some of the clumping inside the willow canopy as did the inclusion of the clumping index into the equation of radiative transfer. However, the values of the clumping index were taken from radiation measurements; also, the *ad hoc* nature of the clumping index indicates that this approach should be used with caution.

The measured canopy transmittance showed that in the middle canopy layers, foliage intercepted radiation as if it was distributed randomly. At the top of the canopy, very large clumping occurs, the origin of which is unknown.

The distribution of leaf inclination angles was found to have a minimal effect on the radiation regime of the stand.

LÜHILAINELISE PÄIKESEKIIRGUSE VÄLI PAJUVÕSAS

Lühilaineline (400–2500 nm) päikesekiirgus mängib olulist rolli taimkatte mikrokliima kujunemisel ja suunab taimede organites toimuvaid biokeemilisi protsesse. Lühilaineline kiirgus määrab taimede kasvu, mõjutab tugevalt energiabilanssi ja on fotosünteesi käimapanev jõud.

Erinevad taimed kasutavad kiirguskeskkonnaga kohanemiseks erinevaid meetodeid ja reageerivad muutuvale kiirgushulgale erinevalt. Kiirgusrežiimi muutlikkus kirjeldab seega ökosüsteemi mitmeid bioloogilisi, füüsikalisi ja keemilisi omadusi.

Peale ökosüsteemi ja selle funktsioneerimise kirjeldamise omab lühilaineline kiirgusväli tähtsat rakendust ka teistel aladel. Taimkatte kaugseire tulemuste töötlemine eeldab teadmist, kuidas taimede organid — lehed, oksad, õied jne. — mõjutavad kiirgusvälja.

Kiirgusmõõtmised toimusid Tartu Observatooriumi (Tõravere, Tartumaa) juurde rajatud kiirekasvulise pajuvõsa istanduses. Istanduse ala oli jagatud kahe pajuliigi, *Salix viminalis*'e ja *Salix dasyclados*'e vahel.

Kiirgusmõõtmiste aparatuur koosnes 6 m pikkusest alumiiniumlatist ja sellel liikuvast vankrikesest. Vankrikesele olid kinnitatud järgmised instrumendid: kaks püranomeetrit alla- ja ülespoole suunatud integraalse kiirgusvoo mõõtmiseks, kaks kvantvastuvõtjat alla- ja ülessuunatud fotosünteetiliselt aktiivse kiirguse mõõtmiseks, miniatuurne bilansomeeter kiirgusbilansi mõõtmiseks ja miniatuurne aktinomeeter — päikeselaikude indikaator. Lati kõrgust võsas sai muuta, et mõõta kiirgusvooge erinevatel kõrgustel võsa sees ja kohal. Paralleelselt mõõtmistega võsas mõõdeti võsa kõrval või selle kohal ka kiirgusfooni.

Istandus rajati 1994. a., pajud lõigati maha aastal 1997; 1998. a. kevadel kasvasid kändudest uued võrsed, algatades võsa uue kasvutsükli. Doktoritöös kasutatud mõõtmised toimusid 1995. – 1999. a. vegetatsiooniperioodidel pilvitutel päevadel. Enamus tööst keskendub 1997. ja 1998. a. mõõtmistulemustele, mis olid võsa jaoks vastavalt esimese kasvutsükli neljas ja teise kasvutsükli esimene kasvuaasta.

Esimesel kasvuaastal võis võsa kirjeldada „silindrilise kihina", mis koosnes peaaegu vertikaalsetest võrsesilindritest. Teise aasta algul kasvasid eelmise aasta lehtede kohale varrel kõrvalharud. Kõrgemal asuvad ja pikemad kõrvalharud moodustasid uue silindrilise kihi, mille alla tekkis lühematele okstele kinnitunud lehtedest peaaegu ühtlane „sume keskkond".

Kirjeldamaks lehepinna jaotust pajuvõsas, koostati allomeetrilised valemid, mis kehtisid vaid lühikesel perioodil nende koostamisel kasutatud biomeetriliste mõõtmiste tegemise hetke lähedal. Allomeetriliste valemite abil arvutati hil-

jem vertikaalse koordinaadina kasutatav kumulatiivne lehepinnaindeks ja teised lehestikku kirjeldavad parameetrid. Detailsete biomeetriliste mõõtmiste abil koostati ka kolmedimensionaalne pajuvõsa mudel, milles lehestik on kirjeldatud vertikaalsetest võrsetest koosnevana.

Töös pakutakse välja pikkade ja kitsaste lehtede kirjeldamiseks sobiv lehekuju valem. Valem sisaldab kolme tundmatut: lehe pikkus, laius ja kujutegur (lehepinna suhe pikkuse ja laiuse korrutisse); need kolm taimelehe geomeetrilist parameetrit on mõõdetavad ka lihtsate vahenditega. Väljapakutud kujufunktsiooni võrreldi mõõdetud *S. viminalis*e ja *S. dasyclados*e lehtede kontuuridega.

Lehe kujufunktsioon sisaldus ka kolmemõõtmelises mudelis lehe kuju kirjeldamiseks, kasutades *S. viminalis*e jaoks määratud lehe kujutegurit.

Täisvarju pikkuste jaotust uuriti nii *S. viminalis*e kui *S. dasyclados*e mõõtmisandmetest; kuna aga *S. dasyclados*es tehtud kiirgusmõõtmiste arv oli väike, on laigupikkuste katakteristikuid uuritud vaid *S. viminalis*e istanduses. Analüüsi tulemusena leiti, et otsese päikesekiirguse läbitulekut taimkattest kirjeldab kõige paremini optiline teepikkus $\tau = L/\cos\vartheta_S$, kus L on kumulatiivne lehepinnaindeks ja ϑ_S päikese seniitnurk, mitte lehtede ja vastuvõtja geomeetriline kaugus teineteisest.

Taimkatte sees mõõdetud kiirgusrežiimi analüüsil leiti taimestiku erineva arhitektuuri mõju, näiteks sama τ väärtuste puhul tekitasid laiemad ja madalamalasuvad *S. dasyclados*e lehed suurema poolvarjuala kui kitsamad *S. viminalis*e lehed. Erinevused täisvarjupiirkondade arvus ja keskmise pikkusega varjude osakaalus annavad alust oletada, et ka täisvarjupiirkondade jaotus taimkatte all on mõjutatud taimkatte struktuurist.

Paju lehestiku struktuuri mõju kirjeldamiseks kiirgusrežiimile kasutati erinevaid meetodeid. Otsese kiirguse intensiivsuse jaotus taimkattes arvutati kolmemõõtmelise võsamudeli abil, arvestades ka päikeseketta lõplikku läbimõõtu. Modelleerimistulemusi võrreldi nii lihtsama mudeliga, kus taimelehed olid paigutatud ruumis juhuslikult, kui ka kiirgusmõõtmistega.

Nii kolmemõõtmeline kui ka võrdlusena kasutatud lihtsam mudel simuleerisid realistlikult kiirguse intensiivsuste jaotust poolvarjupiirkonnas. Kuid arvestades mudelite poolt ennustatud päikeselaigu, poolvarju ja täisvarju erinevaid osakaalusid, on lehe kiirgusrežiim neis kahes modelleeritud lehestikus erinev. Kolmemõõtmelises pajumudelis esinevat lehestiku grupeerumust ei kirjeldanud ka konstantne grupeerumusindeks (parand kirjeldamaks kiirguse läbituleku erinevust eksponentvalemi ennustatust) — grupeerumine oleneb nii mõõtmiskõrgusest kui päikese seniitnurgast.

Kiirguslevi võrrandisse otsekiirguse läbitulekut kirjeldavasse liikmesse lisati parand grupeerumusindeksi arvestamiseks. Taimestiku kiirgusrežiimi modelleerimiseks jagati lühilaineline kiirgus kaheks spektraalseks komponendiks —

fotosünteetiliselt aktiivseks kiirguseks ja lähis-infrapunakiirguseks. Monte Carlo meetodil simuleeriti kiirgusvälja modelleeritud pajuvõsas; diskreetsete ordinaatide meetodit kasutades lahendati kiirguslevi võrrand nii grupeerunud kui grupeerumata taimkatte jaoks.

Kõik kasutatud mudelid andsid mõistlikke tulemusi allapoole suunatud kiirgusvoogude ennustamisel, peegeldunud voogude arvutamisel olid vead suuremad. Taimkatte grupeerumuse mõju kiirgusrežiimile suutis kirjeldada nii Monte Carlo mudel kui grupeerumist arvestav kiirguslevivõrrand, kuid viimases esinev grupeerumisindeks tuli arvutada mõõdetud taimkatte läbilaskvusest. Samuti räägib viimase meetodi kahjuks grupeerumusindeksi *ad hoc* iseloom.

Taimkatte otsekiirguse läbilaske mõõtmised näitasid, et taimkatte keskmised kihid nõrgendavad kiirgust sarnaselt juhusliku lehestikuga. Taimkatte ülakihtides aga esineb tugev grupeerumine, mille päritolu on raske selgitada.

Leiti ka, et lehtede orientatsioon ei avaldanud kiirgusrežiimile olulist mõju.

ACKNOWLEDGEMENTS

First, I would like to thank all my supervisors, Prof. Tiit Nilson, Prof. Hannes Tammet, and most of all, Prof. Juhan Ross for their support. I started to investigate the radiation regime of plant canopies under the supervision of Prof. Juhan Ross, and I sincerely hope that he, if he was still among us, would not disapprove of my treatment of the subject he pioneered several decades ago.

Also I feel indebted towards Vello Ross for the biometrical measurement data this thesis is largely based on, Madis Sulev for his advice on actinometrical matters, and all other scientists and engineers working with radiation measurements at Tartu Observatory.

I would also like to thank Dr. J. B. Stewart, the regional editor of Agricultural and Forest Meteorology, and all the anonymous reviewers of the articles in the LIST OF ORIGINAL PUBLICATIONS as their expertise has contributed to the formulation of the results presented in this thesis.

And last but not least, I express my thanks towards my family and friends for being there when I needed them; especially towards my father, who passed away while I was finishing this manuscript. I hope my friends and family understand what I mean by that without me having to write it on the last page of my PhD thesis.

CURRICULUM VITAE

Matti Mõttus

Citizenship	Estonian
Date and place of birth	24 July 1976, Tartu, Estonia
Address	Tartu Observatoorium 61602 Tartumaa, Estonia
Telephone	+372 741 0278, +372 5565 0659
Fax	+372 741 0205
E-mail	mottus@ut.ee

Education

2000–2004	Doctoral student at University of Tartu, Faculty of Physics and Chemistry
1998–2000	MSc in environmental physics (University of Tartu), "Statistical treatment of penetration of direct solar radiation inside willow coppice"
1994–1998	BSc in physics (University of Tartu) *cum laude*
1983–1994	M. Härma Tartu Secondary School No. 2

Special courses

18.04.–01.05.2001	Hyytiälä and Helsinki, Finland. NORFA Network on Aerosol Dynamics: Atmospheric Aerosols, Formation and Transformation
26.11.–19.12.2001	Stockholm, Sweden. NORFA Network on Aerosol Dynamics: Aerosol, clouds and climate
6.6.–13.6.2003	Riga, Latvia. NORFA course Today's research training—tomorrow's scientific quality

Professional employment

2004–	Research associate, Tartu Observatory
2001–	Temporary assistant at Institute of Environmental Physics, University of Tartu
1999–2004	Engineer, Tartu Observatory
1995–1997	Assistant, Institute of Experimental Physics and Technology, University of Tartu

Scientific work

Scientific interests	Radiation regime of plant canopies—modeling the radiative transfer and canopy transmittance to estimate LAI and canopy structural parameters

ELULOOKIRJELDUS

Matti Mõttus

Kodakondsus	Eesti
Sünniaeg ja -koht	24. juuli 1976, Tartu, Eesti
Aadress	Tartu Observatoorium 61602 Tartumaa
Telefon	+372 741 0278, +372 5565 0659
Faks	+372 741 0205
E-mail	mottus@ut.ee

Hariduskäik

2000–2004	Doktorant Tartu Ülikooli füüsika-keemiateduskonnas
1998–2000	MSc keskkonnafüüsikas (Tartu Ülikool), *Statistical treatment of penetration of direct solar radiation inside willow coppice*
1994–1998	BSc füüsikas (Tartu Ülikool) *cum laude*
1983–1994	M. Härma nim. Tartu 2. Keskkool, hõbemedal

Erialane täiendus

18.04.–01.05.2001	Hyytiälä ja Helsingi, Soome. *NORFA Network on Aerosol Dynamics: Atmospheric Aerosols, Formation and Transformation*
26.11.–19.12.2001	Stockholm, Rootsi. *NORFA Network on Aerosol Dynamics: Aerosol, clouds and climate*
6.6.–13.6.2003	Riia, Läti. NORFA kursus *Today's research training—tomorrow's scientific quality*

Erialane teenistuskäik

2004–	teadur Tartu Observatooriumis
2001–	Meteoroloogia praktikumi juhendaja TÜ keskkonnafüüsika instituudis
1999–2004	insener Tartu Observatooriumis
1995–1997	TÜ eksperimentaalfüüsika ja tehnoloogia instituudi gaaslahenduslabori laborant

Teadustegevus

Teadustöö suunad	Taimkatte kiirgusrežiimi uurimine — kiirguslevi ja otsese päikesekiirguse läbituleku modelleerimine taimkatte arhitektuuri ja lehepinnaindeksi hindamiseks.